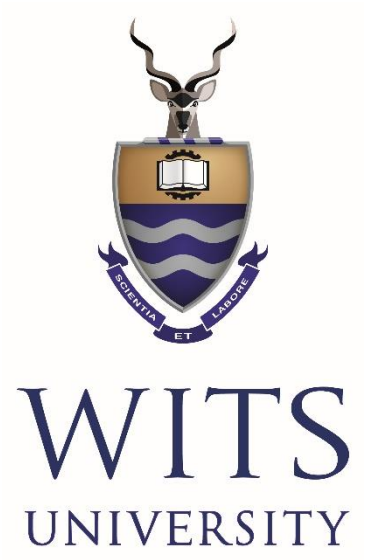

Follow-up soil survey to evaluate regional Pb and Zn soil anomalies in Modimolle, Limpopo Province, South Africa

Submitted in fulfilment of the requirements for the degree of Master of Science

Thato Ntikang

787047

ACKNOWLEDGEMENTS

I would like to express my sincere appreciation to my supervisor, Professor Judith Kinnaird, for thorough guidance with constructive reviews and comments during the running of this project. I'm also grateful to the generosity of South African Council for Geoscience for financial support and resources (geological and geochemical data of the study area) in making this project a reality. I would also like to thank my colleagues Mr Jakobus Elsenbroek and Mr Sibongiseni Hlatshwayo at Council for Geoscience for their invaluable comments, criticisms, recommendations and guidance. Special thanks to my family for their great love, patience, guidance and encouragement during the course of my study. This achievement would not have been possible with your unfailing support.

DECLARATION

I Thato Ntikang declare that this Research Report is my own, unaided work. It is being submitted for the Degree of Master in Science by Coursework and Research Report to the University of the Witwatersrand, Johannesburg, South Africa. It has not been submitted before for any degree or examination in any other University.

Signature: 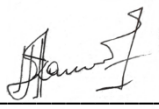 Date: _____

ABSTRACT

The Bushveld Complex was sampled in 1989 as part of the Council for Geoscience (CGS) national geochemical mapping programme. This programme was conducted in order to produce geochemical data to update the geological maps, undertake mineral exploration and determine geochemical baseline concentrations. About 5 kg of surficial soil samples were collected using a sample density of one sample per 1 km^2. Soil samples were collected by means of a helicopter and analysed by a simultaneous wavelength-dispersive X-ray fluorescence spectrometer for TiO_2, MnO, Fe_2O_3T, Sc, V, Cr, Co, Ni, Cu, Zn, As, Rb, Sr, Y, Nb, Zr, Ba, W, Pb, Th and U. These results produced elevated concentrations of several elements and this report focuses on Pb and Zn, which showed elevated concentrations of up to 429 ppm and 1 064 ppm, respectively. Most of these elevated concentrations were localised in areas such as Modimolle, Thabazimbi, Mabopane, Pretoria and Groblersdal among others.

A further follow-up survey was conducted north of Modimolle area to verify these elevated Pb and Zn concentrations, determine whether they indicate potential mineralisation and generate target areas of potential mineralisation. Soil samples were collected at 200 m intervals with a depth of 10–60 cm, prepared and analysed for SiO_2, TiO_2, Al_2O_3, Fe_2O_3, MnO, MgO, CaO, Na_2O, K_2O, P_2O_5, As, Ba, Ce, Co, Cr, Cu, Ga, Hf, Mo, Nb, Nd, Ni, Pb, Rb, S, Sb, Sc, Sn, Sr, Ta, Th, U, V, W, Y, Zn, and Zr by X-ray Fluorescence Spectrometry.

The results showed Pb and Zn ranging between 16–1043 ppm and 28–4564 ppm, respectively, and average concentrations (i.e. 179 ppm and 284 ppm, respectively), which are significantly higher than the regional rock averages of 11 ppm Pb, 147 ppm Zn and regional soil averages of 10 ppm Pb and 50 ppm Zn. About 65 % of Zn concentrations lie in the background range of 0–300 ppm and 35 % within the high concentration range of 300–4650 ppm. Lead showed 11.5 % of concentrations in the background range of 0–100 ppm and 88.5 % within the high concentration range of 100–1100 ppm. High Pb and Zn concentrations (i.e. Pb > 100 ppm and Zn > 300 ppm) coupled with high variance values (Zn = 30613 and Pb = 9186), high maximum concentrations (Zn = 4564 ppm and Pb = 1043 ppm), high mean concentrations (Zn = 284 ppm and Pb = 179 ppm) and positive skewness of Pb and Zn, statistically reflected anomalous characteristics indicating potential mineralisation.

Multivariate analysis produced element associations of Zn-Pb-Cu-Mn which characterises the potential mineralisation of the area. Spatial distribution of Zn, Pb, Cu and Mn anomalies produced target zones mainly along the Swaershoek anticline, indicated a possible structural control on the anomalies. The potential type of mineralisation associated with these Zn-Pb-Cu-Mn anomalies is characterised by Zn-Pb-Cu-Ag (veins, fissure lodes, polymetallic sulphide and Irish style mineralisation), and the potential ore-group is characterised by element assemblages of Zn-Pb-Cu/Zn-Cu-Pb, Pb-Zn-Cu/Pb-Cu-Zn and Cu-Pb-Zn which indicate an ore group rich in Zn, Pb and Cu.

CONTENTS

LIST OF FIGURES

LIST OF TABLES

CHAPTER 1

1.1 Introduction

The Council for Geoscience (CGS) has in previous years embarked on a regional geochemical mapping programme in South Africa. The programme was in accordance with the Geoscience Amendment Act No. 16 of 2010 which mandated the Council for Geoscience to be the custodian of geoscientific information and undertake reconnaissance operations, prospecting research and other related activities in the minerals sector. The programme began in 1973 and it was focused mainly in the Karoo Uranium province and then proceeded to the Northern Cape and Bushveld Complex metallogenic provinces (Figure 1.1). These locations were chosen based on the high likelihood of finding more new deposits in the older lithologies compared to the young lithologies.

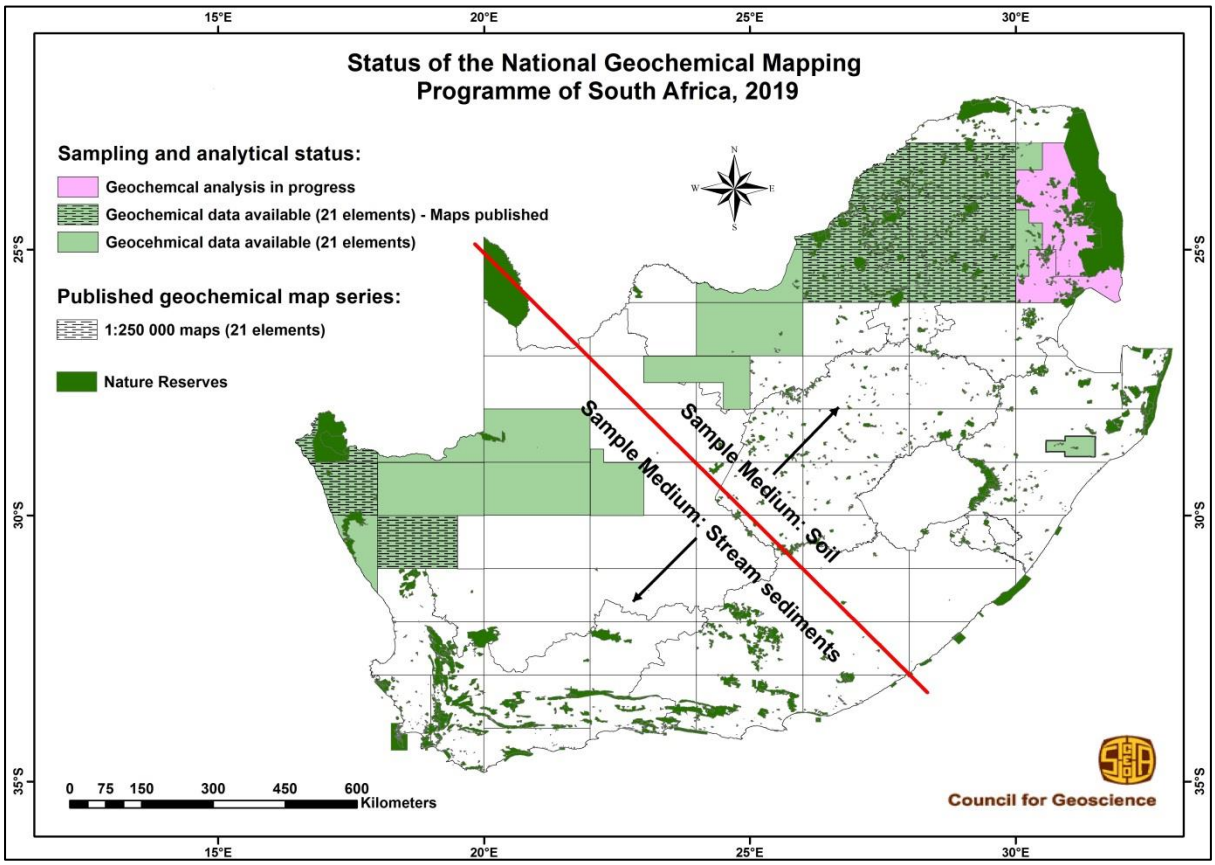

Figure 1.1 Status of the national geochemical mapping programme of South Africa in 2019 (Council for Geoscience).

The objectives of the regional geochemical mapping programme were to conduct regional geochemical soil and first-order stream sediment sampling, create geochemical databases to provide geochemical information in order to complement the existing geological information, determine regional geochemical baseline concentrations of variable lithological units and anomalous concentrations for mineral exploration. The regional geochemical sampling survey was conducted in the manner as to sample the entire country with regard to soil and first-order stream sediment sampling. This led to the entire South Africa being divided into 1:250 000 map units (Figure 1.1) for sampling framework and compilation of geochemical element distribution maps. Collecting samples

of the entire country required a long period of time and significant capital investment especially if the sole means of collecting samples was vehicles. This necessitated a robust sampling method which enabled the entire country to be sampled efficiently. The introduction of a helicopter in 1979 as a means of collecting samples was initiated in order to improve the efficiency of the programme. This substantially increased the sampling rate of the programme whereby up to 400 samples were collected daily. Some of the areas were selected for surficial soil sampling and the others were selected for stream sediment sampling based on the complexities of the terrain.

The collection of samples was conducted with a sampling density of one sample per km^2 and the sample size used was approximately 5 kg. The sampling depth of each sampling medium was 20 cm. Each sample was dry sieved to extract the -75 µm fraction for analysis. The standardised method of analysis for soil and stream sediment samples was carried out by a simultaneous wavelength-dispersive X-ray fluorescence spectrometer (SWDXRF) for TiO_2 (%), MnO (%), Fe_2O_3T (%), Sc (ppm), V (ppm), Cr (ppm), Co (ppm), Ni (ppm), Cu (ppm), Zn (ppm), As (ppm), Rb (ppm), Sr (ppm), Y (ppm), Nb (ppm), Zr (ppm), Ba (ppm), W (ppm), Pb (ppm), Th (ppm) and U (ppm). Recently an additional analysis by DC Arc Emission Spectrography at the Henan Laboratory Peoples Republic of China was conducted for elements such as Pt (ppb), Pd (ppb) and Au (ppb).

Sampling in the Bushveld Complex started in 1989. The regional geochemical results of this survey produced elevated geochemical concentrations of several elements and this research report focusses on Pb, which showed values up to 429 ppm, and Zn with values up to 1 064 ppm. Most of the high regional Pb and Zn concentrations were localised in areas such as Modimolle, Thabazimbi, Mabopane, Pretoria and Groblersdal among others (Figure 1.2 and Figure 1.3). These elevated Pb and Zn concentrations necessitated a follow-up geochemical survey of high-density sampling in order to increase the anomaly contrast against background. In 2014 this follow-up soil survey was conducted in the Modimolle area to verify the elevated Pb and Zn concentrations and determine whether there is potential mineralisation associated with elevated concentrations. A section north of Modimolle town characterised by a high density of elevated Pb and Zn concentrations was targeted for soil sampling, at a sampling density of one sample per 200 m and a sample size was approximately 5 kg.

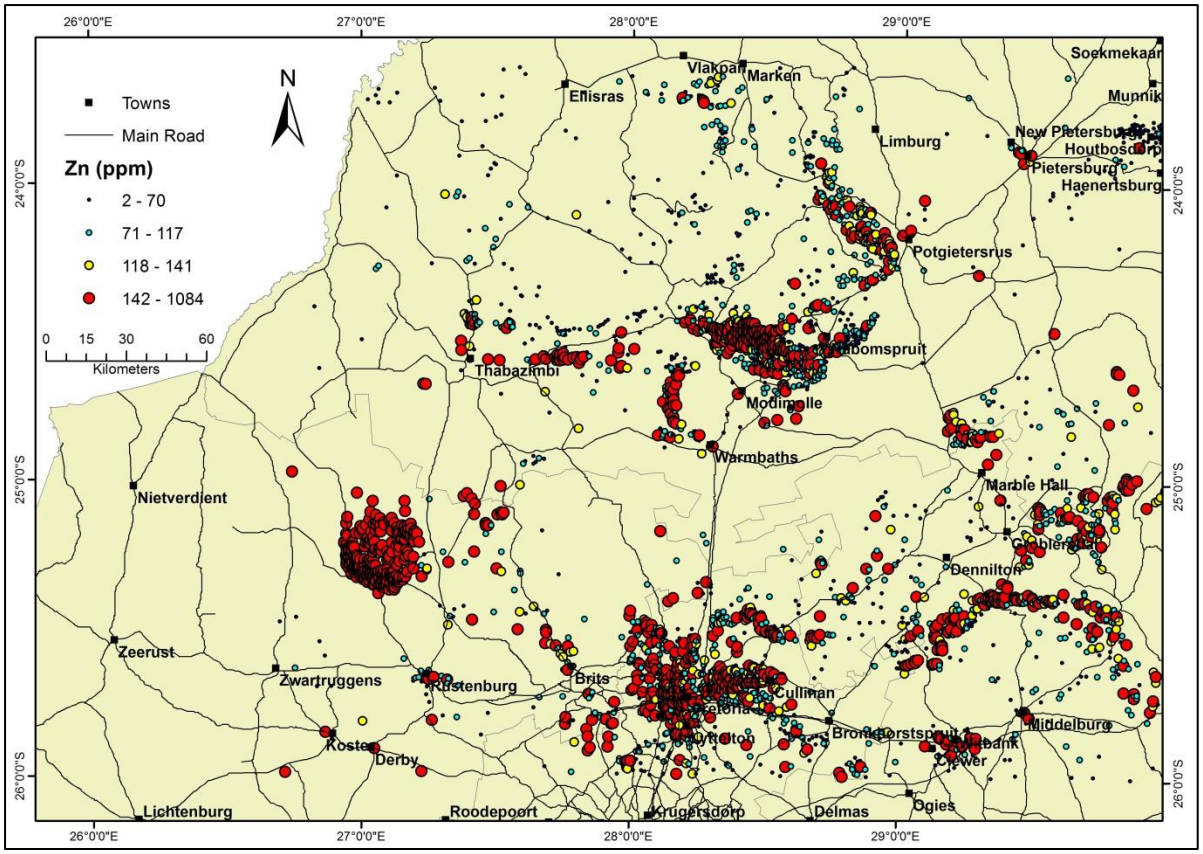

Figure 1.2 Regional geochemical concentrations of zinc (Zn) (CGS ArcGIS database).

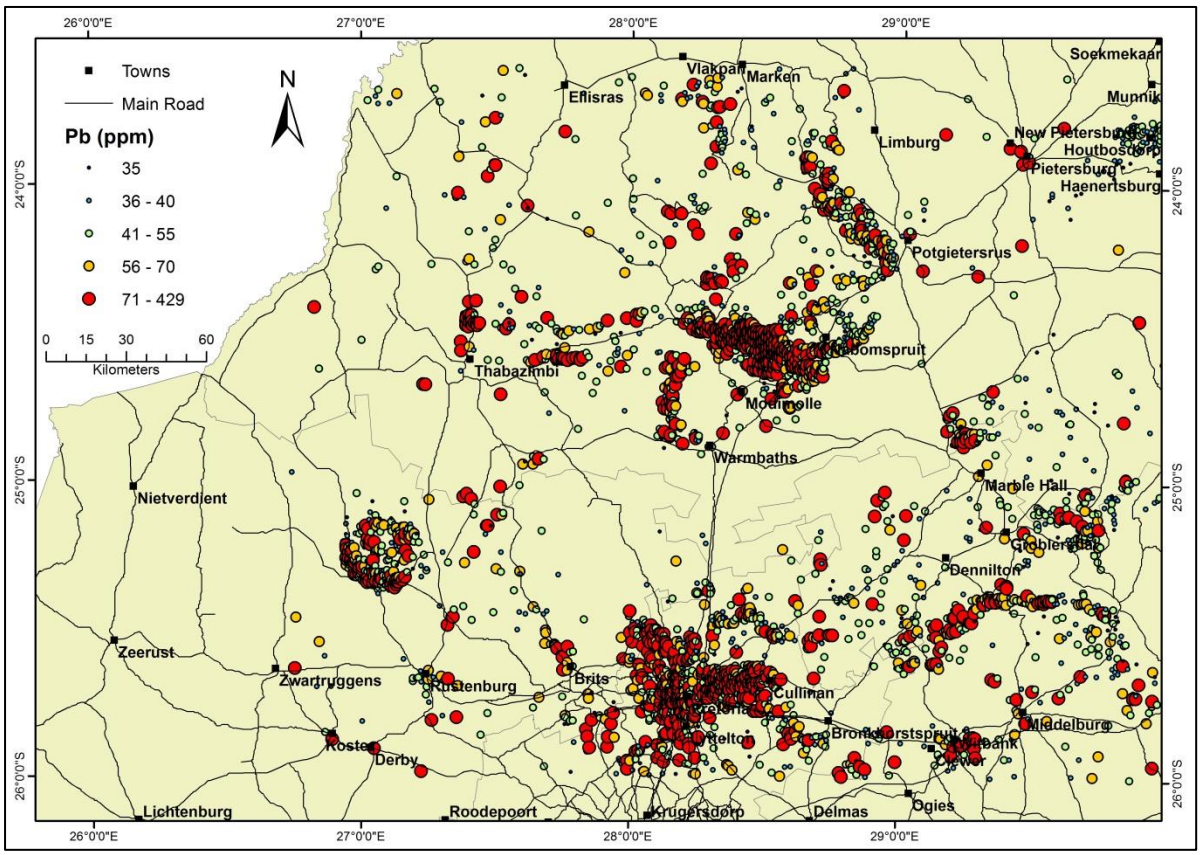

Figure 1.3 Regional geochemical concentrations of lead (Pb) (CGS ArcGIS database).

1.2 Aims and Objectives

This study aims to verify the elevated Pb and Zn concentrations from the regional geochemical survey to assess the anomalous nature of concentrations and identify locations indicating the possibility of mineralisation associated with the anomalous Pb and Zn concentrations. This was to be accomplished by data acquisition, which involved collection of samples at a higher sample density (one sample per 200 m) followed by sample analysis, data quality assessment and interpretation. The author was involved in sample collection, sample preparation and data quality assessment and interpretation. The following objectives were followed in order to realise the aims of the study:

- High density sampling of a 200 m x 200 m grid was utilised for the follow-up soil survey;
- The Pb and Zn concentrations of this study were compared with the elevated Pb and Zn concentrations from a regional geochemical survey to verify their anomalous nature;
- The anomalous Pb and Zn concentrations were evaluated to determine whether they indicate the possibility of mineralisation;
- Potential locations of likely mineralisation were evaluated by using two modes of geochemical exploration (i.e. empirical exploration approach and conceptual exploration approach).

1.3 Location of Study Area

The study area is located 25.5 km north of Modimolle town (formerly known as Nylstroom), Limpopo Province, South Africa. The town lies southeast of the Waterberg District Municipality. The study area falls on the topographic cadastral 1:50 000 map sheets 2428AD, 2428CB and 2428DA. The area lies between latitude 24°29' and 24°32' south, and between longitude 28°23' and 28°30' east. It incorporates about seven farm portions, namely: Zuikerboschfontein 198 KR, Paardeplaats 378 KR, Magalakynsoog 201 KR, Driefontein 379 KR, Geelhoutkloof 202 KR, Kromkloof 203 KR and Wilgeboomsdrift 380 KR. The area is characterised mainly by game and agricultural farms. The agriculture in the area mostly focuses on soft fruits (citrus, peaches, grapes, watermelons), maize and cattle, whereas game farming is mostly wildlife and tourism. In terms of geology, the study area is situated on the felsites of the two young formations of the Rooiberg Group, namely the Kwaggasnek Formation and the Schrikkloof Formation (Figure 1.4).

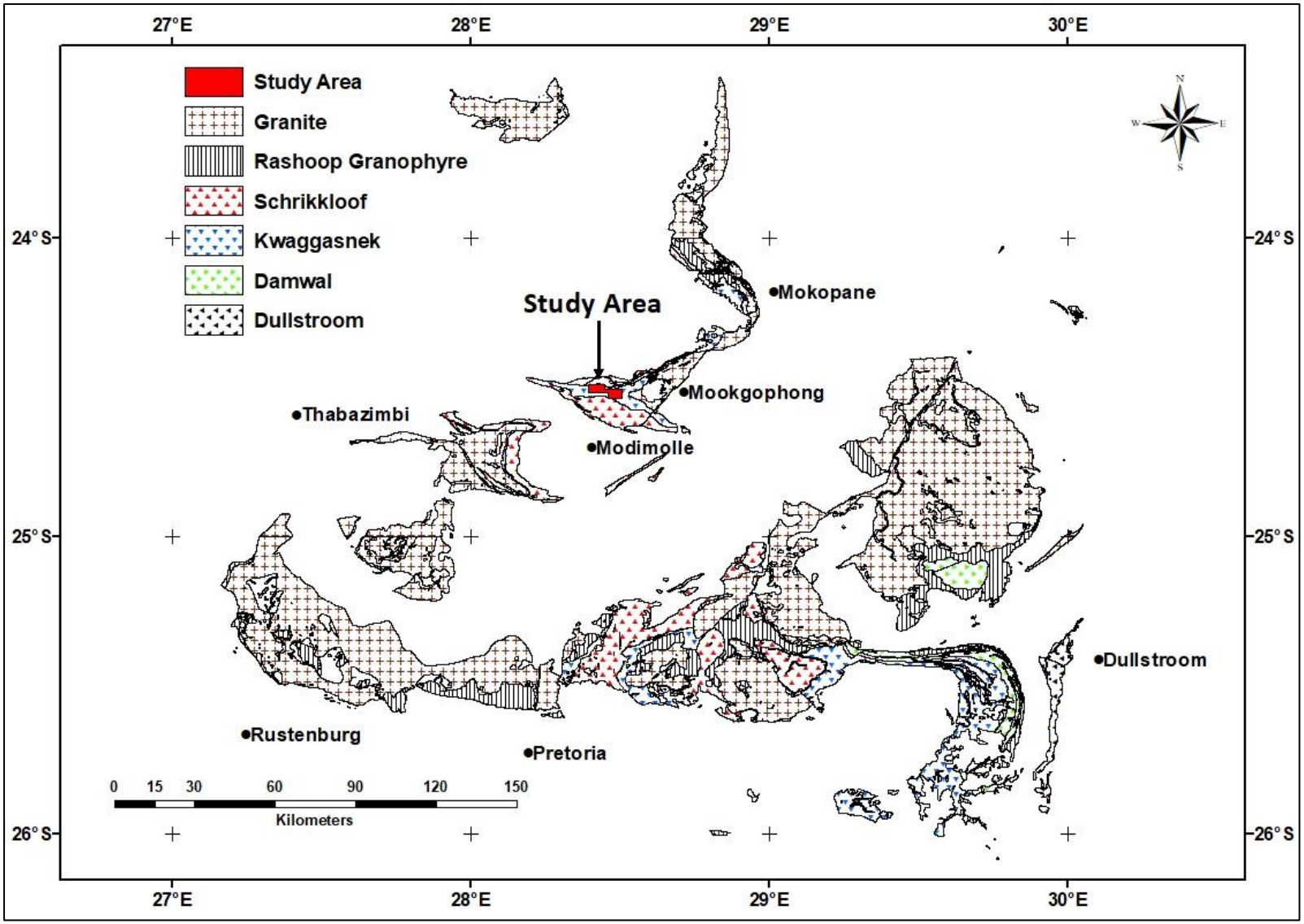

Figure 1.4 The location and geology of the study area in relation to the Rooiberg Group (modified after Schweitzer *et al*., 1995b).

1.3.1 Topography, Drainage and Vegetation

1.3.1.1 Topography

The topography of the study area is characterised by an uneven terrain with hills and low-level mountains. The highest altitude (1620 m above sea level) of the area is on the northwestern part, and the lowest altitude (1400 m above sea level) is on the southeastern part (Figure 1.5). Soils in these moderate to high relief environments tend to have similar geochemical expressions of the underlying lithology due to physical erosion being the dominant dispersion mechanism (Butt and Zeegers, 1992). Moderate to high relief areas also play a crucial role with regard to geochemical anomaly contrasts against background, in a sense that reduction in chemical dispersion and the dominance of physical dispersion tend to result in an increased anomaly/background contrast.

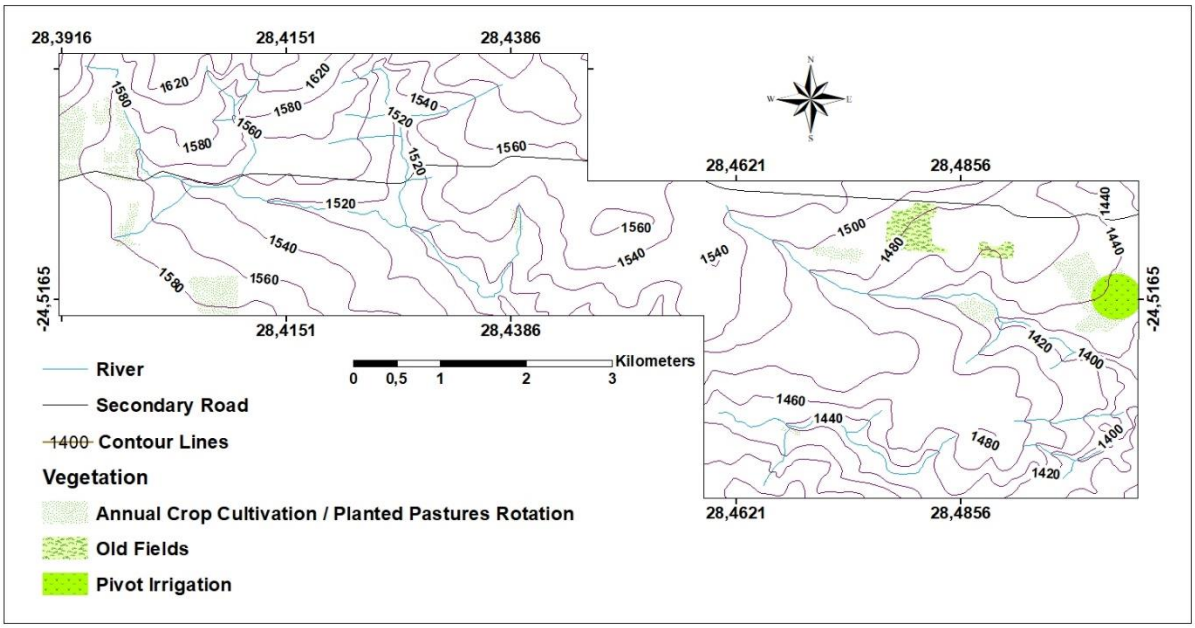

Figure 1.5 The topography of the study area (CGS ArcGIS database).

1.3.2 Landform and Soil Cover

- Landforms

The dominant landform in the area is characterised by a medium-gradient mountain (Figure.1.6A). This type of landform is mainly characterised by a gradient of 15–30 %, that is moderately steep with a relief intensity of 150–300 m.km^{-1} (Jahn *et al*., 2006). Due to the low chemical erosion character of these moderate to high steep terrains, physical erosion tends to dominate as the influential erosion mechanism (Butt and Zeegers, 1992). This mass movement of soil tends to improve downslope geochemical dispersion in colluvial soils (Butt and Zeegers, 1992).

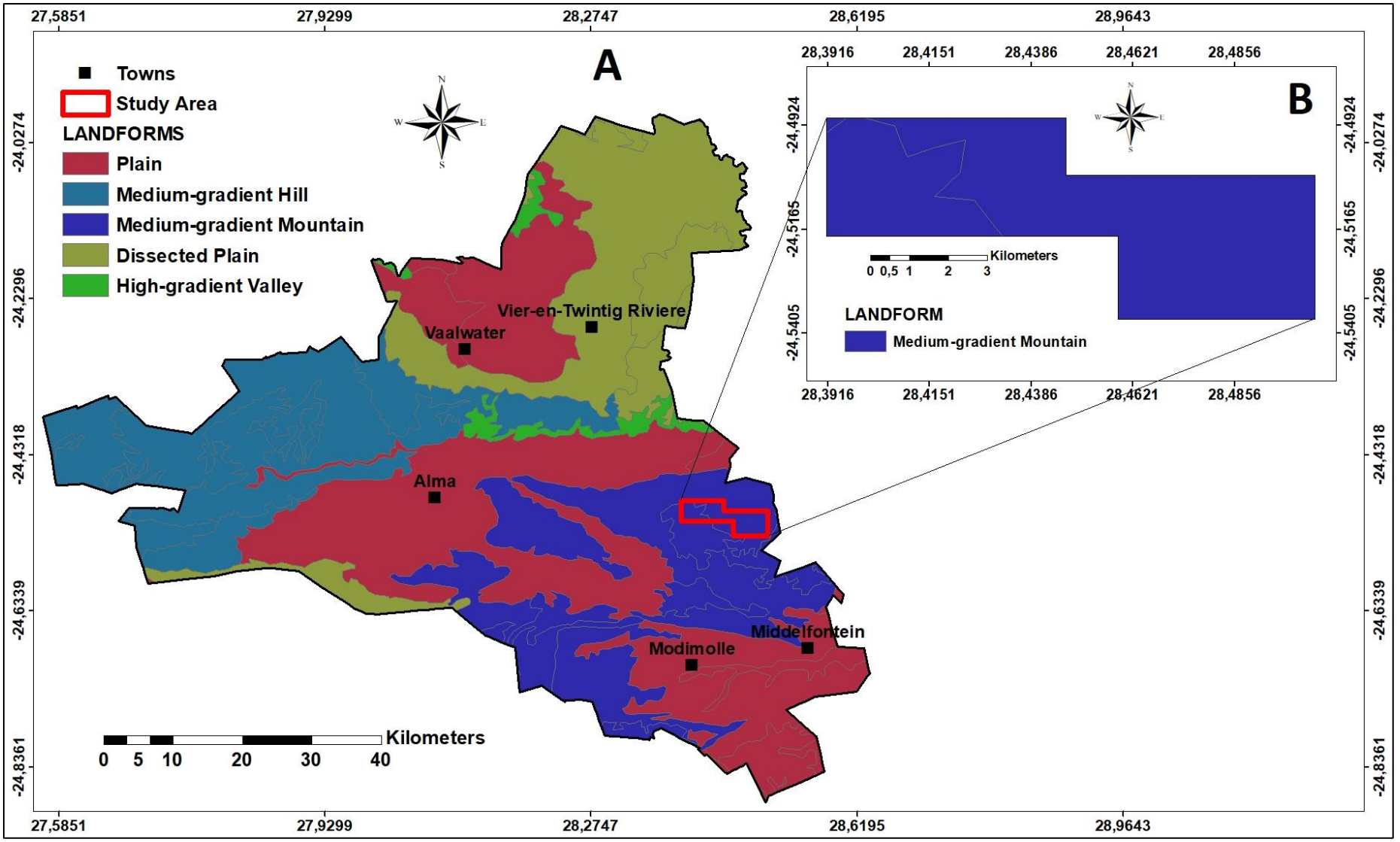

Figure 1.6 The major landform of the study area (FAO, 1988). (A) Regional landforms of Modimolle Local Municipality. (B) Landform of the study area.

- Soil Cover

The soil cover of the area is outlined in Figure 1.7A. It is characterised by two soil types (i.e. Eutric leptosols and Lithic leptosols). Leptosols are young gravelly soils derived from weathered rocks (Kabata-Pendias, 2011; IUSS Working Group WRB, 2015). They are also shallow (generally less than 50 cm) over the bedrock and mostly limited to an A-horizon (Nachtergaele, 2010; IUSS Working Group WRB, 2015). Some of the leptosols tend to be deeper (i.e. 75 cm) containing about <10 % of fine materials (IUSS Working Group WRB, 2015). The IUSS Working Group WRB (2015) constrained the depth of these soils to 25 cm from the bedrock to the soil surface. Leptosols are commonly found in strongly eroded mountainous areas and they have no climatic restrictions (IUSS Working Group WRB, 2015). These soils have <20 % fine material (by volume) and are mainly suitable for forest lands (IUSS Working Group WRB, 2015).

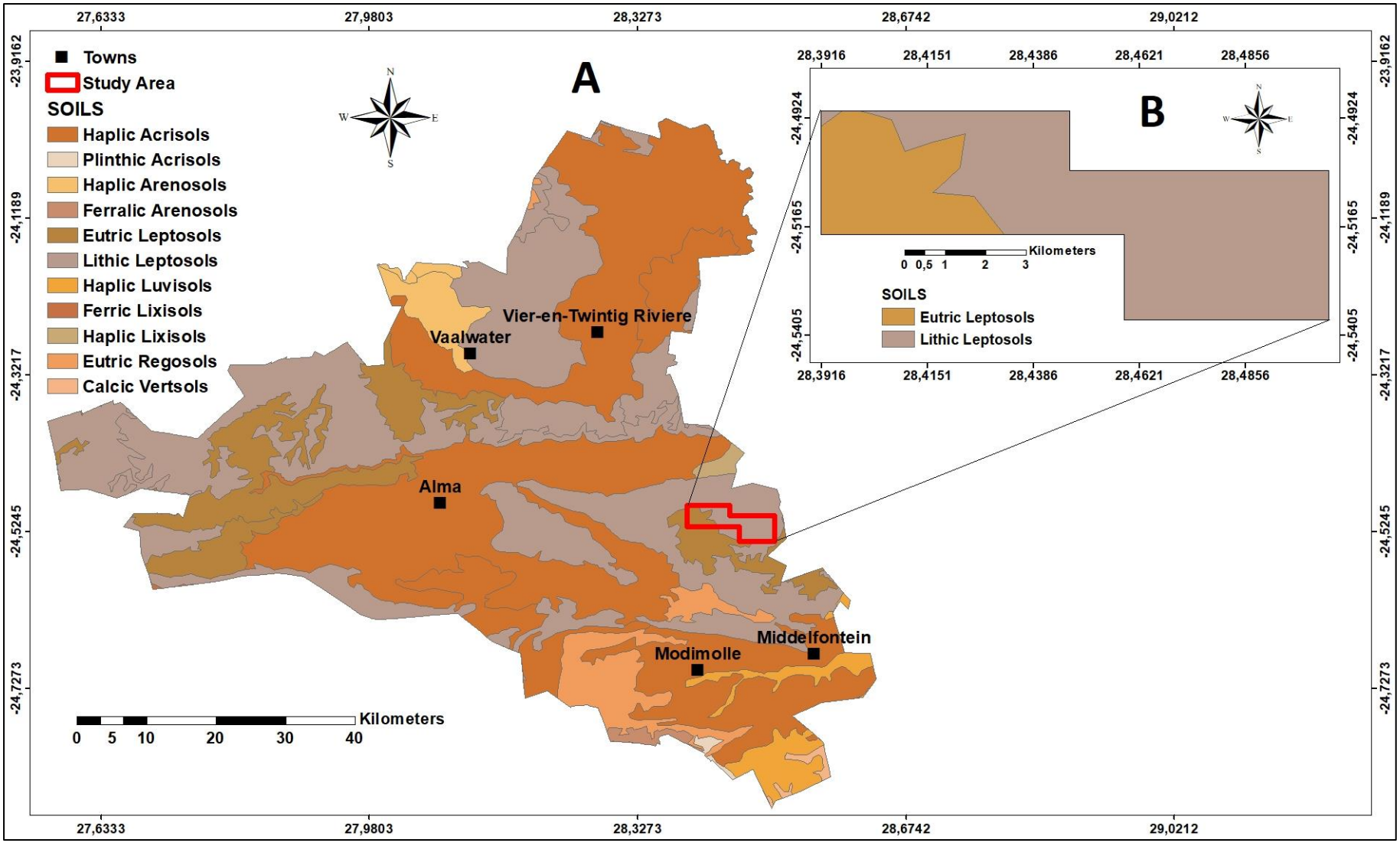

Figure 1.7 The soil cover of the study area showing two types of soils (FAO, 1988). (A) Regional soil types of Modimolle Local Municipality. (B) Soil types of the study area.

Eutric leptosols are mainly localised in the west side of the area, covering only about one third of the entire area. According to the FAO (2001), these soils are characterised with a base saturation (in 1 MNH4OAc at pH 7) of 50 % or more between 20 and 100 cm from the soil surface or within a 5 cm thick horizon directly above a lithic contact. In some instance eutric leptosols tend to be characterised by a relatively large depth (between 20 and 100 cm) compared to the lithic leptosols (IUSS Working Group WRB, 2015). The lithic leptosols cover about two thirds of the area, extending towards the east side of the area. These soils are very shallow and gravelly, with the depth of the bedrock being ≤10 cm from the soil surface (Nachtergaele, 2010; IUSS Working Group WRB, 2015).

CHAPTER 2

Geological Setting

2.1 Regional Geological Setting

The Paleoproterozoic Rooiberg Group is a thick package of silicic volcanic rocks forming the roof of the Bushveld Complex (Rhodes, 1977; Cheney and Twist, 1991; Schweitzer *et al*., 1995a). This group has a thickness of about 5 km and a volume of approximately 300 000 km^2, which due to erosion has had its area of occurrence reduced from 200 000 km^2 to about 67,000 km^2 (Lenhardt and Eriksson, 2012). The Rooiberg Group stratigraphy (Figure 2.1) is characterised mainly by four formations (SACS, 1980; Lenhardt and Eriksson, 2012; Mathez *et al*., 2013), which according to Rhodes (1977) and Lenhardt *et al*. (2017) have been interrupted by the intrusion of Rustenburg Layered Suite (RLS), Rashoop Granophyre Suite and Lebowa Granite Suite (Figure 2.1). These formations in ascending order include the Dullstroom, Damwal, Kwaggasnek and the Schrikkloof formations (Schweitzer, 1987; Schweitzer *et al*., 1995a; Lenhardt and Eriksson, 2012). They are conformably overlain by the clastic sedimentary rocks of mid-Proterozoic Waterberg Group (Ericsson *et al*., 1997; Armitage *et al*., 2007), which are intercalated with minor interbedded volcanics (Figure 2.1).

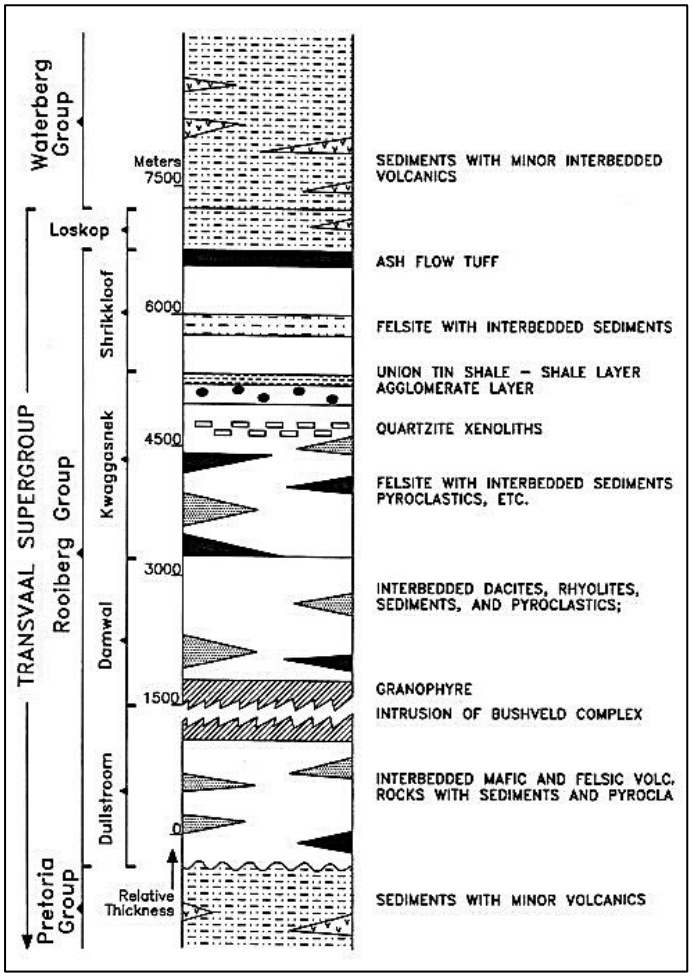

Figure 2.1 The generalised stratigraphy of the Rooiberg Group as proposed by Buchanan and Reimold (1998). Adapted from Coetzee (1970), Council of Geosciences (1978), Clubley-Armstrong (1980), Cheney and Twist (1991), Eriksson *et al*. (1994) and Schweitzer *et al.* (1995a).

Regionally the Dullstroom and Damwal formations are localised southeast of Rooiberg Group whereas the Kwaggasnek and Schrikkloof formations are mainly in the south-central and NW section of the Rooiberg Group (Lenhardt and Eriksson, 2012). The outcrop distribution is largely in the NNW section originating from Mokopane extending through Modimolle towards the Rooiberg area and a southern section originating from Vergenoeg and extending to Middelburg and Sekhukhuni Plateau (Twist and French, 1983). The outcrops in the NNW section occur as discrete roof rocks overlying the Bushveld granites and granophyres, and only Kwaggasnek and Schrikkloof have regional persistent lithostratigraphic markers (e.g. quartzite xenoliths and the Union Tin Member), which can be correlated throughout the region (Figure 2.1). In the southern section the Rooiberg Group outcrops overlie the Bushveld granite towards the southwest and the Rustenburg Layered Suite towards the southeast (Twist and French, 1983; Hatton and Schweitzer, 1995).

Numerous hypotheses have been postulated regarding the origin of the Rooiberg Group (Rhodes, 1975; Sharpe *et al*., 1981; Hatton 1988; Harmer and Gruenewaldt, 1991; Hatton, 1995; Hatton and Schweitzer, 1995; Robb *et al*., 2000; Gunther *et al*., 2018). Its formation is associated with the partial melting of the lower crust by heat from the large volume of mantle-derived magma ponded at the base of the crust (Sharpe *et al*., 1981; Hatton, 1995; Hatton and Schweitzer, 1995). However, the magnesian character of the Dullstroom Formation and ferroan character of the Damwal, Kwaggasnek and Schrikkloof formations led Mathez *et al*. (2013) to suggest that the Rooiberg Group is a product of igneous differentiation of Bushveld mafic liquids. Twist and French (1983) also suggested that the Rooiberg Group is a derivation of cyclic differentiation of magma, whereas Hatton, (1988) compared the rocks of this Group to the continental flood-basalt and the volcanic aggregates produced in the vicinity of the continental margin. Other authors (Hunter, 1974; Hatton and Schweitzer, 1995; Schweitzer *et al*., 1997; Robb *et al*., 2000; Gunther *et al*., 2018) suggested contemporaneous emplacement of Rooiberg lavas and mafic phases of the Bushveld Complex. The hypothesis of the formation of the Rooiberg Group by simultaneous impact of asteroids and comets (Rhodes, 1975; Elston, 1992) was discounted by Buchanan and Reimold (1998), citing lack of evidence for classifying lower Rooiberg Group as an impact melt breccia and quartz paramorphs after tridymite as indicative of impact.

The radiometric dating of the Rooiberg Group proved to be complex with various ages postulated for its formation (Walraven and Hattingh, 1993; Walraven, 1997; Harmer and Armstrong, 2000). The dating complexity arose from extensive alteration attributable to hydrothermal fluids which caused the open-system behaviour of Rb-Sr and Pb-Pb isotopic systems until 1.6–1.0 Ga (Harmer and Farrow, 1995). This led to a range of isotopic ages (2061 ± 2 to 2052 ± 48 Ma) being proposed by several authors (Walraven *et al*., 1987; Schweitzer *et al*., 1995a; Walraven, 1997; Harmer and Armstrong, 2000; Buick *et al*., 2001; Lenhardt and Eriksson, 2012) for the Rooiberg Group. The age of the Rooiberg Group, which was thought to be precise (Vantongeren *et al*., 2010), was suggested by Walraven (1997) who put forward the Pb-Pb evaporation age of 2061 ± 2 Ma based on two zircon populations obtained from the Kwaggasnek rhyolite.

The Rooiberg lavas consist of basaltic to rhyolitic rocks with fine-grained pyroclastic rocks of tuff, phreatic tuff, lithic and vitric tuff shale, volcanic mudflows and sedimentary intercalations (Twist and French, 1983; Twist, 1985; Schweitzer *et al*., 1995a; Harmer and Armstrong, 2000). The deposition of the sedimentary intercalations by sandy fluvial and lacustrine processes (Lenhardt and Eriksson, 2012) is attributed to the period of dormancy of the Rooiberg Group (Coetzee, 1970; Twist and French, 1983;

Schweitzer *et al*., 1994; Ehlers and du Toit, 2002). Some of these sedimentary intercalations contain structures such as cross-bedding, channel fillings, planar and flow-banding, spherulites, amygdales, vesicles and pillow structures (Twist and French, 1983). Most of the Rooiberg Group rocks are massive, microporphyritic, red-brown to grey, epicrustal acidic volcanics with a glassy groundmass embedded by phenocrysts of mainly feldspars and quartz (Twist and French, 1983; Schweitzer *et al*., 1995a; Buchanan *et al*., 1999).

Most of the Rooiberg Group structures formed because of the intrusion of the Bushveld Complex (Twist and French, 1983). Some of these structures in the northwest section (from Mokopane to Rooiberg) are characterised by a series of folds and faults trending E–W (Twist and French, 1983) (Figure 2.2). In the Rooiberg area, the felsites rest on the limbs of the east-trending anticline dipping at 10–12° N–S, whereas in the Loskop Dam-Middelburg district they dip at 55–70° southwards on the northern limb of the southwest plunging syncline characterising the Middelburg basin (Twist and French, 1983). On the southern limb of this southwest plunging syncline the felsites dip at 15–30° towards the north, and on the east limb they have a similar dip (15–30°) towards the west (Twist and French, 1983).

Clear eruptive centres and deposition of the Rooiberg lava are still a matter of debate (Lenhardt *et al*., 2017). However, the petrogenetic association of these lava with the Bushveld magmatic event (Cawthorn, 2013; Mathez *et al*., 2013) suggests that its eruption was controlled by the prominent Thabazimbi-Murchison Lineament (Zeh *et al*., 2015; Lenhardt *et al*., 2017). The eruption of the early magma (i.e. Dullstroom magma) was continuous and resulted in massive lava with less pyroclastic and sedimentary intercalations, whereas the later volcanism (Damwal to Schrikkloof magma) had pauses dominated by deposition of sediment (Lenhardt and Eriksson, 2012). These hiatuses could have been related to the reactivations of the Thabazimbi-Murchison Lineament (Good and de Wit, 1997).

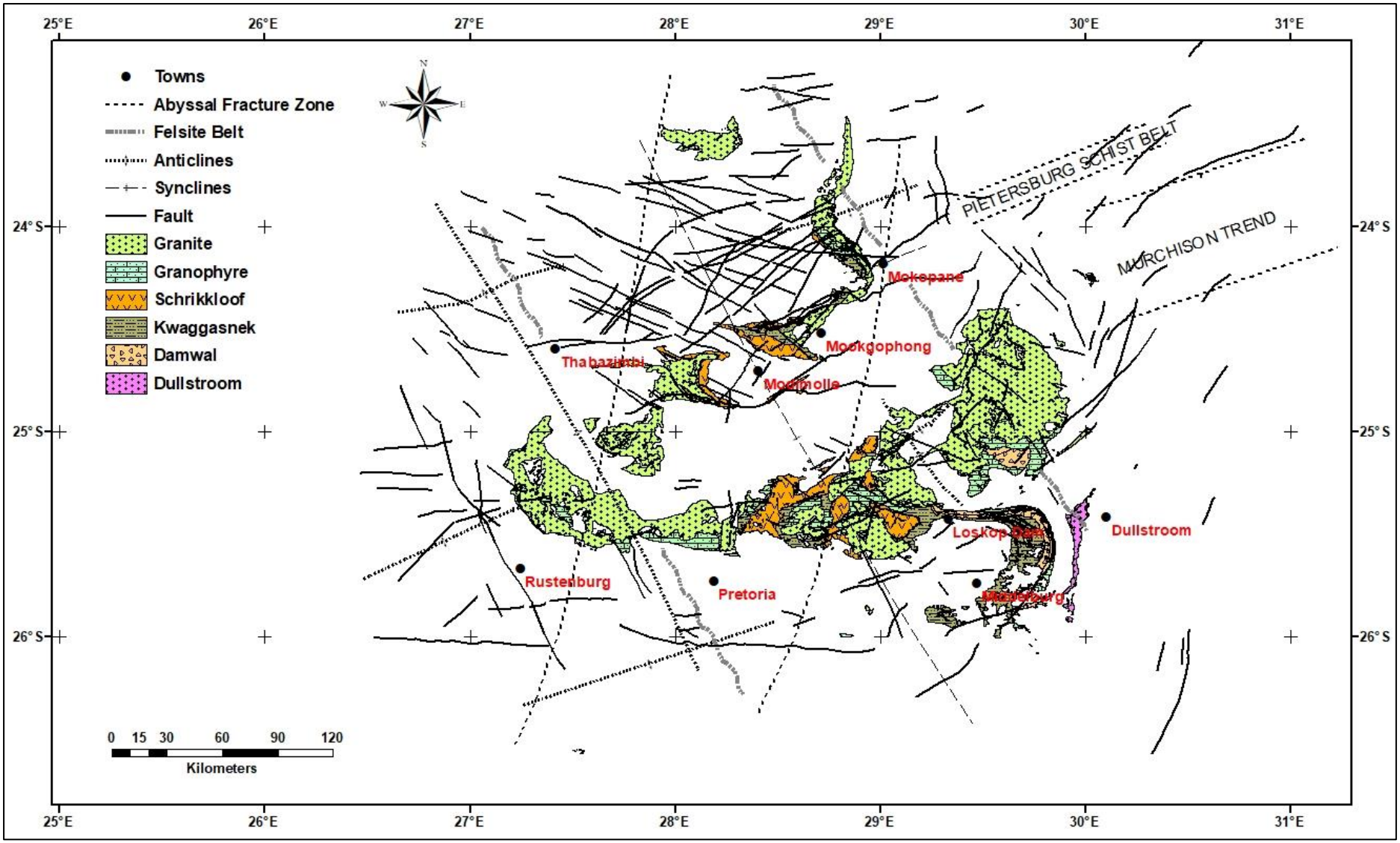

Figure 2.2 The regional major structures in relation to the Rooiberg Group (modified after Hunter, 1973, 1976).

2.2 Local Geology

The local geology is characterised by two young formations of the Rooiberg Group (i.e. Schrikkloof- and Kwaggasnek formations) (Table 2.1). These felsites north of Modimolle have poorly exposed outcrops and are characterised as fractured grey to reddish quartz-feldspar porphyritic felsites intercalated with variable sedimentary aggregates of agglomerates and shales (Coetzee, 1970; Twist and French, 1983; Armitage *et al*., 2007). In the upper portion of the Kwaggasnek Formation, a zone of quartzite xenoliths (1–3 m in thickness) also occurs beneath the agglomerates (Schweitzer *et al*., 1995a). These quartz-feldspar porphyritic felsites have a flow banding texture with corroded quartz and feldspar phenocrysts embedded in the finely mottled light-grey groundmass (Coetzee, 1970). Armitage *et al*. (2007) also observed green pinitoid grains and lithophysae in some felsites. Most of the felsites are extensively altered, contain mainly quartz, feldspar, hydrated iron oxides, magnetite, chloritisation, sericitisation, spherulite and pseudo-spherulite crystals of unknown origin (Coetzee, 1970). Other pale felsites contain a pilotaxitic texture characterised by a glassy groundmass with aligned lath-shaped plagioclase (Coetzee, 1970).

Table 2.1 Lithological description of the Schrikkloof and Kwaggasnek formations in Modimolle (Schweitzer *et al*., 1995a).

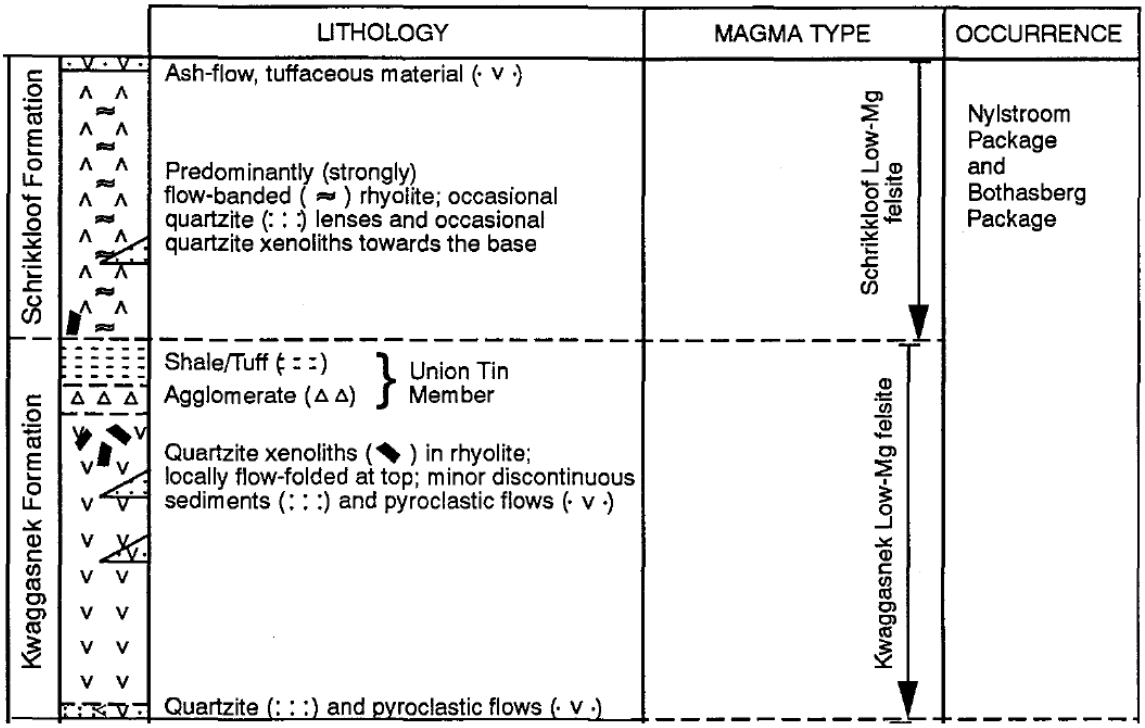

2.2.1 Kwaggasnek Formation

The Kwaggasnek Formation is dominated mainly by porphyritic and non-porphyritic lavas at the base, which are overlain by flaggy flow-banded pinkish-red felsites (Twist, 1985). These low-Mg felsites in the lower portion are considered crystallised and partially mobilised (Rhodes and du Plessis, 1976). Rhodes and du Plessis (1976) attributed this extensive crystallisation and remobilisation to the intrusion by granite and gabbro. Ascending towards the middle part of the formation, some minor sedimentary intercalations become more apparent (Schweitzer *et al*., 1995a). At the top, Kwaggasnek

rocks are mainly flow banded with intercalations of quartzite xenoliths, agglomerates and the shale (tuff) layer of the Union Tin Member (Rhodes and du Plessis, 1976; Schweitzer *et al*., 1994; Schweitzer *et al*., 1995a). The shaly tuff horizon overlies the agglomerates, forming an interface dividing the Kwaggasnek and Schrikkloof formations (De Bruiyn, 1980; Schweitzer *et al*., 1994).

2.2.2 Schrikkloof Formation

This formation in the Modimolle area is characterised by low-Mg pinkish-red felsites, which are flow-banded, sparsely porphyritic to non-porphyritic and invariably sericitised (Twist, 1985; Schweitzer *et al*., 1995a). The base of this formation is marked by felsites with a quartzite xenolith zone, and is overlain by volcanic breccia and ash tuffs (Rhodes and du Plessis, 1976; Schweitzer *et al*., 1995a). Towards the middle of the formation the rocks are mainly flow banded with an intercalation of quartzites lenses and volcanic breccia, whereas at the top, flow folded felsites, ash-flows and tuffaceous aggregates become more apparent (Rhodes and du Plessis, 1976; Schweitzer *et al*., 1995a).

2.2.3 Local Structural Geology

The major structures of the study area are characterised by the major regional ENE–WSW trending Welgevonden Fault and the WNW–ESE trending Swaershoek anticline (Figure 2.3). The western branch of the Welgevonden Fault cuts across the Swaershoek anticline towards the middle of the area. Other minor structures towards the northwest part of the area also traverse across the Swaershoek anticline. Some these minor structures in the local Rooiberg rocks are characterised by numerous small veins, which Armitage *et al*. (2007) described as steep to subvertical quartz veins.

The Welgevonden Fault is described by Temperley (1975) as a heavily silicified fault which is a member of a 270 km fault system, characterised by tear, reverse and overthrust faults that extends from Thabazimbi to Zebediela. It dips towards the north at various angles between 45°–90° (Temperley, 1975). In some locations, the Welgevonden Fault crops out as quartz veins and there are some mineralised springs in some locations of the fault (Temperley, 1975). It has been regarded as an extension of Zebediela Fault (Armitage *et al*., 2007), even though they are unconnected (Temperley, 1975). The fault system to which it belongs (i.e. Thabazimbi-Murchison Lineament fault system) (Du Plessis and Walraven, 1990), is described by Basson (2019) as characterised by a left-lateral, transpressional shear. Other faults which belong to this fault system include the Ysterberg-Planknek Fault and Zebediela Fault, and together with the Welgevonden Fault are regarded as the southern margin of the northern Limb of the Bushveld Complex (Oberthur *et al*., 2018).

The Swaershoek anticline which is considered cogenetic with the Nylstroom syncline and Zwartkloof anticline (Armitage *et al*., 2007), extends from Bakoendkrans in the northwest, cutting across the study area and the Lebowa granite towards the south of Mookgophong (Figure 2.3). According to Armitage *et al*. (2007), this anticline is characterised by a westward gentle plunge with slightly bowed axial traces.

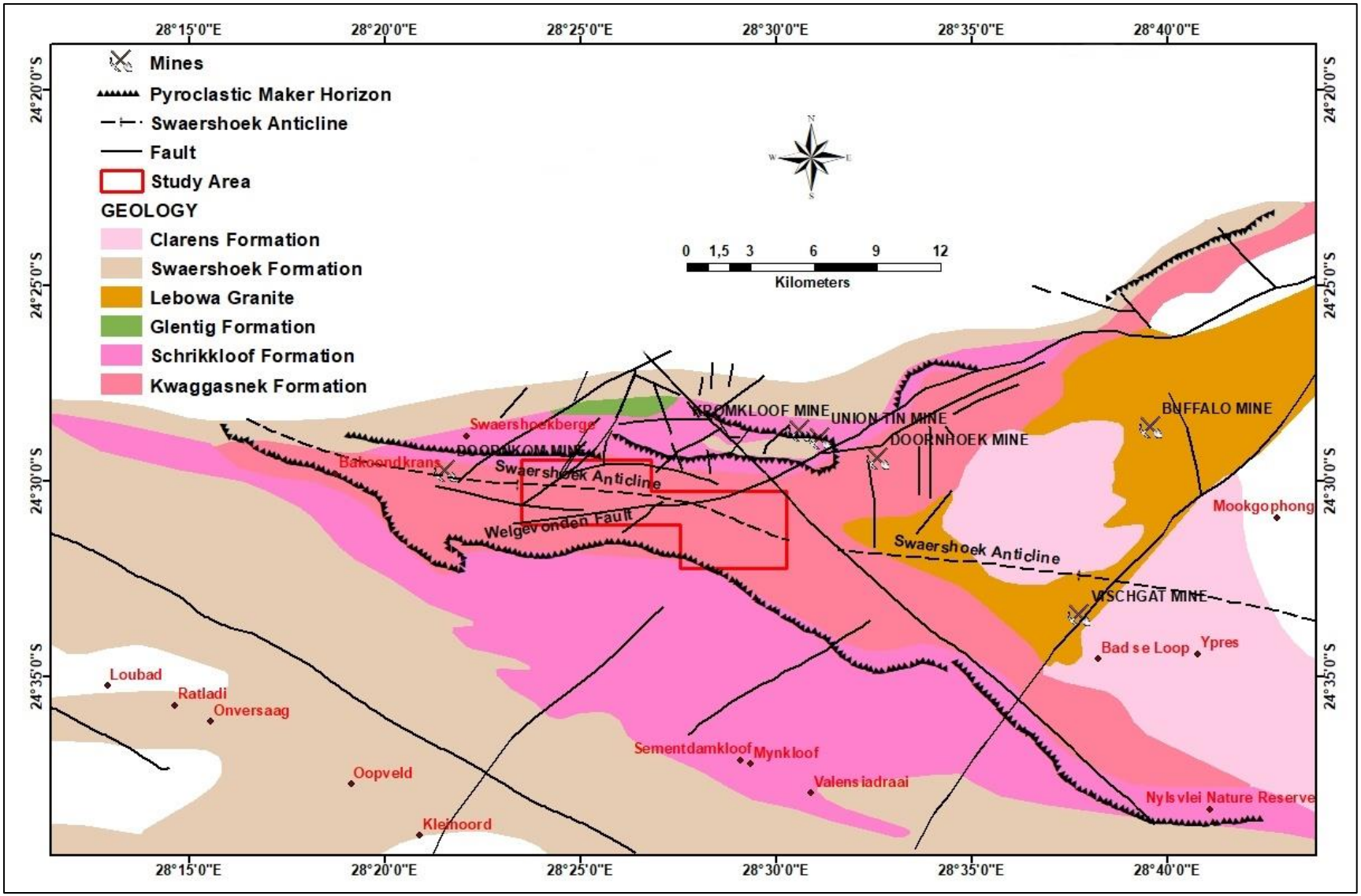

Figure 2.3 Local structures in relation to the study area (modified after Crocker, 1979).

2.2.4 Local Mineralisation

Several proposals have been put forward regarding the mineralisation of the Rooiberg Group (Robb *et al.*, 1994; Schweitzer *et al.*, 1994; Harmer and Farrow, 1995). According to Robb *et al*. (1994) this endogranitic and exogranitic polymetallic mineralisation of the Rooiberg Group is associated with the intrusion of Bushveld granites. This was corroborated by Harmer and Farrow (1995), who attributed the formation of this mineralisation to evolving hydrothermal fluids from the Lebowa Granite Suite. Four regional events pertaining to the Rooiberg Group mineralisation were put forward by Schweitzer *et al*. (1994), one of which (i.e. third phase of mineralisation associated with base metals in Table 2.2) is associated with the enrichment of Pb and Zn in the Kwaggasnek Formation.

Table 2.2 Mineral commodities of Kwaggasnek and Schrikkloof formations (modified after Schweitzer *et al*., 1994). (2) Second phase of mineralisation, (3) Third phase of mineralisation, (4) Fourth phase of mineralisation.

	LITHOLOGY	MAGMA TYPE	MINES	COMMODITY
Schrikkloof Formation	Ash-flow, tuffaceous material (· v ·) Predominantly (strongly) flow-banded (≈); occasional quartzite (: : :) lenses and occasional quartzite xenoliths towards the base	Schrikkloof Low-Mg felsite	Salomons Temple Welgevonden Century Hoekberg Zwartkloof Vergenoeg	Sn Sn Sn Sn F F } (4)
Kwaggasnek Formation	"Union Tin Tuff" and derivatives (= = =) Agglomerate (Δ Δ) Quartzite xenoliths ( ) in felsite-locally flow-folded at top; minor discontinuous sediments (: : :) and pyroclastic flows (· v ·) Quartzite (: : :) and pyroclastic flows (· v ·)	Kwaggasnek Low-Mg felsite	Union Tin Welgelegen Waterberg Tins Localised Diggings	Sn Sn Sn } (4) Arsenopyrite (2) and Base Metals (3)

This third phase of mineralisation formed due to the contact metamorphism during the final stages of the formation of the Rustenburg Layered Suite (RLS), and it affected the Dullstroom and Kwaggasnek formations (Schweitzer *et al*., 1994). The circulation of base metal-rich fluids facilitated the formation of mineralisation when it moved to and from the heat source, enriching the upper portion of the Dullstroom and lower portion of the Kwaggasnek volcanics with Pb and Zn (Schweitzer *et al*., 1994). The origin of the anomalous Zn concentrations is associated with the RLS whereas the anomalous Pb concentrations are considered to be derived from the volcanics of the Rooiberg Group (Schweitzer *et al*., 1994).

CHAPTER 3

Methodology

3.1 Soil Sampling

The soil samples were collected from the topsoil at a depth of 10–60 cm and the ideal sample weight was approximately 5 kg (Figure 3.1). The sampling grid used was 200 m x 200 m. In some parts of the area, the topsoil sampled was mainly fine-grained containing mostly sand (particle size >63 µm), silt (particle size >2 µm) and clay (particle size <2 µm) with a brown to reddish colour. In other parts, especially close to outcrops, the top soil was coarse-grained with a light brown colour. Since the area is characterised by a savanna environment, the top soil is mainly covered by grass.

Figure 3.1 The top soil sampling medium and sampling depth of 10–60 cm.

3.2 Sample Preparation

The sample preparation procedure included removal of coarse organic matter (twigs, grass, etc.) in the sample material, dry sieving of samples and pulverisation of the samples to powder form for 2–3 minutes using the planetary ball mill. A powder briquette was pressed from the -75 µm fraction using a PVA binder. The remainder of the sieved samples was retained for future use. The use of this fine sample material for analysis is predicated on the orientation studies which suggested that most of the elements analysed for are concentrated in the fine fraction (-75 µm), i.e. above the detection limit for the analytical technique used (Beeson *et al.*, 1978; Labuschagne *et al.*, 1993).

3.3 QA/QC for Sample Preparation

In a batch of samples, the first sample and every twentieth sample were sieved using a small hand-held sieve. Before sieving, the sample was weighed using the calibrated scale and then it was sieved in small portions to avoid blocking of the sieve pores. When a larger number of the sample fraction was greater than 75 microns the milling was repeated until 95 % of sample material was less than 75 microns. Two samples were taken randomly for particle size analysis from batches after milling and sieving. A technique which uses the laser diffraction method was used to determine the particle size distribution of samples. This was conducted to indicate whether the sieve used was in sufficiently good condition or whether it needed to be replaced.

3.4 Geochemical Extraction

The glass disks and wax pellets were analysed by a PANalyticalAxios X-ray fluorescence spectrometer equipped with a 4 kW Rh tube for the following major oxides and trace elements: SiO_2, TiO_2, Al_2O_3, Fe_2O_3, MnO, MgO, CaO, Na_2O, K_2O, P_2O_5, As, Ba, Ce, Co, Cr, Cu, Ga, Hf, Mo, Nb, Nd, Ni, Pb, Rb, S, Sb, Sc, Sn, Sr, Ta, Th, U, V, W, Y, Zn and Zr. The steps to calibrate the instrument accuracy and precision and the reference materials used are described by Elsenbroek (1995, 1996). The detection limits of the major oxides and trace elements are displayed in Appendix 2. A drift correction was made after every tenth unknown sample by means of an internal glass-disc monitor. The resulting stability of analyses was checked on a daily basis per batch of samples analysed, using in-house powder briquette monitors of various concentrations. The precision and concentrations for these monitors are displayed in Appendix 2. These monitors generally have a precision better than 5 %, except in the case of MnO, Sn, Sb, W and U with precisions of 10 %, 29 %, 72 %, 33 % and 14 %, respectively (Appendix 2).

3.5 Geochemical Data Evaluation

The geochemical data was processed by replacing zeros, negative values and values below the detection limits with a quarter of the second minimum value. The data was evaluated using various software packages (e.g. ArcGIS, IoGas and SPSS) to obtain information in accordance with the objectives of the study.

3.6 Data Interpretation

3.6.1 Comparison of Regional and Local Zn and Pb Concentrations

The Pb and Zn concentrations of regional and follow-up surveys were compared in terms of reproducibility and refinement of concentrations. The concentrations were also compared in terms of the range, average concentrations, number of background and anomalous concentrations and whether elevated follow-up Pb and Zn concentrations indicated potential mineralisation. Indication of anomalous concentrations was determined on the basis Pb and Zn concentrations being greater than the soil threshold concentrations (Pb = 100 ppm and Zn = 300 ppm) which indicate potential mineralisation (Reedman, 1979).

3.6.2 Univariate Statistics

Soil geochemistry was analysed from the statistical summary. This analysis was conducted to determine the variation of geochemical signatures of major oxides and trace element with regard to their mean, range, minimum and maximum concentrations. The variance and skewness of Pb and Zn were also analysed to determine whether they have statistical traits of potential mineralisation. These statistical mineralisation traits include high maximum concentrations, high mean, high variance and positive skewness (Govett, 1983).

3.6.3 Multivariate Statistics

The inter-element relationships in this context were determined by correlation matrix and principal component analysis (PCA). This inter-element relationship will aid in characterising the local potential mineralisation associated with Pb and Zn anomalies. The correlation matrix in this instance measures mainly the strength and linearity of relationship between elements, whereas the principal component analysis complements with additional simultaneous spatial variation context of inter-element relationship.

3.6.3.1 Geochemical Correlation

The strength and linearity of the geochemical association between trace elements and major oxides were quantified with the aid of correlation coefficients, using the Pearson method. The correlation matrix was generated from log-transformed data. In terms of correlation interpretation, there are no absolute rules for generating critical intervals of correlation coefficients (Akoglu, 2018; Cooksey, 2020). But there have been some heuristic intervals proposed by researchers for the interpretation of correlation coefficients (Cohen, 1988; Chan, 2003; Munro, 2005; Brace *et al*., 2006; Dancey & Reidy, 2007; Ratner, 2009; Rezaei *et al*., 2018; Cooksey, 2020). The most widely used correlation intervals were proposed by Cohen (1988), and they include ± 0.1 (weak), ± 0.3 (moderate) and ± 0.5 (strong). In this study, the emphasis is aimed mainly on the strong correlation coefficients ($r \geq 0.5$). The correlation coefficients less than 0.5 (i.e. weak and moderate coefficients) are regarded as poor and those in $0.5 \leq r \leq 1$ are arbitrarily subdivided as follows for distinction:

- 0–0.5: poor,
- 0.5–0.6: fair,
- 0.6–0.7: good,
- 0.7–0.8: very good,
- 0.8–1: excellent

The confidence levels that were used were 95 and 99 percent (Appendix 3). The correlation at 95 % was considered geologically significant, whereas at 99 %, the relationship was considered strongly significant and associated with anomalies. The 99 % confidence level is indicated by two asterisks (**) whereas 95 % is marked by one asterisk (*). It should be noted that the correlations incorporate all samples and, as a result, the correlation signals are slightly diluted. The coefficients range between -1 and +1. The + and - signs merely serve to indicate the directions in which the proportions change: (+) indicates that both elements increase and decrease by a certain quantified proportion and (-) indicates that if one element increases, the other decreases by the same proportion (Appendix 3).

3.6.3.2 Principal Component Analysis

The principal component analysis (PCA) was used to classify the elements to reflect their geological and mineralisation settings. The PCA was carried out using log-transformed data, based on the rotation method of Varimax with Kaiser Normalisation. The low eigenvalues of variables with minimum influence or variability in each component were suppressed in order to project only those high eigenvalues of variables with high variability in a component. The principal component characterising the target potential mineralisation was mapped to illustrate its target areas and spatial variation. The map was produced by means of the inverse distance weighted (IDW) interpolation method in ArcGIS.

3.6.4 Background and Anomalous Concentration

The selection of threshold percentile, which separates anomalous from background concentrations was conducted using mean + 'α' x standard deviation (α = integers). The disadvantage of using mean + α x std deviation method is that it requires the geochemical data to be normally distributed which is not the case in most situations. In some situations, the use of mean + 'α' multiples of the standard deviation also tends to misclassify concentrations whereby some of the background concentrations are classified as anomalous and some anomalous concentrations are classified as background. In order to minimise these disadvantages, the geochemical data was log-transformed before classification of concentrations (Appendix 1). The thresholds which separate the anomalies from background concentrations, were also kept at the 90th percentile to reduce misclassification of concentrations. These thresholds were also scrutinised against regional rock average concentrations, local average concentrations, as well as the generalised soil threshold concentration which indicate mineralisation from Reedman (1979). Regional rock average concentrations were derived from regional geochemical data (Appendix 8) from Mathez *et al*. (2013).

3.6.5 Spatial Distributions of Paragenetic Elements

The mapping of spatial distribution was conducted to indicate elemental spatial associations and zones of special interest with respect to potential mineralisation. The spatial distribution maps of elements characterising potential mineralisation from the multivariate analysis were created in ArcGIS based on the formula mean + 'α' standard deviation (α = integers).
The RGB (red, green and blue) classification maps of elements characterising potential mineralisation were created using ioGAS software. These classification maps were created to illustrate the locations where anomalies of three elements occur concurrently. Individual and combinations of elements are represented by their respective individual and combinations of RGB colours as illustrated in Figure 3.2. Only concentrations which are greater than the local threshold concentrations are assigned an RGB colour (Figure 3.2). The black colour represents background concentrations. The grey colour defines the target locations with concurrent anomalies which might indicate the likelihood of mineralisation.

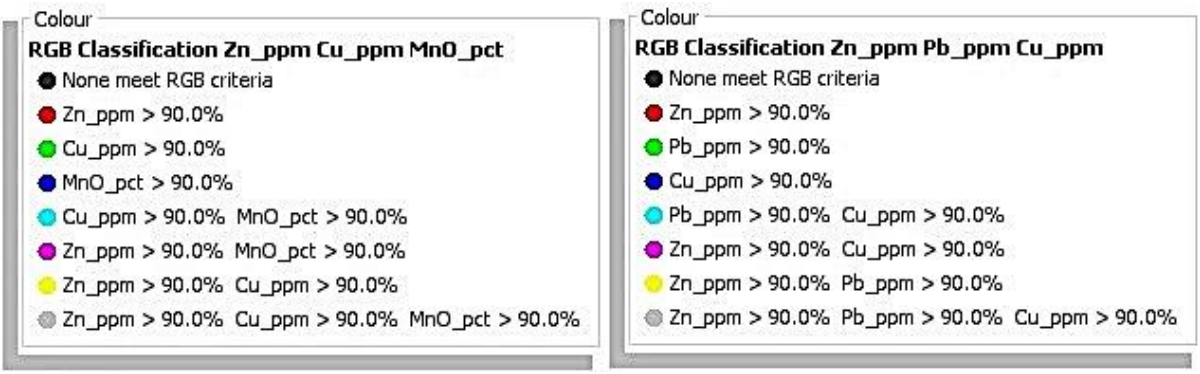

Figure 3.2 The RGB colour codes of the concentration percentages.

3.6.6 Potential Style of Mineralisation

The potential style of mineralisation associated with the local Pb and Zn anomalies was determined with the aid of an average zinc ratio (ZR) [i.e. ZR = 100Zn/(Zn + Pb)]. This ratio is useful in providing information on the style of mineralisation at an early stage of exploration (Hudson and Large, 1987). It is controlled mainly by relative concentrations of Pb and Zn, mechanism of metal solution from the source rocks, saturation and non-saturation of base metal, chemistry of metal-bearing solutions and efficiency of metal deposition (Hudson and Large, 1987). The importance of the mean zinc ratio in classifying mineralisation styles was demonstrated by Huston and Large (1987) when they used it to classify the vein-style granite-related mineralisation in the Mount Read volcanics of Tasmania (Stolz *et al*., 1994). They developed a set of zinc ratio parameters (i.e. mean zinc ratio ranges, standard deviation ranges and histogram distribution patterns) in order to differentiate various deposits.

This method is useful for C-horizon soil and drill hole sampling in poorly understood targets (Huston and Large, 1987). It must also be applied with a reasonable population of samples in order to be effective. A minimum 15 samples are required for the method to be effective (Huston and Large, 1987). Explanation of zinc ratio relies on the pattern of the zinc ratio histogram, the standard deviation and the mean zinc ratio value (Hudson and Large, 1987). These histogram parameters must be used together in order to characterise the potential style of mineralisation (Hudson and Large, 1987).

The calculation of the local mean zinc ratio was carried out using only anomalous concentrations of Zn and Pb. Since Pb and Zn have different local threshold concentrations, the lower local threshold was selected to accommodate both elements. About 19 samples were used to calculate the mean zinc ratio. The mean zinc ratio of the area was compared with the standardised ZR parameters (Table 3.1) of mineralisation styles from Huston and Large (1987).

Table 3.1 The standardised ZR parameters of mineralisation styles (Huston and Large, 1987).

Zn-Pb-Cu-Ag-Au Volcanogenic Massive Sulphide Deposits			**Zn-Pb-Ag (Veins, Fissure lodes, Polymetallic Sulphide and Irish style) Deposits**		
Mean	Standard Deviation	Histogram Distribution	Mean	Standard Deviation	Histogram Distribution
66–77	<15	Normal	39–75	>23	Skewed

3.6.7 Potential Ore Group Classification

The ore group classification was conducted to determine the potential ore group that characterises the potential mineralisation of the area. The classification is based on the characteristic ranges of average magnitude of three ratios (i.e. copper ratio [CR = 100Cu/(Cu + Zn)], zinc ratio [ZR = 100Zn/(Zn + Pb)] and lead ratio [PR = 100Pb/(Pb + Cu)]) in ore groups. According to Antony (1999) these three ratios are useful indicators in mineral exploration and can be used to classify varieties of base metal sulphide deposits.

The mean local CR and PR were calculated from 25 samples with anomalous concentrations of Zn, Pb and Cu. The CR, ZR and PR of the area were compared with the standardised ore groups (Table 3.2) defined by Antony (1997) in order to determine which ore group characterises the potential mineralisation of the area.

Table 3.2 Standardised ore groups defined by Antony (1997).

Ratios	**Cu-rich ore groups**				
CR = 100Cu/(Cu + Zn)	>90		50–90		
	Cu		Cu-Zn/Cu-Zn-Pb		
ZR = 100Zn/(Zn + Pb)	0–100	>80	50–80	20–50	<20
	Cu	Cu-Zn	Cu-Zn-Pb	Cu-Pb-Zn	Cu-Pb
PR = 100Pb(Pb + Cu)	<10		10–50		
	Cu		Cu-Pb/Cu-Pb-Zn		
Ratios	**Zn-rich ore groups**				
CR = 100Cu/(Cu + Zn)	<50				
	Zn-Cu/Zn-Cu-Pb/Zn-Pb-Cu/Zn-Pb				
ZR = 100Zn/(Zn + Pb)	>90		50–90		
	Zn-Cu		Zn-Cu-Pb/Zn-Pb-Cu/Zn-Pb		
PR = 100Pb(Pb + Cu)	-				
Ratios	**Pb-rich ore groups**				
CR = 100Cu/(Cu + Zn)	-				
ZR = 100Zn/(Zn + Pb)	10–50		<10		
	Pb-Zn-Cu/Pb-Cu-Zn/Pb-Zn		Pb-Cu		
PR = 100Pb(Pb + Cu)	>50				
	Pb-Cu, Pb-Zn-Cu/Pb-Cu-Zn/Pb-Zn				

3.6.8 The Fuzzy Logic Modelling

Fuzzy logic modelling is a knowledge driven exploration method which is mainly used in greenfield exploration. The method is based on the conversion of spatial evidential components (i.e. energy driving the fluids, ligands, source of metals, transport of fluids, trap and outflow of fluids) of conceptual mineral system (Figure 3.3) into fuzzy sets. This is carried out by the following three processes:

- Fuzzification of spatial evidential data, which involves creating a predictive model by assigning weights to geological features of a mineral system to produce fuzzy predictor maps (also known as fuzzy membership value maps);
- Secondly, fuzzy predictor maps are logical integrated using fuzzy set operators to produce fuzzified mineral potential maps (Figure 3.4);

- Finally, the output fuzzy mineral potential maps are defuzzified for better analysis in determining the probability of occurrence of mineralisation.

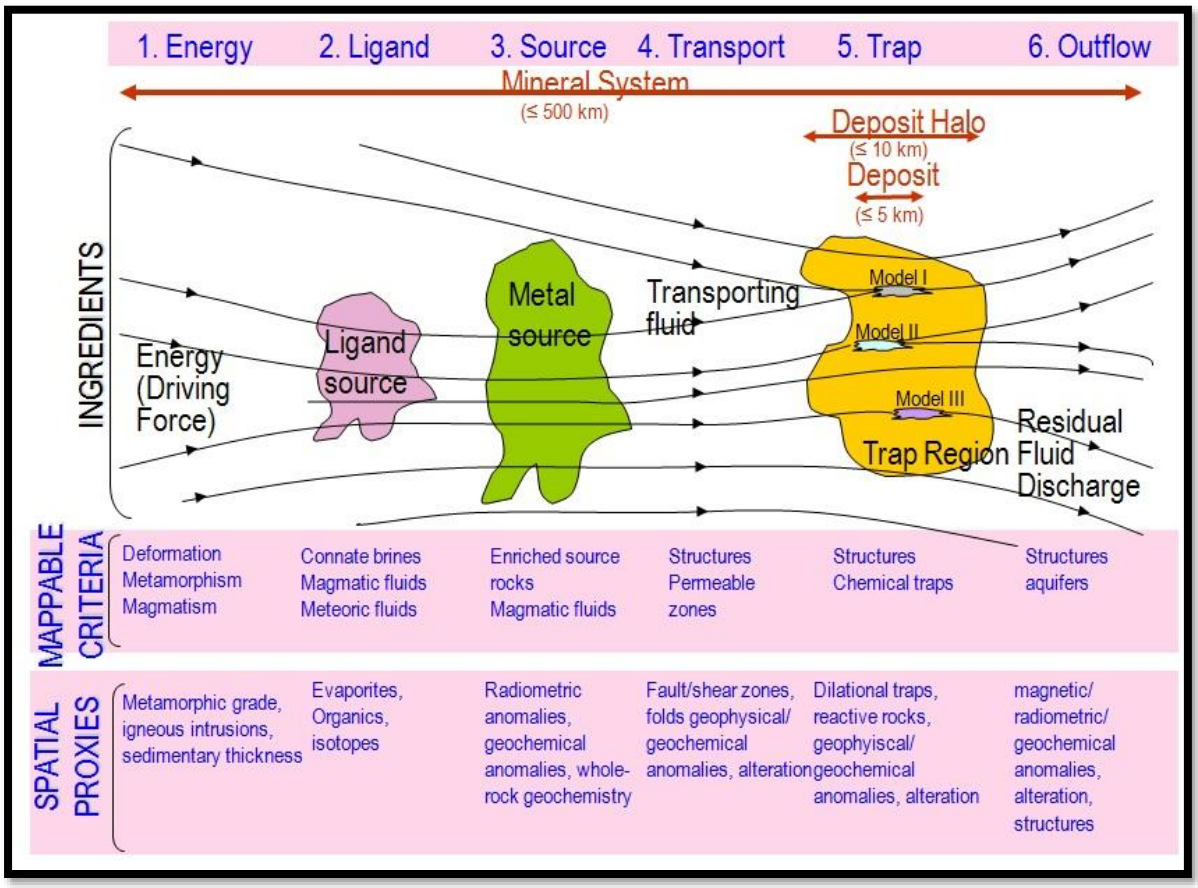

Figure 3.3 The mineral system model illustrating the connections of geological processes required to form mineralisation (modified after Knox-Robinson and Wyborn, 1997).

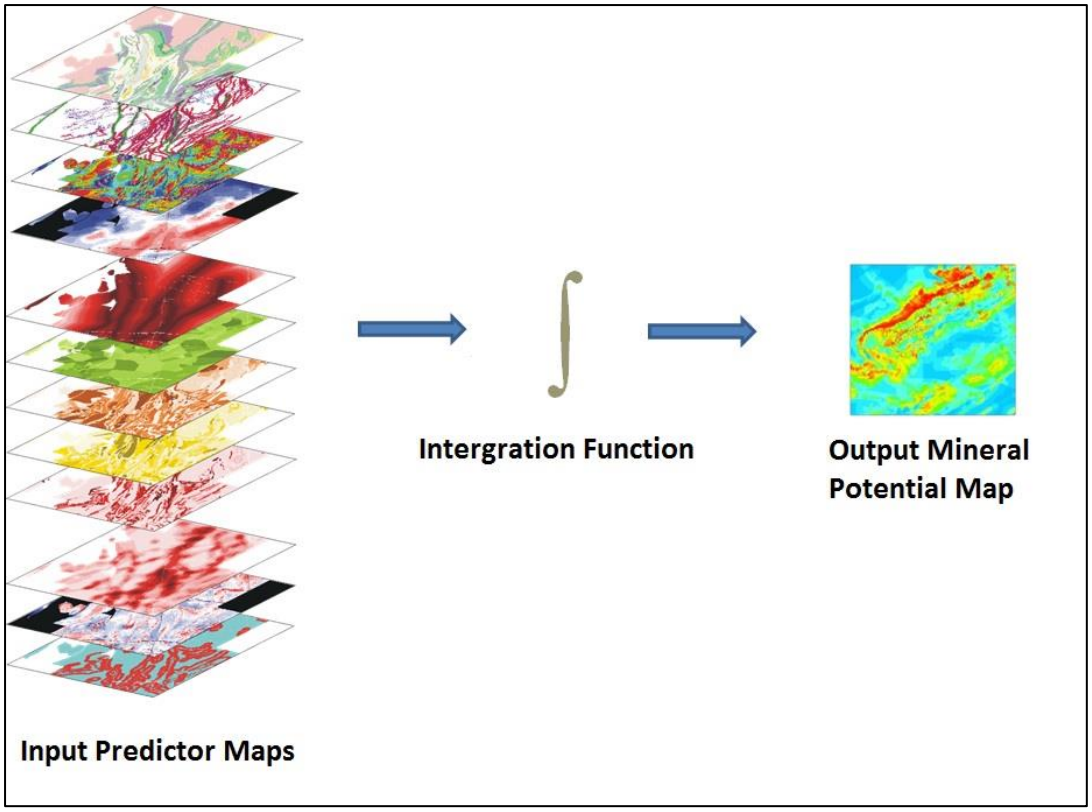

Figure 3.4 The model structure for the combination of predictor maps to produce prospectivity maps (modified after Porwal and Chudasama, 2016).

The theory of the fuzzy logic model states that if X represents multiclass data whose classes are characterised by x, then a fuzzy set *A* in X is described by the following equation:

$$A = (x, \mu_A(x)) \mid x \in X$$

In the equation above, $\mu_A(x)$ is a membership function of x in A which maps X to a membership space (Zimmermann, 1985; Carranza, 2009). This fuzzy membership works by classifying the input data between two sets, 0 and 1 to generate fuzzy membership values maps (predictor maps). The assignment of weights to the data can be done in three ways. The first approach is subjective where the weights and membership values are assigned manually, the second approach entails building conditional queries to assign membership values and the third approach uses software tools to assign weights and membership values.

The integration of these fuzzy membership value maps is then conducted by a set of fuzzy set operators which include fuzzy AND, fuzzy OR, the fuzzy algebraic product, the fuzzy algebraic sum and fuzzy gamma (Table 3.3).

Table 3.3 The fuzzy operators (after Bonham-Carter, 1994).

Fuzzy AND	This could also be called as Min-operator as it creates an output, which is controlled by the smallest fuzzy membership values at each location. It results in a conservative estimate of set membership, with a tendency to produce small values and minimum areas. This operator is used to find the areas where all the evidence used needs to be present for the hypothesis to be true.
Fuzzy OR	This could be called the Max-operator as it creates an output whose membership values are controlled by the maximum values of any of the input maps. By using this operator, any positive evidence may be sufficient to suggest favourability.
Fuzzy Algebraic Product	The combined fuzzy membership values tend to be very small owing to the effect of multiplying several numbers less than 1. The output is always smaller than, or equal to, the smallest contributing membership value.
Fuzzy Algebraic Sum	The result is always larger (or equal to) the largest contributing membership value.
Fuzzy Gamma	This is defined in terms of the fuzzy algebraic product and the fuzzy algebraic sum, being a combination of these two operations.

In this work, the assignment of weights and membership values was carried out using ArcGIS software to produce fuzzy predictor maps (Appendix 4, 5 and 6) with membership values ranging between 0 and 1. This method of assigning weights using a software is used here because it is mostly applied when the mineralisation of the area is not well understood (Porwal and Chudasama, 2016).

The spatial evidential components (i.e. geochemical and structural data) outlined in Table 3.4 were used to create fuzzy predictor maps. The predictor maps include the proximity to faults because most of the deposits tend to form in close proximity to fault systems and the faults also act as pathways for fluids, high fault density functioning as a trap and anomalous geochemical concentrations. In order to extract locations with high proximity to structures, high structural density and geochemical anomalies, the evidential data was classified [by mean + 'α' standard deviation (α = integers)] subsequent to euclidean distance, kernel density and interpolation calculations before the assignment of weights. The elements selected for geochemical predictor maps include those generated from the elemental association characterising the potential mineralisation of the area.

Table 3.4 The selection of predictor maps to be used in the mineral system of the study area.

Essential Evidential Data	**GIS Processing**	**Predictor Maps**
Faults (distance to faults)	Euclidean distance calculations and assignment of weights	Proximity to Pathways
Faults (high fault density)	Kernel density calculations and assignment of weights	Proximity to Physical traps
Geochemical concentrations of elements	Interpolation of geochemical concentrations and assignment of weights	Geochemical anomalies

The multistep used to generate the defuzzified mineral potential maps (or prospectivity maps) are outlined in Figure 3.5. The predictor maps were combine using the fuzzy gamma overlay operator to produce the fuzzified mineral potential maps (Appendix 7) with membership values ranging between 0 and 1, depicting the areas of low favourabilty (0) to high favourability (1) in terms of mineralisation.

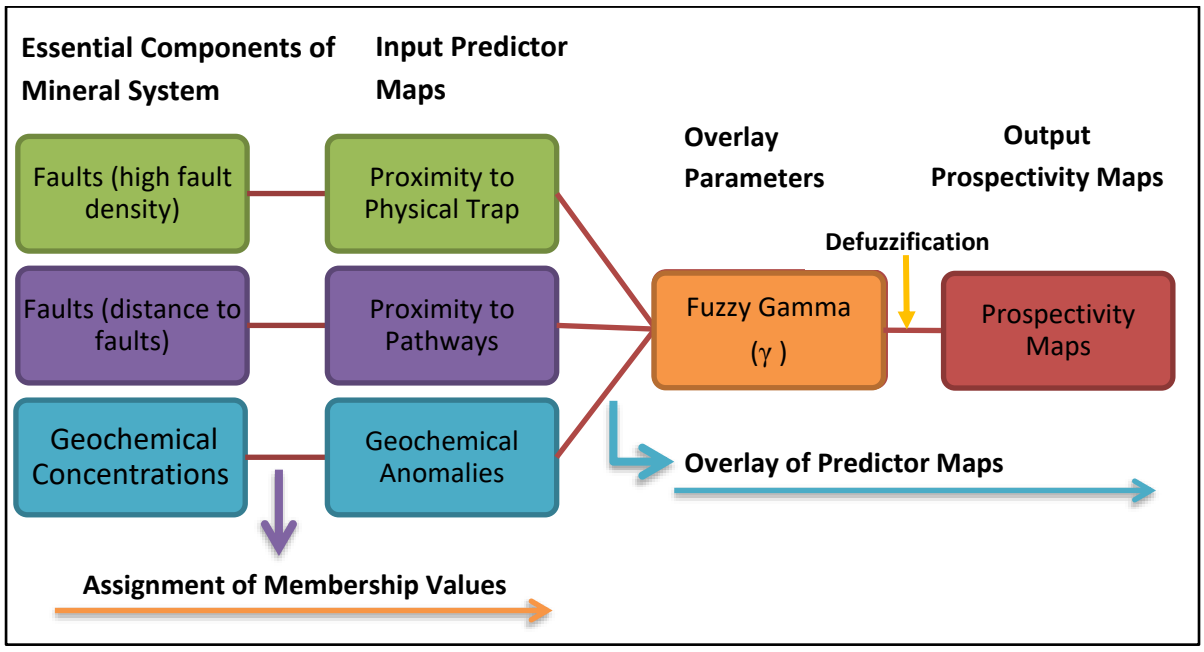

Figure 3.5 The multistep process of the fuzzy gamma network used to integrate the fuzzy predictor map.

This fuzzy Gamma operator is a combination of fuzzy Algebraic Sum and the fuzzy Algebraic Product as outlined in equation (1) (Zimmermann and Zysno, 1980).

$$\mu_{A\,i,comp}(x) = \left(\prod_{i=1}^{m} \mu_i\,(x)\right)^{(1-\gamma)} \left(1 - \prod_{i=1}^{m}(1-\mu_i\,(x))\right)^{\gamma} \quad (1)$$

where x ∈ X, $0 \leq \gamma \leq 1$

At γ = 0, the Gamma operator is equal to the fuzzy Algebraic Product whereas, at γ = 1, the Gamma operator is equal to the fuzzy Algebraic Sum.

The calculation of the fuzzy membership values is based on the following equation;

$$\mu_A\,(x_{ij}) = \begin{cases} 0 & for\ S_{ij} = S_{min} \\ \dfrac{S_{ij} - S_{min}}{S_{max} - S_{min}} & for\ S_{max} > S_{ij} > S_{min} \\ 1 & for\ S_{ij} = S_{max} \end{cases} \quad (2)$$

The score which is characterised by (S_{ij}) measures the weight of the i^{th} class of map *j*. This is calculated by the following equation;

$$S_{ij} = \frac{W_i x W_j}{\sum_{j=1}^{n} W_j} \quad (3)$$

where W_i is the weight of the i^{th} class and W_j is the weight of the j^{th} map (Zimmermann and Zysno, 1980).

The values of γ used to combine the input predictor maps and also assess the quality of the prospectivity maps were 0, 0.25, 0.5, 0.75 and 1. These values were varied in order to determine the range which produces best representativeness of anomalies. Subsequent to an overlay process, the final fuzzy mineral potential maps were defuzzified by classification [using mean + 'α' x standard deviation (α = integers)] in order to recognise areas which are prospective and non-prospective. Defuzzification classes included low background, high background, threshold, anomalies and significant anomalies.

The author processed the data from a selection of mineral system components (i.e. high fault density, distance to faults and geochemical anomalies), creation of predictor maps (i.e. proximity to physical trap, proximity to fluid pathways and geochemical anomalies), overlaying the predictor maps, defuzzification and the production of the last output prospectivity maps.

CHAPTER 4

Results

4.1 Empirical Exploration Approach

4.1.1 Comparison of regional and local Zn and Pb concentrations

About 98.4 % of the regional Zn concentrations lie within the lowest range of 1–150 ppm (Figure 4.1A). The overall percentage of concentrations in the background range (0–330 ppm) is 99.7 % whereas the 0.3 % of high concentrations is in the >300 ppm range (Table 4.1). With regard to relative significant anomalies, the highest regional Zn concentration lies within the range of 1050–1200 ppm. The average regional concentration is also low at 50 ppm Zn.

Regional Pb has most of the concentrations (99.62 %) lying within the lowest range, which is also a background range of 0–100 ppm, whereas in the high concentration range (>100 ppm), the percentage is low at 0.38 % (Figure 4.1B). In terms of anomalies, the highest concentration is in the range of 420–479 ppm (Figure 4.1B). The regional average of Pb is also slightly low at 10 ppm.

With regard to the local Zn concentrations, most (i.e. 62.38 %) of the concentrations lie between high background of 150–300 ppm (Figure 4.1C). This range is followed by a high concentration range of 300–450 ppm with 32.8 % of Zn concentrations. The background range (>300 ppm) has 65.2 % of concentrations, whereas the high concentration range (>300 ppm) has 34.8 % (Table 4.1). The highest concentration lies in the range of 4500–4650 ppm, which is significantly high. The average of 284 ppm Zn is also relatively higher than the average (50 ppm) of the regional survey.

In terms of local Pb concentrations, the range of 100–200 ppm has the highest number (60.11 %) of concentrations (Figure 4.1D). This is followed by 200–300 ppm range with the 20.75 % samples. The overall percentage of concentrations in the background range (<100 ppm) is 11.5 % whereas the high concentration range (>100 ppm) has 88.5 % (Table 4.1). The local highest concentration of Pb lies within the range of 1000–1100 ppm. The average concentration is also significantly higher at 179 ppm Pb than the regional average of 10 ppm.

Table 4.1 Comparison of regional and follow-up Zn and Pb in terms of the number of samples with background and anomalous concentrations related to soil thresholds for mineralisation.

		Regional Survey		**Follow-up Survey**	
	Soil Threshold for Possibility of Mineralisation	**Number of Concentrations in Background (i.e. Zn < 300 ppm and Pb < 100 ppm)**	**Number of Anomalous Concentrations (i.e. Zn > 300 ppm and Pb > 100 ppm)**	**Number of Concentrations in Background (i.e. Zn < 300 ppm and Pb < 100 ppm)**	**Number of Anomalous Concentrations (i.e. Zn > 300 ppm and Pb > 100 ppm)**
Zn	300 ppm	99.7 %	0.3 %	65.2 %	34.8 %
Pb	100 ppm	99.6 %	0.4 %	11.5 %	88.5 %

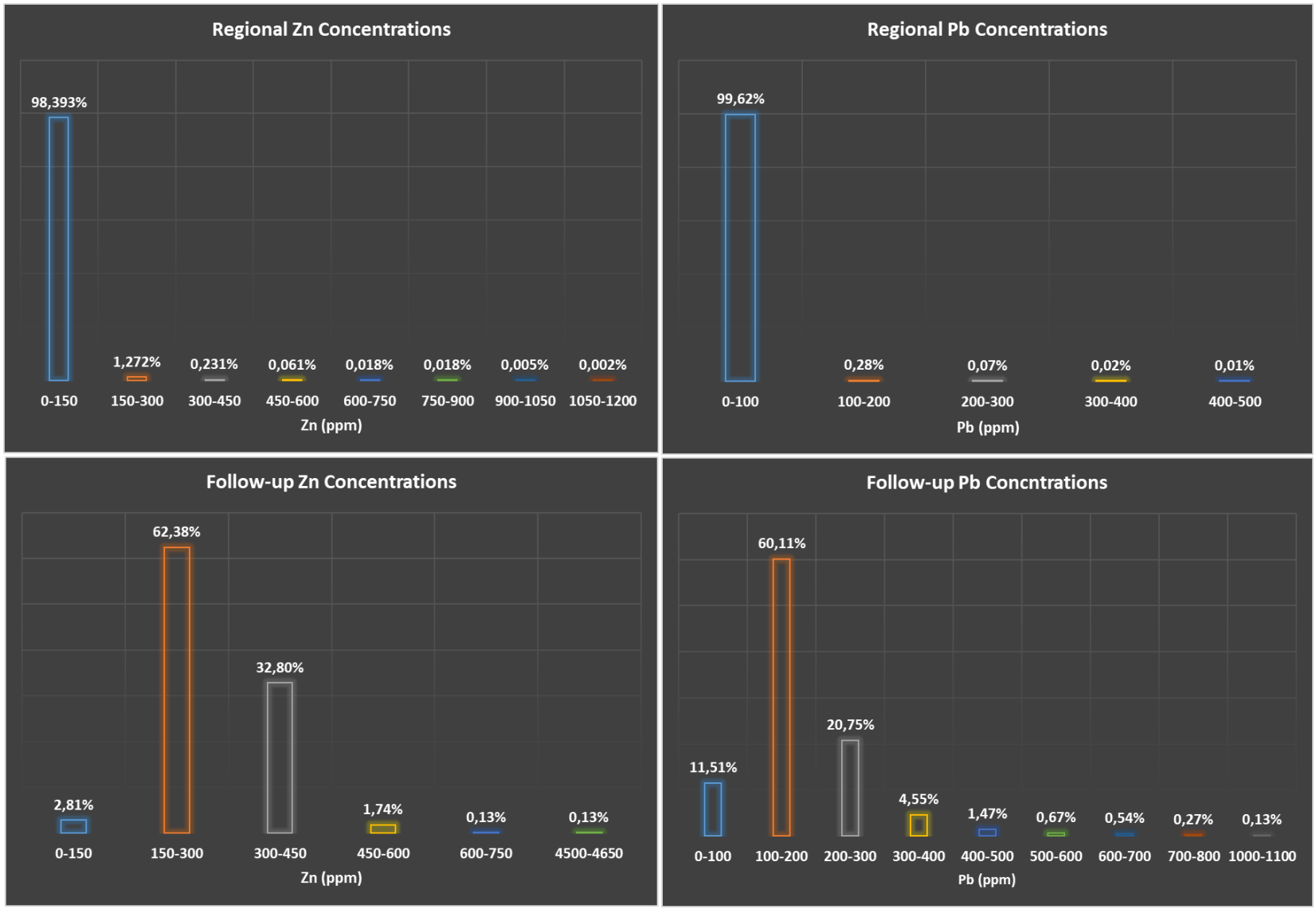

Figure 4.1 Comparison of regional and local concentrations of Pb and Zn.

4.1.2 Descriptive Statistics

4.1.2.1 Major and Minor Elements

The box and whisker plots (Figure 4.2) indicate high concentrations of SiO_2, Al_2O_3 and Fe_2O_3 reaching maximum concentrations of 73.55 %, 15 % and 13.84 %, respectively (Table 4.2). These oxides also have high average concentrations of 54.21 % SiO_2, 10.79 % Al_2O_3 and 7.25 % Fe_2O_3 (Table 4.2) accompanied by relatively high standard deviation and high range concentrations (i.e. 64.12 %, 13.34 % and 13.03 %, respectively). These statistical attributes indicate inherent weak central clustering and high variability of concentrations. This variability is also demonstrated by relatively high variances (18.88 SiO_2, 1.9 Al_2O_3 and 3.43 Fe_2O_3) compared to the other oxides. Silica has a relatively high negative skewness (-2.99) compared to moderately skewed Al_2O_3 (-0.92) and fairly symmetrical Fe_2O_3 (0.12) concentrations (Table 4.2).

The other oxides such as K_2O, TiO_2, MnO, MgO, CaO, Na_2O and P_2O_5 occur in relatively low concentrations, with maximum concentrations of <4 % (Figure 4.2). This is also indicative of the significant narrow range of box and whiskers displayed in Figure 4.2. These narrow box and whiskers are also attributed to a relatively low standard deviation (Table 4.2), indicative of high central clustering. These oxides are also characterised by low mean values (i.e. 1.57 % K_2O, 0.76 % TiO_2, 0.14 % MnO, 0.07 % MgO, 0.20 % CaO, 0.01 % Na_2O and 0.12 % P_2O_5) accompanied by low variance values (Table 4.2). Manganese oxide has the relatively highest positive skewness (11.42) compared to all oxides (Table 4.2). All the oxides are characterised by a smaller number of outliers (Figure 4.2).

4.1.2.2 Trace Elements

Trace elements characterised by the relatively highest maximum concentrations include Ba (1225 ppm), Pb (1649 ppm), S (1649 ppm) and Zn (4564 ppm) (Table 4.2). The range values of these elements are also high at 1184 ppm Ba, 1027 ppm Pb, 1640 ppm S and 4536 ppm Zn, accompanied by a high standard deviation of 103 ppm Ba, 96 ppm Pb, 156 ppm S and 175 ppm Zn. Elements such as Pb (179 ppm), Zn (284 ppm), Rb (184 ppm) and Zr (549 ppm) show higher average concentrations (Table 4.2) compared to the mean background concentrations in soils (i.e. 27 ppm Pb, 70 ppm Zn, 68 ppm Rb and 267 ppm Zr). The average concentrations of Pb (179 ppm) and Zn (284 ppm) are higher than the baseline range values (i.e. Pb: 56–100 ppm and Zn: 185–200 ppm) for South African soils.

Other trace elements which have relatively moderate to high maximum concentrations include As (374 ppm), Cu (265 ppm), Rb (316 ppm) and Zr (790 ppm). Tin and W show relatively high concentrations in relation to background concentrations in soils (i.e. <0.1–10 ppm Sn with an average of 2.5 ppm Sn and <0.17–<5 ppm W with an average of 1.7 ppm W), ranging between 0.79–29 ppm Sn and 0.75–31 ppm W with average concentrations of 9 ppm Sn and 11 ppm W. Trace elements which show the relatively highest variance among all trace elements include Ba (10592), Pb (9186), Rb (1176), S (24198), Zn (30613) and Zr (3828), suggesting high variability in the data. The box and whiskers plots in Figure 4.3 and 4.4 also show this variability, where Ba, Pb, Rb, S, Zn and Zr show wide ranges. The other trace elements have relatively low to moderate variance. The elements with fairly symmetrical data include Ce, Cr, Ga, Rb, Sc and U. Elements with moderately skewed data include Nd, Th, Y and Zr and the remaining elements are characterised by a highly skewed distribution of concentrations (Table 4.2). Zinc, Ba, Pb and S elements also have outliers, with Zn having relatively the highest outlier compared to all elements (Figure 4.3 and 4.4).

Table 4.2 Descriptive statistics of major, minor oxides and trace elements (major and minor oxides are measured in percentage whereas trace elements are measured in ppm).

(n = 747)	Minimum	Maximum	Range	Mean	Std. Deviation	Variance	Skewness
Major Oxides (%)							
SiO_2	9.43	73.55	64.12	54.21	4.35	18.88	-2.99
TiO_2	0.13	1.29	1.16	0.76	0.11	0.01	0.34
Al_2O_3	1.65	15.00	13.34	10.80	1.38	1.91	-0.92
Fe_2O_3	0.81	13.84	13.03	7.32	1.85	3.43	0.12
MnO	0.01	1.78	1.77	0.14	0.08	0.01	11.42
MgO	0.0005	0.45	0.45	0.07	0.10	0.01	1.15
CaO	0.02	1.72	1.70	0.20	0.11	0.01	6.95
Na_2O	0.000025	0.12	0.12	0.01	0.02	0.0005	2.30
K_2O	0.21	3.21	2.99	1.57	0.41	0.17	0.69
P_2O_5	0.01	0.38	0.37	0.12	0.03	0.00	1.87
Trace Elements (ppm)							
As	1.0	374	373	14	20	394	11
Ba	41	1225	1184	377	103	10592	2
Ce	15	183	168	96	18	334	0.5
Co	1.0	35	34	7	4	15	2
Cr	11	129	117	69	11	125	0
Cu	5	265	259	67	24	579	1.5
Ga	3	32	29	21	4	14	0
Hf	3	21	18	16	2	3	-1.3
Mo	0.3	11	11	1.0	1.1	1.2	3
Nb	5	67	62	27	6	34	2
Nd	7	119	112	52	11	127	0.8
Ni	2	49	47	20	6	30	1.1
Pb	16	1043	1027	179	96	9186	3
Rb	31	316	285	184	34	1176	0
S	9	1649	1640	372	156	24198	2
Sb	0.7	7	7	1.1	1.0	0.9	3
Sc	0.6	24	24	7	4	12	0.5
Sn	0.8	29	28	8	4	17	2
Sr	3	65	62	25	7	44	2
Ta	0.7	19	19	3	3	7	1.1
Th	1.1	32	31	16	3	12	0.9
U	0.8	13	12	7	1.3	2	0
V	4	146	142	43	16	269	2
W	0.8	31	31	11	4	13	1.3
Y	8	100	92	48	7	44	0.8
Zn	28	4564	4536	284	175	30613	20
Zr	93	790	697	549	62	3828	-0.9

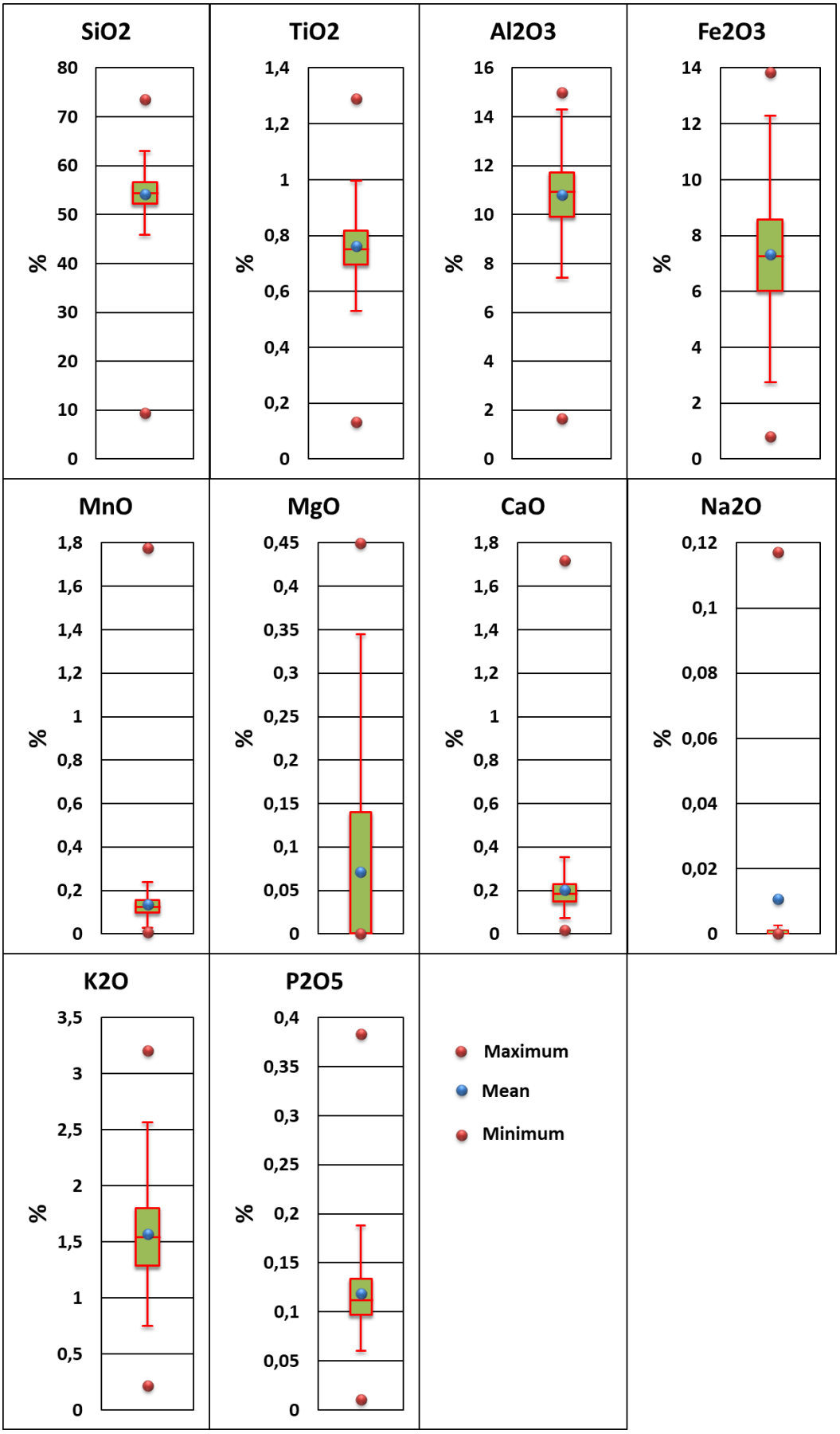

Figure 4.2 Box and whisker plot of major and minor oxides.

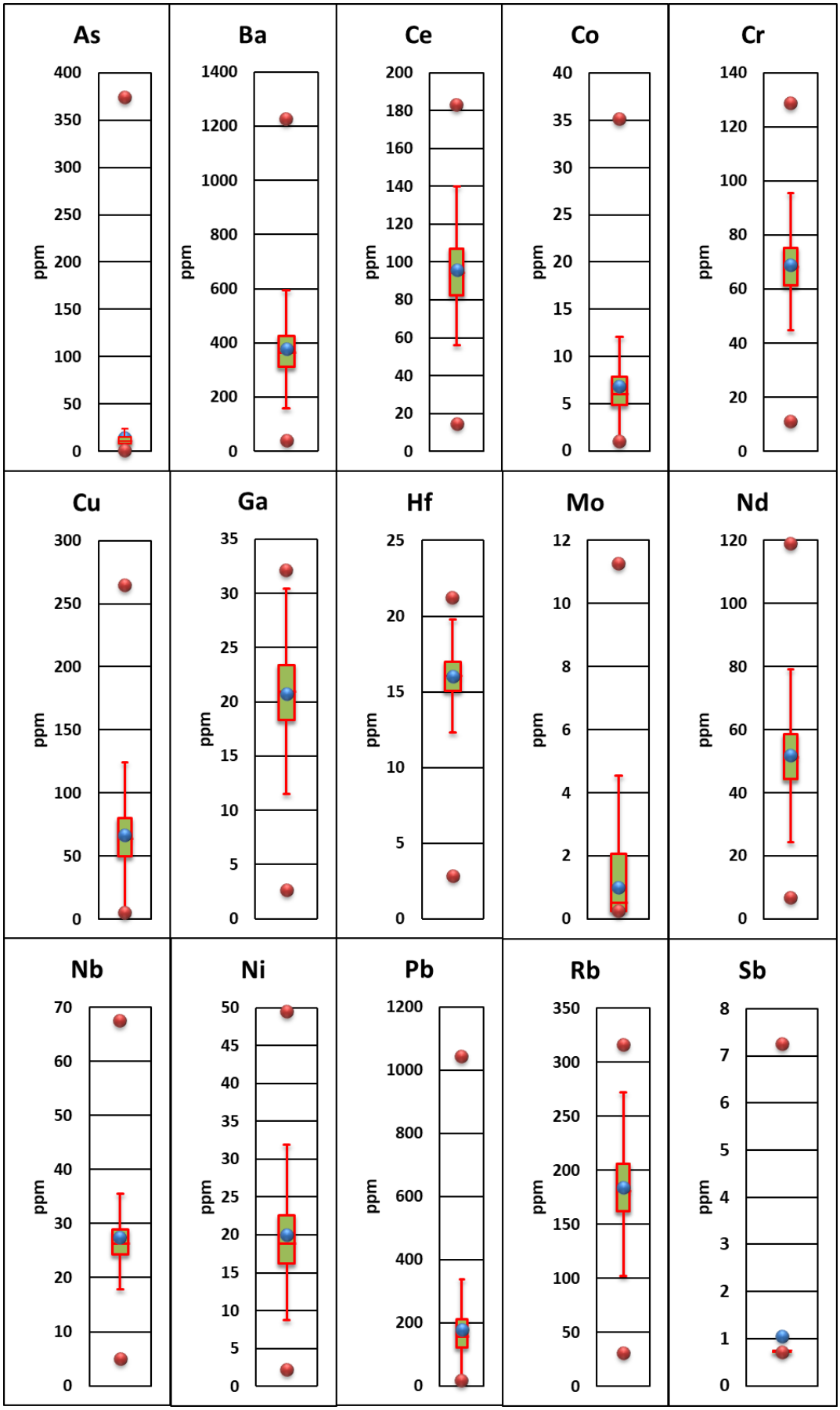

Figure 4.3 Box and whisker plots of trace elements.

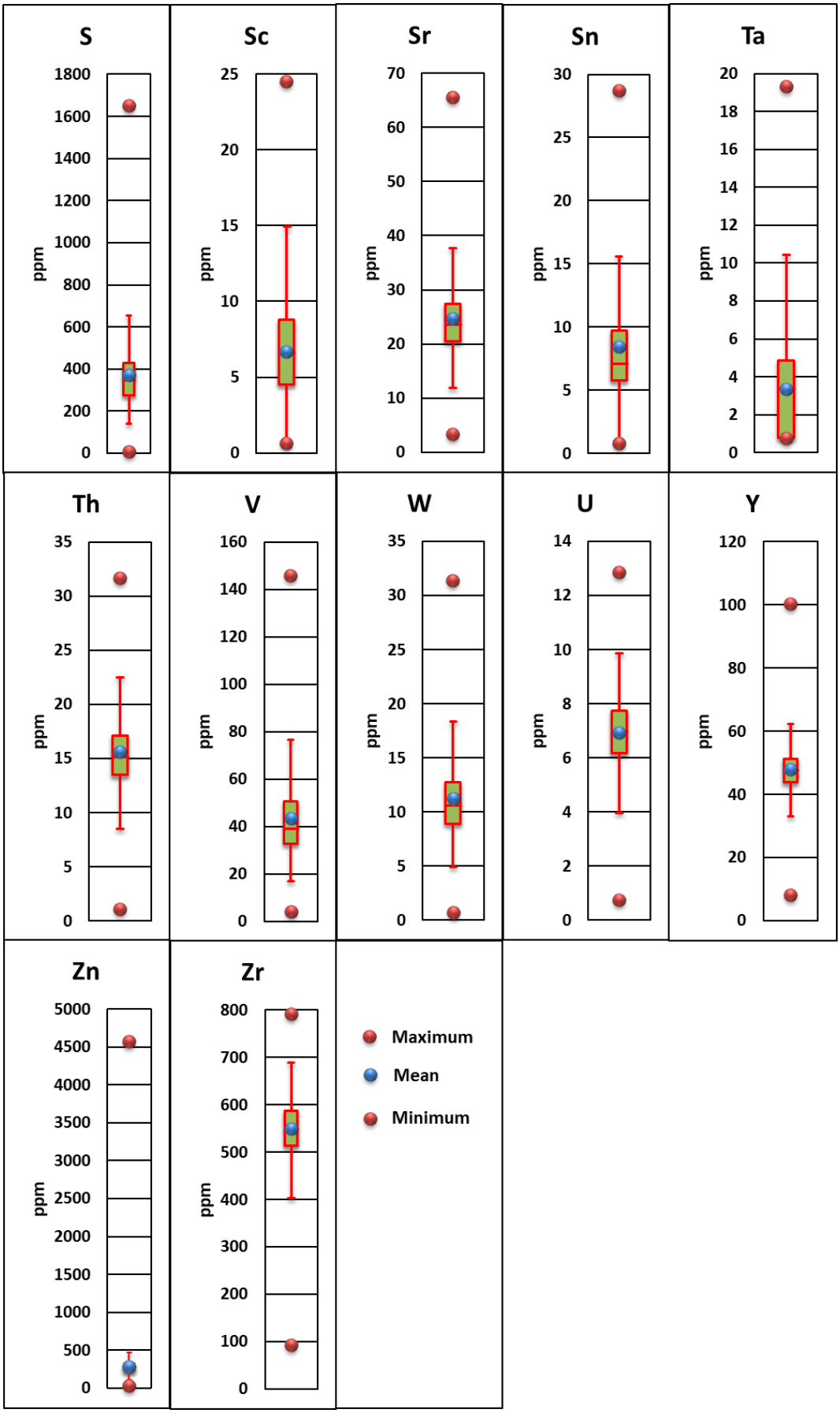

Figure 4.3 Continued.

4.1.3 Multivariate Analysis

4.1.3.1 Correlations

Only degrees of correlation with positive coefficient ranges >0.5 were selected to represent a meaningful association between elements. Coefficient ranges <0.5 are considered as having a low degree of correlation and they are discounted. The correlation matrix (in Appendix 3) produced several inter-element associations of lithological and mineralisation settings which include:

- Mn-Zn-Pb-Cu-Ni: Base metal mineralisation index
- Ca-P-S-Sr: Carbonate and phosphate index
- Ti-P-Cr-Ni-V-Zr: Laterite index
- Al-Ba-Ce-Nb-Nd-Rb-Th-U-Y-Zr: Felsic index, also reflects a pegmatitic composition
- Ti-Al-Fe-P-Co-Cr-Cu-Ni-V: Ultramafic index
- Si-Ti-Al-Cr-Hf-Th-U-Y-Zr: Index of granite, syenitic pegmatite and also reflects the presence of heavy minerals.

The elemental association which describes the potential Pb and Zn mineralisation of the area is Mn-Cu-Ni-Pb-Zn. In this association, Zn is highly correlated only with Pb, Cu and Mn. Lead solely correlates highly with only Cu and Zn. Nickel in contrast solely correlates highly with Cu whereas Mn correlates with Cu and Zn. Lead has good positive correlation with Cu (0.632) and fair correlation with Zn (0.521) (Appendix 3). Zinc also has fair correlation with Mn (0.576) (Appendix 3). Copper has a fair correlation with Mn (0.514) and Ni (0.539).

4.1.3.2 Principal Component Analysis (PCA)

The PCA generated 10 components (Table 4.3), with geochemical associations comparable to those obtained with correlation matrix.

- 1st component: Fe-Ti-V-Ni-Co-Cr-Sc. This elemental association reflects mafic to ultramafic systems.
- 2nd component: Al-K-Nd-Ce-Y-Rb-U. This association reflects a pegmatitic composition.
- 3rd component: Ca-P-S-Sr-Ba which indicate the presence of carbonate and phosphates. Phosphorus and Ca in soil tend to form low solubility secondary phosphate minerals (e.g. plumbogummite and pyromorphite).
- 4th component: Si-Hf-Zr. This association indicates granite, syenitic pegmatites and also the presence of heavy minerals.
- 5th component: Mn-Zn-Pb-Cu. These elements characterise the base metal mineralisation. This association is also comparable with the geochemical signature of the polymetallic vein deposits of base metals associated with felsic intrusions.
- 6th component: Sn-W-Nb-Th association which characterises Sn-W mineralisation. This association is also characteristic of pegmatite and veins systems.
- 7th component: Mg-Na. This association may indicate the presence of salts.
- 8th component: Ta-Ga.
- 9th component: Mo-Ga-As-Sb. These elements tend to be more mobile in alkaline environments, especially around polymetallic deposits. They also occur in epithermal systems.

- The 10th component: As-Ga.

The component which shows traits of Pb and Zn mineralisation is the 5th component. This component is characterised by a strong correlation between Zn, Pb, Cu and Mn. The spatial distribution of 5th component in Figure 4.4 indicates the locations where the association Zn-Pb-Cu-Mn is prominent. These zones occur along the NE–SW trending Swaershoek anticline and also along fault lines and lithological contacts particularly in the northwestern part of the area. Zones of high intensity of Zn-Pb-Cu-Mn became weaker away from the anticline structure.

Table 4.3 The Principal Component Analysis illustrating correlations between major oxides and trace elements which characterise various geological and mineralisation settings denoted by coloured frames.

Rotated Component Matrix										
	Component									
	1	2	3	4	5	6	7	8	9	10
V	,916			,114						
Ni	,904			,119	,218					
TiO2	,783	,186	,189	,367			-,112	-,129	-,157	
Co	,716			-,179	,254			,294		
Cr	,648		,171	,382	,121	,145	-,127	-,262	,112	,118
Fe2O3	,542	,131	,122		,133	,140		,505	,389	-,235
Sc	,481	,276		-,107		-,160	,307	,242		
Nd		,835					-,128			
Ce		,797		-,109	,102	,153			,119	,163
Y	,154	,763	,135	,355		,147		,169		
Rb		,601	,171	,159	,227	,414		-,122	-,419	
Al2O3	,452	,541	,183	,393	,242				,204	-,147
K2O	-,296	,518	,333	,176		,324			-,443	
U	,199	,472		,363	,331	,293		,243		-,220
CaO			,876	,105	,112	-,184				
S	,119	,143	,848	,144	,135			-,193	,114	
P2O5	,494		,658		,178	,248		-,143	,138	
Sr	-,143	,398	,631	,180					-,379	,208
Ba		,511	,541	,185				,262	-,377	-,145
SiO2		,139	,196	,873	,106					
Hf	,186			,845	,135			,161		
Zr	,265	,252	,317	,755	,116	,238				
Pb	,105	,149			,776	,213	,106		,212	,324
Zn	,101	,164	,261	,238	,761				-,153	-,135
Cu	,386			,136	,722	,164				-,137
MnO	,325		,349	,122	,592			,286		-,160
W		,290	-,174	,119	,337	,651	,152	,159	-,176	,270
Nb	,235	,388		,236	-,249	,647		,137		
Sn	,154		,103		,267	,625	-,207	,168	,157	-,296
Th	,270	,564		,250		,581		,122		
MgO							,899			
Na2O						,102	,892			
Ta		,105	-,189			,187		,774		,143
Ga	,138	,470						,500	,230	
Mo		,125			,102				,793	
As	-,191			,139		,171		-,108	-,123	,801
Sb	,133				-,101	-,161		,163	,137	,665

Extraction Method: Principal Component Analysis. Rotation Method: Varimax with Kaiser Normalization.

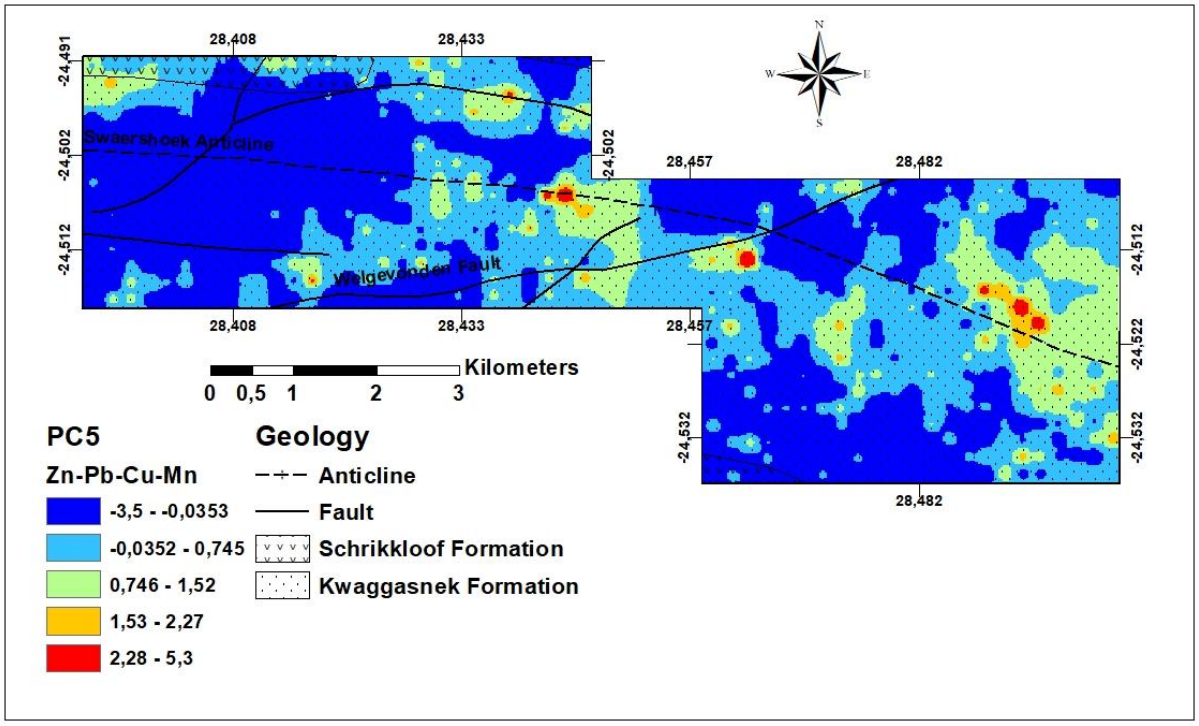

Figure 4.4 The spatial distribution of PCA 5 that characterises the Zn-Pb-Cu-Mn association.

4.1.4 Background and Anomalous Concentrations of Paragenetic Elements

The threshold values of Pb, Zn and Cu for the 68 percentile are 252 ppm, 368 ppm and 91 ppm, respectively (Table 4.4). Comparison of these Pb, Zn and Cu thresholds to soil threshold concentrations indicating potential mineralisation (i.e. Pb > 100 ppm, Zn > 300 ppm and Cu > 100 ppm) indicates that Pb (252 ppm) and Zn (368 ppm) are within the potential mineralisation threshold limits (i.e. >100 ppm and >300 ppm, respectively), whereas Cu (91 ppm) is less than the potential mineralisation threshold limit (i.e. >100 ppm). These 68 % threshold values are also less than the maximum concentrations (i.e. 1043 ppm Pb, 4564 ppm Zn and 265 ppm Cu) as in some case when working with log-transformed data, calculated threshold values tend to be greater than the maximum concentrations. Compared to regional rock average concentrations (i.e. 11 ppm Pb, 147 ppm Zn and 12 ppm Cu), these 68 % threshold concentrations are greater.

In terms of the 90 % threshold values, Pb, Zn and Cu have threshold concentrations of 336 ppm, 451 ppm and 115 ppm, respectively. These threshold values are well above the soil thresholds (i.e. Pb > 100 ppm, Zn > 300 ppm and Cu > 100 ppm), which indicate the possibility of mineralisation. There are a few high concentrations classified as background concentrations for Pb (between 100 ppm and 336 ppm) and Zn (between 300 ppm and 451 ppm). This observation also applies for high concentrations of Cu, but to a less extent. In order to distinguish these high concentrations from the low background concentrations, they are classified as high background concentrations (Table 4.5). The 90 % threshold concentrations (i.e. 336 ppm Pb, 451 ppm Zn and 115 ppm Cu) are also less than the maximum concentrations (i.e. 1043 ppm Pb, 4564 ppm Zn and 265 ppm Cu) and greater than the regional rock average concentrations (i.e. 11 ppm Pb, 147 ppm Zn and 12 ppm Cu).

The misclassification of anomalous concentrations is also apparent in 95 % thresholds, which have significantly higher threshold values (i.e. Pb = 395 ppm, Zn = 504 ppm and Cu = 132 ppm). Most of the

anomalous concentrations of Pb (between 100 ppm and 395 ppm), Zn (between 300 ppm and 504 ppm) and Cu (between 100 ppm and 132 ppm) are excluded by the 95 % thresholds. These excluded concentrations are well within the anomalous range when compared to the soil threshold values (i.e. >100 ppm and >300 ppm, respectively), which indicate the possibility of mineralisation.

The 68 % threshold failed to meet the requirement of classifying anomalies of all three elements (Pb, Zn and Cu). This is evident in the Cu threshold value of 91 ppm, which is lower than the soil threshold which indicates mineralisation. In terms of declassification of anomalous concentrations, both 90 % and 95 % classified some anomalous concentrations as background concentrations. This misclassification of anomalous concentrations is to a large extent in a 95 percentile because of significantly high threshold values. In comparison between 68 %, 90 % and 95 % thresholds, the 90 % threshold is relatively suitable to classify the anomalous concentrations.

Table 4.4 The threshold concentrations ore-forming elements and their pathfinder elements.

	Regional Rock Geochemical Data	Local Soil Geochemical Data					
	Regional Average Concentrations	Maximum Concentrations	Analytical Values				Soil concentration indicating potential mineralisation
			Mean	Mean + Std. Dev. (68 %)	Mean + 1.64485xStd. Dev. (90 %)	Mean + 2x Std. Dev. (95 %)	
MnO (%)	0.13	1.78	0.12	0.19	0.24*	0.28	Use as an indicator element in geochemical exploration (Reedman, 1979)
Cu (ppm)	12	265	63	91	115*	132	>100 (Pohl, 2011, (Reedman, 1979)
Pb (ppm)	11	1043	161	252	336*	395	>100 (Reedman, 1979)
Zn (ppm)	147	4564	268	368	451*	504	>300 (Reedman, 1979)

* Selected threshold concentrations separating background and anomalous concentrations.

Table 4.5 Concentration ranges describing the background, threshold and anomalous concentrations.

	Low Background	High Background	Threshold	Anomalies	Significant Anomalies
MnO (%)	<0.12	0.12–0.24	0.24	0.24–0.28	>0.28
Cu (ppm)	<63	63–115	115	115–132	>132
Pb (ppm)	<161	161–336	336	336–395	>395
Zn (ppm)	<268	268–451	451	451–504	>504

4.1.5 Spatial Distribution of Zn, Pb, Cu and MnO

Significant anomalous concentrations of MnO (0.29–1.78 %) are trending in a NW–SE direction, along the Swaershoek anticline (Figure 4.5A). Most of significantly anomalous MnO concentrations (0.29–1.78 %) occur on both sides of the anticline, and a high number of them are localised towards the southeast part of the area. The anomalous concentrations (0.25–0.28 % MnO) also follow the same trend of the anticline. Significant anomalous concentrations of Cu (133–265 ppm) also follow the trending pattern (NW–SE) of MnO along the anticline, with most the significant anomalies (133–265 ppm Cu) localised towards the southeast of the area (Figure 4.5B). The anomalous concentrations of copper (116–132 ppm Cu) are mostly localised towards the southeast of the area.

Significant anomalous concentrations (396–1043 ppm) of Pb also follow the same NW–SE trend as those of Cu and MnO (Figure 4.5C). These concentrations (396–1043 ppm Pb) occur mainly in the central part of the study area, forming a NW–SE trend and localised along the NW–SE anticlinal structure. Some of these significant anomalous concentrations also occur in the northwest and northeast part of the area, mainly along lithological contacts and fault lines (Figure 4.5C). The anomalous concentrations (337–395 ppm Pb) also follow the same NW–SE trend. Significant anomalous concentrations (505–4564 ppm) of Zn show a similar NW–SE trend in Figure 4.5D, and most of these anomalies occur mainly in the central part and towards the southeast part of the area. Most of these anomalies are also aligned and localised mainly along the Swaershoek anticline.

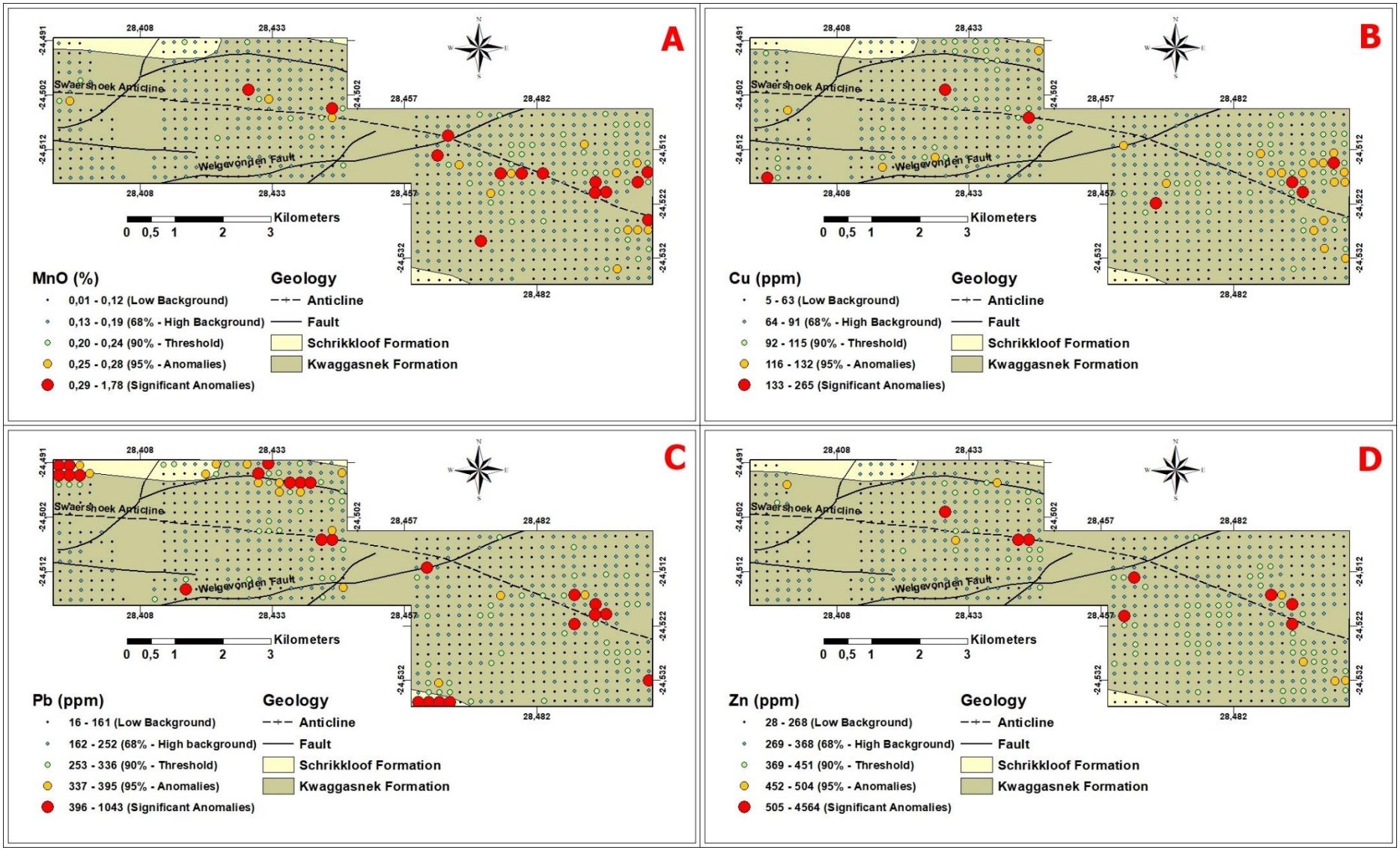

Figure 4.5 The spatial distribution of MnO (A), Cu (B), Pb (C) and Zn (D).

4.1.6 The RGB Classification Zn, Pb, Cu and MnO

The target anomalies shown in grey in Figure 4.6 represent anomalies of Zn, Pb and Cu, which are >90 % threshold, and these occur in zones 1 to 5. Zones 1 and 2 occur directly on the structural features. The zones 2–5 form a NW–SE trend along the Swaershoek anticline. From zone 2 towards the southeast along the anticline, the zones start to occur a certain distance away from the Swaershoek anticline.

Anomalies of Zn, Pb and MnO which are >90 % threshold in zones 1, 3 and 4 (Figure 4.7) also show a similar trend along the Swaershoek anticline. These zones are similar to the locations of Zn, Pb and Cu anomalies along the anticline. The other anomaly of Zn, Pb and MnO in zone 2 occurs at the intersection of the Welgevonden Fault and the other secondary fault.

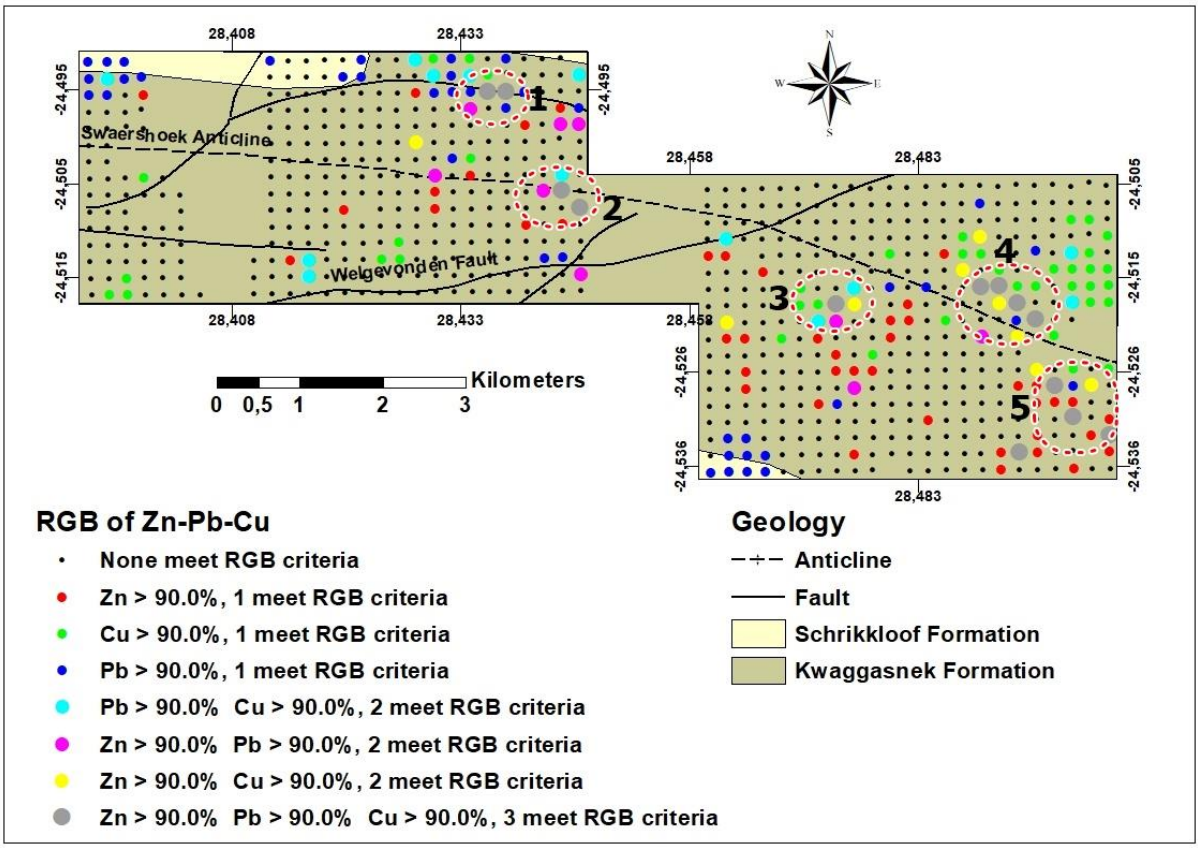

Figure 4.6 The RGB classification map of Zn, Pb, Cu. The map illustrates the locations where >90 % anomalies of Zn, Pb and Cu occur concurrently.

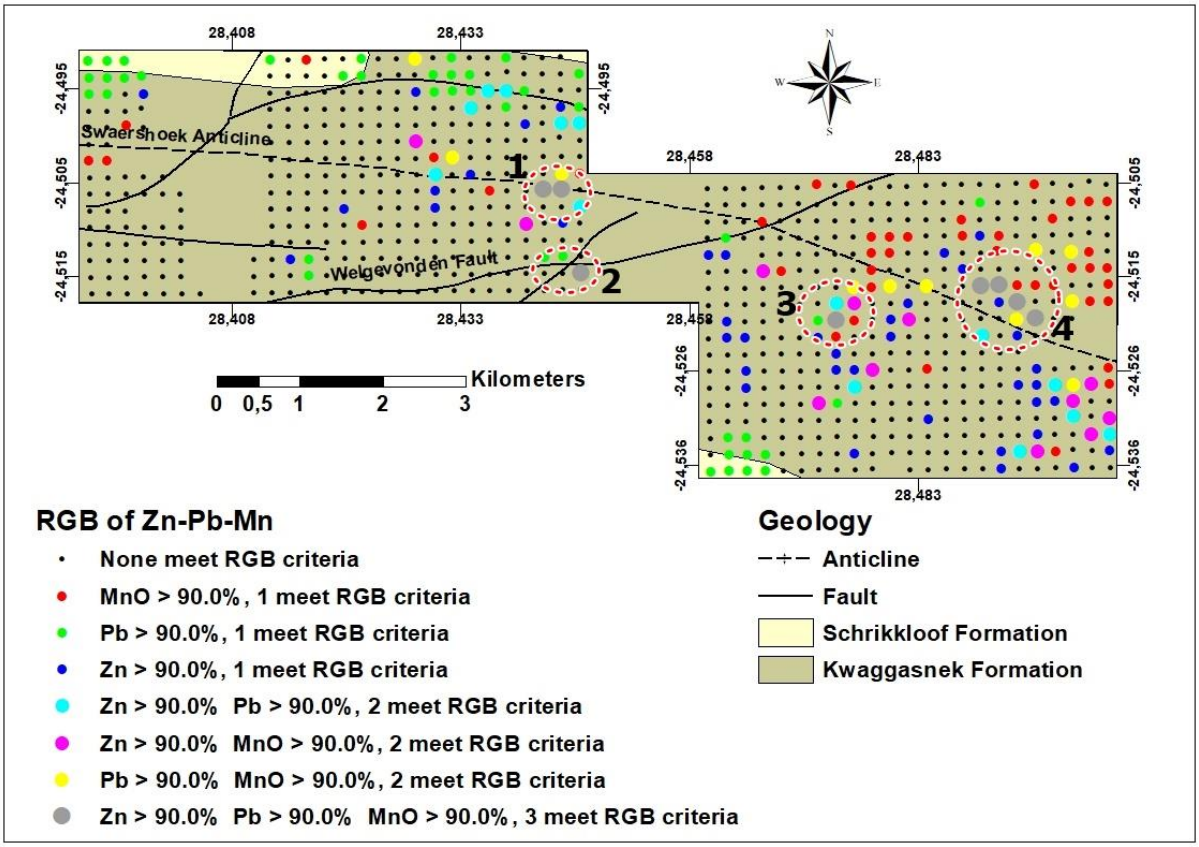

Figure 4.7 The RGB classification of Zn, Pb and MnO. The map illustrates the locations where >90 % anomalies of Zn, Pb and MnO occur concurrently.

4.1.7 Potential Style of Mineralisation

The average zinc ratio [ZR = 100Zn/(Zn + Pb)] shown in Table 4.6 was calculated using 19 samples with anomalous concentrations of Pb and Zn, which are above the threshold of 336 ppm (i.e. Pb > 336 ppm and Zn > 336 ppm). The histogram in Figure 4.8A shows a skewed distribution, indicated also by the skewness of -0.6 in Table 4.6. This skewness value is between -1 and -0.5, indicating negative moderate skewness. This variability is also shown by the Zn vs Pb diagram (Figure 4.8B), showing a high number of samples lying above the line Zn = 0.895Pb (i.e. Zinc Ratio = 47) characterised by a small variation and other samples below the line characterised by a large variation. These two populations are also shown in Figure 4.8C, depicting a population with more samples above the mean zinc ratio line and the population with less samples below the line.

The ZR distribution has a range of 35–57 and low average of 47 with a standard deviation of 7 (Table 4.6). The range of the ZR lies between two ranges [i.e. 1–10 (Pb-rich and Zn-poor) and 90–10 (Zn-rich and Pb-poor)], indicating comparable enrichment proportions in both Zn and Pb. In comparison with the expected high regional mean ZR of 93 (Table 4.7), the low average ZR of 47 indicates that it's not influenced by lithology.

In summary, the distribution of zinc ratios is skewed, coupled with a low average zinc ratio and low standard deviation. In comparison with properties of other mineralisation styles in Table 4.8, the mean ZR of the area falls in the range of 39–75, coupled with the skewed distribution of the ZR values (Table 4.8). The minor difference arises from the standard deviations, i.e. the standard deviation of the area

ZR falls within the range of <15 and out of the range of >23. Comparison to these two mineralisation styles indicates that the histogram properties of local zinc ratio are more similar to those of Pb-Zn-Ag (veins, fissure lodes, polymetallic sulphide and Irish style).

Table 4.6 The statistical summary of zinc ratio [ZR = 100Zn/(Zn + Pb)].

Mean	Std. deviation	Variance	Skewness	Range	Minimum	Maximum
47	7	44	-.6	23	35	57

Table 4.7 The average ZR of the area compared to the expected ZR of the regional Kwaggasnek rhyolite**.**

Regional Kwaggasnek Rhyolite (Average values)			Average ZR of the Study Area
Zn (ppm)	Pb (ppm)	100Zn/(Zn + Pb)	100Zn/(Zn + Pb)
147	11	93	47

Table 4.8 The ZR parameters of the area compared to the standardised ZR parameters of mineralisation styles.

ZR Parameters of the Area			Standardised ZR Parameters of Mineralisation Styles					
			Zn-Pb-Cu-Ag-Au Volcanogenic Massive Sulphide Deposits			Zn-Pb-Ag (Veins, Fissure lodes, Polymetallic Sulphide and Irish style) Deposits		
Mean	Standard Deviation	Histogram Distribution	Mean	Standard Deviation	Histogram Distribution	Mean	Standard Deviation	Histogram Distribution
47	7	Skewed	66–77	<15	Normal	39–75	>23	Skewed

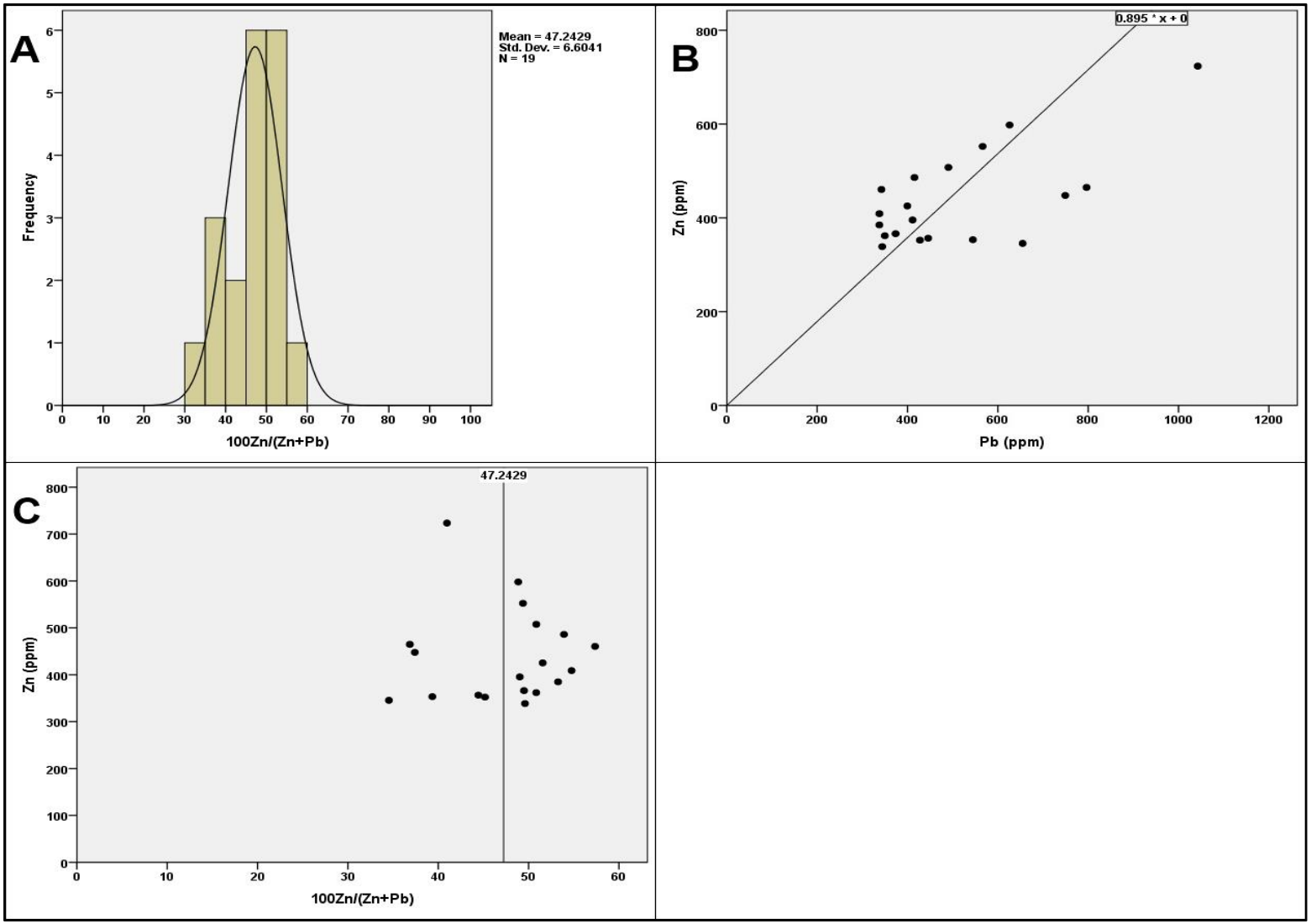

Figure 4.8 The relationship between Zn, Pb and ZR (zinc ratio). (A) Histogram of ZR. (B) Scatterplot of Zn and Pb. (C) Scatterplot of Zn and ZR showing the average of the ZR.

4.1.8 Potential Ore Group Classification

The average of the copper ratio [CR = 100Cu/(Cu + Zn)] and lead ratio [PR = 100Pb/(Pb + Cu)] shown in Table 4.9 were calculated using 25 samples with anomalous concentrations of Cu, Pb and Zn, which are above the threshold of 115 ppm (i.e. Cu > 115 ppm, Pb > 115 ppm and Zn > 115 ppm). The CR values fall within the range of 18–43, with low average CR of 28 and low standard deviation of 6 (Table 4.9). These low CR values indicate an increase of Zn compared to Cu. The range (35) of PR is slightly higher between 49 and 84, with slightly higher average of 68 and low standard deviation of 10 (Table 4.9). A high average PR of 68 indicates a higher increase in Pb concentrations than in Cu.

The average CR (28) of the area is higher than the expected regional average CR of 8, indicating an increment of both Cu and Zn in the area (Table 4.10). The Zinc ratio of felsic rocks is generally high as indicated by the regional average ZR of 93. However, the average ZR of the study area is very low at 47, indicating a significant increase of both Pb and Zn. The average PR of 68 (Table 4.10) is also higher than the regional average PR of 48, indicating an increase in Pb.

In comparison with the CR, ZR and PR parameters of ore groups in Table 4.11, the local average CR of 28 is <50, falling in the category of the Zn-rich ore groups (i.e. Zn-Cu, Zn-Cu-Pb/Zn-Pb-Cu/Zn-Pb). The local average ZR of 47 is also <50, falling between the two ranges of Cu-rich ore group (i.e. 0–100: Cu and 20–50: Cu-Pb-Zn) and one of Pb-rich ore group (i.e. 10–50: Pb-Zn-Cu/Pb-Cu-Zn/Pb-Zn). The local average PR of 68 falls in the range of >50 characterised by Pb-rich ore groups (i.e. Pb-Cu and Pb-Zn-Cu/Pb-Cu-Zn/Pb-Zn). These CR, PR and ZR parameters of the area, result in the overall element assemblages of Zn-Pb-Cu/Zn-Cu-Pb, Pb-Zn-Cu/Pb-Cu-Zn and Cu-Pb-Zn, which characterise the ore group of the area.

Table 4.9 The statistical summary of copper ratio (CR) and lead ratio (PR) of the area.

	Mean	Std. deviation	Variance	Skewness	Range	Minimum	Maximum
CR	28	6	35	0.6	25	18	43
PR	68	10	104	0.02	35	49	84

Table 4.10 Comparison of the average copper ratio (CR), zinc ratio (ZR) and lead ratio (PR) of the area and the regional Kwaggasnek rhyolite.

Average CR, ZR and PR of the Area	100Cu/ (Cu + Zn)	28
	100Zn/ (Zn + Pb)	47
	100Pb/ (Pb + Cu)	68
Regional Kwaggasnek Rhyolite (Average Values)	Cu	12 ppm
	Pb	11 ppm
	Zn	147 ppm
	100Cu/ (Cu + Zn)	8
	100Zn/ (Zn + Pb)	93
	100Pb/ (Pb + Cu)	48

Table 4.11 The ore group definitions with their characteristic ranges of average ZR and CR. Shaded ore groups correspond with CR, PR and ZR of the area.

Ratios	**Cu-rich ore groups**				
CR = 100Cu/(Cu + Zn)	>90		50–90		
	Cu		Cu-Zn/Cu-Zn-Pb		
ZR = 100Zn/(Zn + Pb)	0–100	>80	50–80	20–50	<20
	Cu	Cu-Zn	Cu-Zn-Pb	Cu-Pb-Zn	Cu-Pb
PR = 100Pb(Pb + Cu)	<10		10–50		
	Cu		Cu-Pb/Cu-Pb-Zn		
Ratios	**Zn-rich ore groups**				
CR = 100Cu/(Cu + Zn)	<50				
	Zn-Cu/Zn-Cu-Pb/Zn-Pb-Cu/Zn-Pb				
ZR = 100Zn/(Zn + Pb)	>90		50–90		
	Zn-Cu		Zn-Cu-Pb/Zn-Pb-Cu/Zn-Pb		
PR = 100Pb(Pb + Cu)	-				
Ratios	**Pb-rich ore groups**				
CR = 100Cu/(Cu + Zn)	-				
ZR = 100Zn/(Zn + Pb)	10–50			<10	
	Pb-Zn-Cu/Pb-Cu-Zn/Pb-Zn			Pb-Cu	
PR = 100Pb(Pb + Cu)	>50				
	Pb-Cu, Pb-Zn-Cu/Pb-Cu-Zn/Pb-Zn				

4.2 Conceptual Exploration Approach

4.2.1 Zn-Pb-Cu-Mn Anomalies

The maps presented in Figure 4.9 to Figure 4.10 where A, B, C, D and E represent defuzzified mineral potential maps (prospectivity maps) produced from fuzzy membership value maps overlaid by γ = 0, γ = 2.5, γ = 0.5, γ = 0.75 and γ = 1, respectively. Figure 4.19A represents a more constricted prediction model of Zn-Pb-Cu-Mn anomalies. The distribution pattern of significant Zn-Pb-Cu-Mn anomalies follows the alignment of the NW–SE trending Swaershoek anticline. These significant Zn-Pb-Cu-Mn anomalies are bounded by a very thin dispersion of lower anomalies. These lower anomalies are bounded by a wide and randomly oriented dispersion of low and high background concentrations.

In Figure 4.9B (γ = 0.25) the dispersion of significant and lower anomalies increased, with more of the moderate concentrations (i.e. high background to threshold) being highlighted. The distribution pattern of all anomalies still follows the NW–SE trend of the anticline. In the northeast part of the area, concentrations above the threshold increase along the lithological contacts. Increasing γ (0 to 0.25) also resulted in the increased dispersion of moderate concentrations, particularly in locations leading away from anomalies and the apex of the Swaershoek anticline. The dispersion of background concentrations was not affected by the increase of γ (from 0 to 0.25).

All anomalies in Figure 4.9C have slightly increased with the increase of γ = 0.25 to γ = 0.5. On the east side of the area (Figure 4.9C), the increase in dispersion of anomalies stretches away from the Swaershoek anticline, more particularly around the significant anomalies. The random wide dispersion of moderate concentrations doubled in size along the anticline with increase of γ = 0.25 to γ = 0.5. In

contrast, the dispersion of high background concentrations decreased slightly with an increase of γ from 0.25 to 0.5. The distribution of background concentrations is slightly affected by an increase of γ from 0.25 to 0.5.

An increase in γ from 0.5 to 0.75 (Figure 4.9D) resulted in an overall minor change in all anomalies. Moderate concentrations also increased slightly, particularly in the east side than the west side of the area. Lower background concentrations slightly decreased whereas higher background concentrations increased (Figure 4.9D).

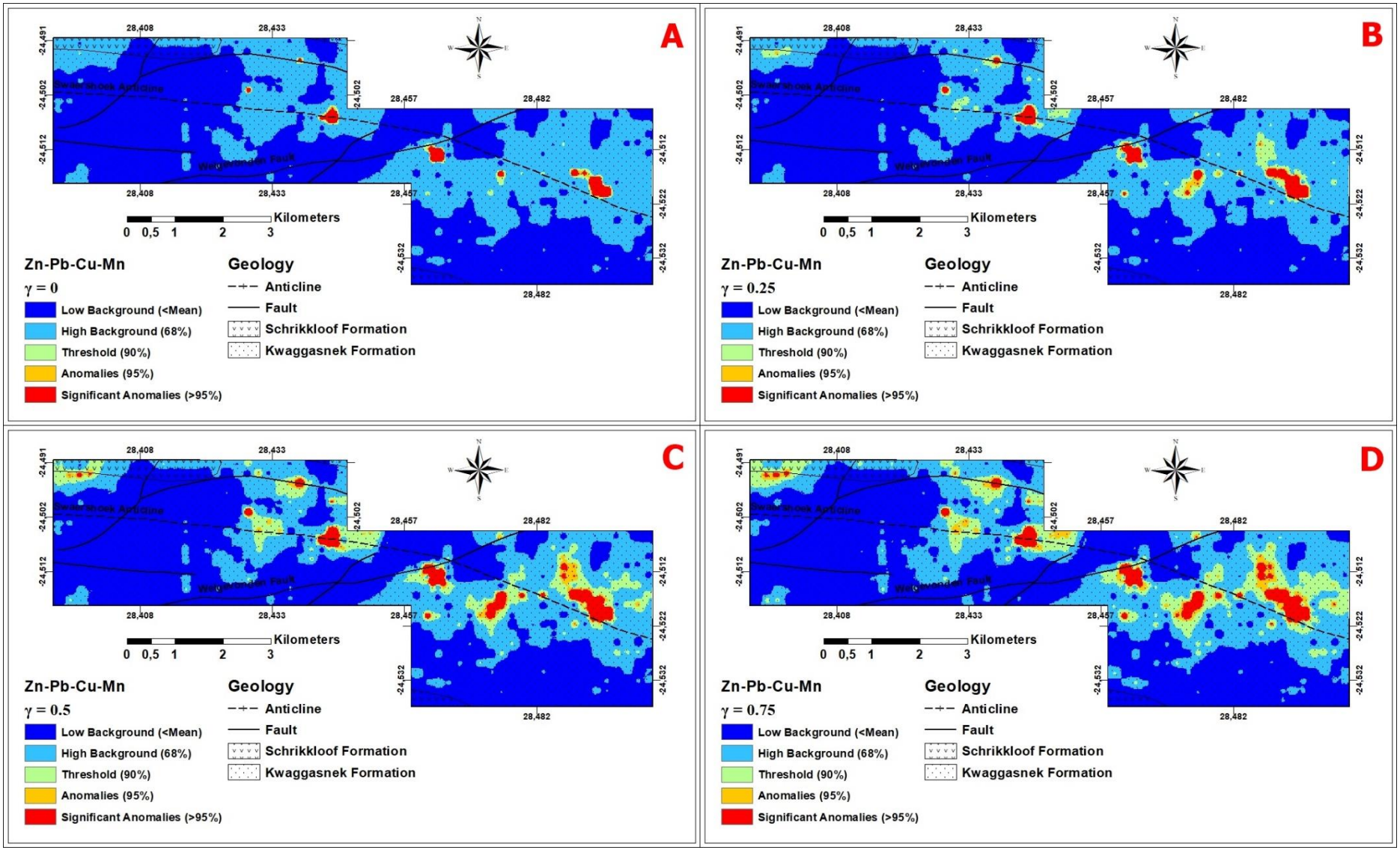

Figure 4.9 Defuzzified mineral potential maps of Zn-Pb-Cu-Mn for (A) γ = 0, (B) γ = 0.25, (C) γ = 0.5 and (D) γ = 0.75.

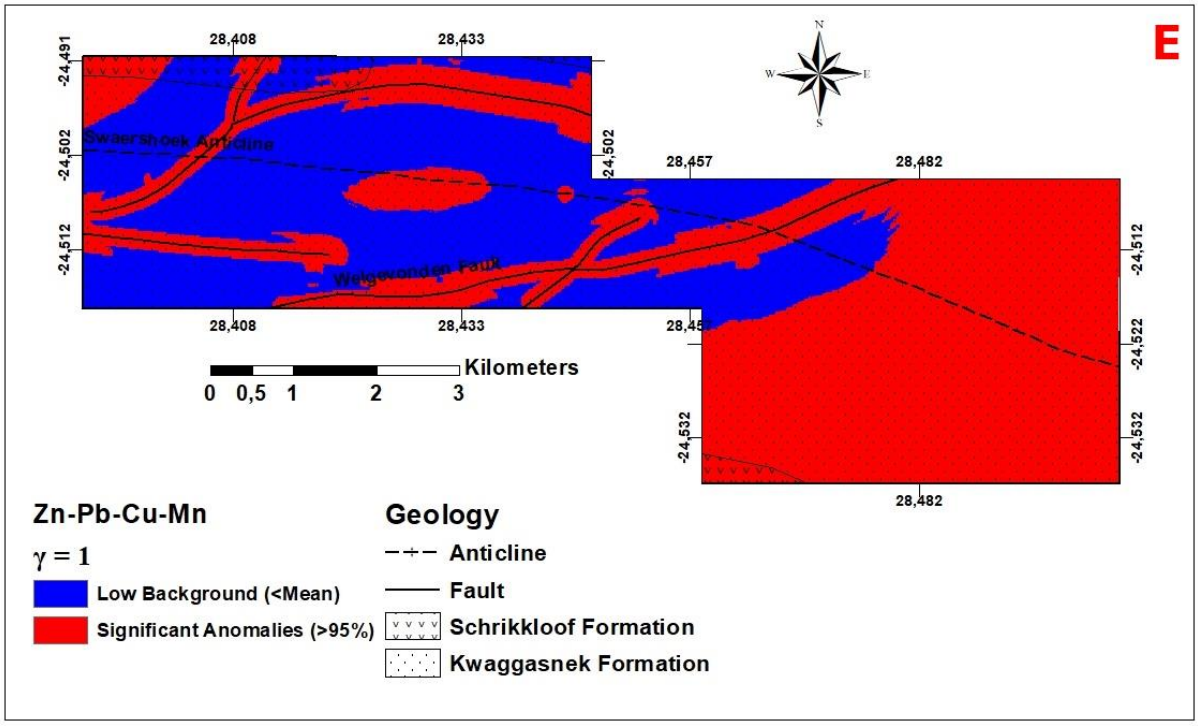

Figure 4.10 Defuzzified mineral potential map of Zn-Pb-Cu-Mn for γ = 1.

An increase of γ from 0.75 to 1 produced significantly exaggerated false anomalies (Figure 4.10E). Concentrations below the threshold limit are highlighted inaccurately as significantly anomalous. This indicates that the range of γ (0–0.75) has high prediction rate than γ = 1 in terms of localising the Zn-Pb-Cu-Mn anomalies. In terms of optimum proportion of prospective area, the more refined anomalies in Figure 4.9A (γ = 0) has an overall prediction rate, representing an optimum proportion of prospective areas.

CHAPTER 5

Discussion and Conclusions

5.1 Discussion

This study investigated the anomalous nature of the regional geochemical data in the Modimolle area, which indicates elevated concentrations of Pb and Zn. These regional elevated concentrations generated from the low-density sampling of one sample per km^2 indicates a requirement for the follow-up survey to verify the elevated Pb and Zn concentrations and determine whether they indicate potential mineralisation. This follow-up soil survey used a high sampling density method of one sample per 200 m to verify these Pb and Zn concentrations and to determine the associated potential mineralisation.

The following approaches were applied in order to investigate the anomalous nature of Pb and Zn concentrations and their likelihood to indicate potential mineralisation:

- The initial step involved comparison of Pb and Zn regional geochemical concentrations with corresponding concentrations of this follow-up study to verify their anomalous inclination.
- Lead, zinc and other associated elements were evaluated using an empirical exploration method to determine whether they indicate the possibility of mineralisation. Locations with likelihood of mineralisation were also generated with the aid of a spatial elemental distribution. An attempt was also made to determine the potential mineralisation style and ore group associated with the potential mineralisation.
- A complementary conceptual exploration method to the empirical exploration method was applied to determine the locations which show enrichment and likelihood of mineralisation.

Assessment of the Zn concentrations indicated that 99.7 % of the regional Zn concentrations lies within the background range of 0–300 ppm, with a lower number (0.3 %) of concentrations in the higher concentration range of >300 ppm. However, the number of concentrations in the background range decreased in the local area, with 65 % of concentrations lying in a background range (i.e. 0–300 ppm) and 35 % lying within the higher concentration range of >300 ppm. In terms of average concentrations, the local area has an average of 284 ppm Zn, which is higher than the regional soil average of 50 ppm, regional rock average of 147 ppm Zn (Mathez *et al*., 2013), mean background concentration in soils of 70 ppm Zn (Kabata-Pendias, 2011) and the average range of Zn (185–200 ppm) in South African soils (Herselman *et al*., 2005). With regards to Pb, 99.6 % of regional concentrations lie between the background range of 0–100 ppm, with 0.4 % of concentrations lying within the higher concentration range of >100 ppm. The local area however has a reduced number (11.5 %) of Pb concentrations in the background range of 0–100 ppm, and elevated number (88.5 %) of concentrations in the higher concentration range of >100 ppm. The average Pb concentration (179 ppm) of the local area is also higher than the regional soil average of 10 ppm, the regional rock average of 11 ppm Pb (Mathez *et al*., 2013), mean background concentration in soils of 27 ppm Pb (Kabata-Pendias, 2011) and baseline range (56–100 ppm Pb) of South African soils (Herselman *et al*., 2005).

The increased number of Pb and Zn concentrations in the higher concentration ranges (Pb > 100 ppm and Zn > 300 ppm) in the local area, indicate the presence of Pb and Zn anomalies. This is also

substantiated by the relatively higher maximum concentrations (4564 ppm and 1043 ppm, respectively), high mean concentrations (284 ppm and 179 ppm, respectively), high variance values (Zn = 30613 and Pb = 9186) and also positive skewness in the distribution of data. These statistical characteristics are analogous to a typical statistical character of anomalous concentrations indicating potential mineralisation (Bolotnikov and Kravchenko, 1970, Cameron and Baragar, 1971; Govett and Pantazis, 1971; Garrett, 1973; Tauson and Kozlov, 1973; Govett and Goodfellow, 1975). In addition, Pb and Zn are characterised by average concentrations (Pb = 179 ppm and Zn = 284 ppm), which are comparable to the soil threshold concentrations (i.e. Pb > 100 ppm and Zn > 300 ppm) proposed by Pohl (2011) and Reedman (1979) which indicate potential mineralisation.

The Zn-Pb-Cu-Mn inter-element association produced from inter-element correlation and PCA, characterises the potential mineralisation of the area. The mineralisation characterised by these geochemical signatures of Zn, Pb, Cu, Mn and associated with felsic intrusion is comparable to the polymetallic vein mineralisation (Cox, 1986). Mapping of the Zn-Pb-Cu-Mn association produced target locations distributed in a NW–SE pattern along the Swaershoek anticline and in the northwestern part of the area along fault line and lithological contacts. The intensity of the Zn-Pb-Cu-Mn association decreases in peripheral areas away from the Swaershoek anticline and the structures particularly in the northwest part of the area. The distribution of these target zones along the structural features suggests a structural control on the Zn, Pb, Cu and Mn anomalies.

In terms of the spatial distribution of individual Zn, Pb, Cu and Mn values, their anomalous concentrations produced distribution trends which are analogous to each other. High concentrations (369–4564 ppm) of Zn trend in a NW–SE direction, with highest concentrations (807–4564 ppm) occurring towards the central part of the area and decreasing towards the NW and SE directions. Higher concentrations of Pb (337–1043 ppm), Cu (116–265 ppm) and of Mn (0.25–1.78 %) also follow the same NW–SE trend similar to Zn. The distribution of all Pb, Zn, Cu and Mn anomalies (i.e. >336 ppm Pb, >451 ppm Zn, >115 ppm Cu and >0.24 % MnO) occur along the Swaershoek anticline in discrete locations. The RGB method, which selected only the anomalous concentrations of Zn, Pb, Cu and Mn lying over a 90 percentile, also produced a discrete anomaly distribution trending along the Swaershoek anticline. Some remnants of these anomalies in the northwest part of the area occur along lithological contact and fault lines.

The conformal distribution of Pb and Zn anomalies with the Swaershoek anticline indicates that the fluids carrying these anomalies might have passed through the Swaershoek anticline. The structure which might have facilitated this movement of fluids is the Welgevonden Fault which cuts the Swaershoek anticline in the middle of the study area. The source rocks of anomalous Zn concentrations might have been the mafic rocks of the RLS which are traversed by the Planknek-Ysterberg Fault system south of Mokopane (Armitage *et al*., 2007; Oberthur *et al*., 2018). Since the Welgevonden Fault merges with the Planknek-Ysterberg Fault system south of Mokopane (Armitage *et al*., 2007), its plausible the Welgevonden-Planknek-Ysterberg fault system might have aided as a conduit that facilitated the circulation of hydrothermal fluids from deeper mafic rocks of the RLS (van den Kerkhof *et al*., 2018) towards the surface. In terms of anomalous concentrations of Pb, Schweitzer *et al*. (1994) indicated that they might have been leached from the acidic volcanics of the Rooiberg Group. This is plausible since the chemical composition of the thermal waters from springs such as Die Oog, Rhemardo, Lekkerrus and Libertas, which are situated along the Welgevonden Fault (Temperley, 1975) reflect the compositional characteristics of the Rooiberg Group (Olivier *et al*., 2008).

In order to understand the type of mineralisation, which can possibly be associated with the Zn-Pb-Cu-Mn anomalies, the mean zinc ratio [ZR = (100Zn/(Zn + Pb)], standard deviation and the distribution of the ZR values calculated from the anomalous concentrations (Pb > 336 ppm and Zn > 336 ppm) were compared with the standardised ZR parameters of Zn-Pb-Ag (veins, fissure lodes, polymetallic sulphide and Irish style) and Zn-Pb-Cu-Ag-Au VMS mineralisation styles from Huston and Large (1987). The local mean ZR of 47 lies between the standardised mean ZR range of 39–75, which classify a group characterised by Pb-Zn-Ag (veins, fissure lodes, polymetallic sulphide and Irish style) (Huston and Large, 1987; Stolz *et al*., 1994). However, the standard deviation of 7 is less than the threshold of >23 for Zn-Pb-Ag (veins, fissure lodes, polymetallic sulphide and Irish style) and within the <15 threshold of Zn-Pb-Cu-Ag-Au VMS mineralisation style. In contrast, the histogram distribution of the ZR indicated skewed distribution of values, analogous to the skewed ZR distribution of Pb-Zn-Ag (veins, fissure lodes, polymetallic sulphide and Irish style) and differing from the normal distribution of Zn-Pb-Cu-Ag-Au VMS mineralisation style. This comparison indicates that the ZR parameters of the area are comparable to those of the Pb-Zn-Ag (veins, fissure lodes, polymetallic sulphide and Irish style) mineralisation style.

The mean ZR of the area is not influenced by lithology, indicated by the difference between the low mean ZR (47) of the area and the high regional lithological mean ZR of 93. This drop of mean ZR is associated with the increase in Pb and Zn concentrations, possibly due to mineralisation process.

In comparison with the other ore group parameters, the copper ratio [CR = 100Cu/(Cu + Zn)] of 28 lies in the range of <50 which is characterised by Zn-rich ore groups (i.e. Zn-Cu, Zn-Cu-Pb/Zn-Pb-Cu/Zn-Pb). The copper ratio which is <50, does not only signify dominance of Zn but also of Pb (Anthony, 1999). The zinc ratio [ZR = 100Zn/(Zn + Pb)] of 47 is also <50, and it lies between two ranges of Cu-rich ore group (i.e. 0–100: Cu and 20–50: Cu-Pb-Zn) and one of Pb-rich ore group (i.e. 10–50: Pb-Zn-Cu/Pb-Cu-Zn/Pb-Zn). The lead ratio [PR = 100Pb/ (Pb + Cu)] of 68 is >50, reflecting an ore group of Pb-Cu, Pb-Zn-Cu/Pb-Cu-Zn/Pb-Zn. These parameters indicated an ore group characterised by an assemblage of Zn-Pb-Cu/Zn-Cu-Pb (Zn-rich), Pb-Zn-Cu/Pb-Cu-Zn (Pb-rich) and Cu-Pb-Zn (Cu-rich). These element assemblages indicate that the potential Zn-Cu-Pb-Mn mineralisation of the area is characterised by an ore group which is rich in Zn, Pb and Cu.

The results of the fuzzy model produced comparable locations with regard to Zn-Pb-Cu-Mn anomalies. The γ = 0 prediction produced a more contracted view of the Zn-Pb-Cu-Mn anomalies. As the values of γ increases from 0.25 to 0.75, the anomalies became more pronounced, highlighting even the faint anomalies along the lithological contacts. Most of the Zn-Pb-Cu-Mn anomalies occur along the NW-SE trending Swaershoek anticline structure, suggesting structural control. Some of the Zn-Pb-Cu-Mn anomalies occur along lithological contacts and fault lines, particularly in the northwestern part of the area. In terms of the optimum proportion in the prospective area, smaller areas with significant anomalous concentrations are ideal in narrowing the search area and increasing the prospect of finding mineralisation. Therefore, the more refined anomalies produced by prediction model γ = 0, represent an optimum proportion of prospective areas.

5.2 Conclusions

This study indicated that the elevated regional concentrations of Pb and Zn are acceptable by reproduction of comparable and some higher concentrations in the follow-up survey. The higher

follow-up Pb and Zn concentrations give validation to the elevated regional concentrations, highlighting even the anomalous concentration (Pb > 100 ppm and Zn > 300 ppm), which indicates potential mineralisation as compared to soil threshold concentrations for mineralisation.

These anomalous concentrations characterised by Zn-Pb-Cu-Mn, bear characteristics of Zn, Pb and Cu rich mineralisation (i.e. Zn-Pb-Cu/Zn-Cu-Pb, Pb-Zn-Cu/Pb-Cu-Zn, Cu-Pb-Zn), analogous to a group of veins, fissure lodes, polymetallic sulphide and Irish style mineralisation. The Zn-Pb-Cu-Mn anomalies occur as discrete target zones along the Swaershoek anticline and also lithological contacts and fault lines, particularly in the northwestern part of the area. The alignment of the anomalies with the structure might be the indication that they are structurally controlled.

REFERENCES

Akoglu, H., 2018. User's guide to correlation coefficients. Turkish Journal of Emergency Medicine, 18, 91–93.

Antony, J.P., 1997. Geochemistry and significance of ore grouping of the Ingaldhal sulphide deposit, Karnataka craton, India. unpub. Ph. D thesis IIT, Bombay, 147pp.

Antony, J.P., 1999. Ore Group Classification - A Case Study from Ingaldhal Sulphide Deposit, Karnataka Craton, India. Gondwana Research, 2, 67–77.

Armitage, P.E.B., McDonald, I. and Tredoux, M., 2007. A geological investigation of the Waterberg hydrothermal platinum deposit, Mookgophong, Limpopo Province, South Africa. Transactions of the Institution of Mining and Metallurgy, Section B, 116, B113–129.

Basson, I.J., 2019. Cumulative deformation and original geometry of the Bushveld Complex. Techtonophysic, 750, 177–202.

Beeson, R., Brunke, E.G. and Dent, R.H., 1978. Preliminary results from a regional geochemical survey in the Northwestern Cape Province. In: W.J. Verwoerd (Editor), Mineralisation in metamorphic terrains. Special Publication, Geological Society of South Africa, 4, 189–203.

Bolotnikov, A.F. and Kravchenko, N.S., 1970. Criteria for recognition of tin-bearing granites. Dokl. Akad. Nauk S.S.S.R., 191, 186–187.

Bonham-Carter, G.F., 1994. Geographic information systems for geoscientists: modeling with GIS. Pergamon Press, 398pp.

Brace, N., Kemp, R. and Snelgar, R., 2006. SPSS for Psychologists: A guide to data analysis using SPSS for Windows (3rd Edition). London: Routledge.

Buchanan, P.C. and Reimold, W.U., 1998. Studies of the Rooiberg Group, Bushveld Complex, South Africa: no evidence for an impact origin. Earth Planet Sci. Lett., 155, 149–165.

Buchanan, P.C., Koeberl, C. and Reimold, W.U., 1999. Petrogenesis of the Dullstroom Formation, Bushveld magmatic province, South Africa. Contributions to Mineralogy and Petrology, 137, 133–146.

Buick, I.S., Maas, R., Gibson, R., 2001. Precise U-Pb titanite age constraints on the emplacement of the Bushveld Complex, South Africa. J. Geol. Soc. Lond., 158, 3–6.

Butt. C.R.M. and Zeegers. H., 1992. Regolith Exploration Geochemistry in Tropical and Subtropical Terrains. Handbook of Exploration Geochemistry. Vol. 4. Elsevier, Amsterdam, 3–512.

Cameron, E.M. and Baragar, W.R.A., 1971. Distribution of ore elements in rocks for evaluating ore potential: frequency distribution of copper in Coppermine River Group and Yellowknife Group volcanic rocks, N.W.T., Canada. In: R.W. Boyle and J.I. McGerrigle (Editors), Geochemical Exploration. Can. Inst. Min. Metall., Spec., 11, 570–576.

Carranza, E.J.M., 2009. Geochemical anomaly and mineral prospectivity mapping in GIS. Handbook of Exploration and Environmental Geochemistry vol. 11. Elsevier, Amsterdam, 210–227.

Cawthorn, R.G., 2013. The Residual or Roof Zone of the Bushveld Complex, South Africa. Journal of Petrology 54, 1875–1900.

Chan, Y.H., 2003. Biostatistics 104: correlational analysis. Singapore Med. J., 44, 614–619.

Cheney, E.S. and Twist, D., 1991. The conformable emplacement of the Bushveld mafic rocks along a regional unconformity in the Transvaal succession of South Africa. Precambrian Research, 52, 115–132.

Clubley-Armstrong, 1980. Petrochemical of the Rooiberg Group and overlying Loskop Formation north of Middelburg, southeastern Transvaal. Ann. Geol. S. Afr.,14/2, 11–28.

Coetzee, G.L., 1970. The Rooiberg felsites series north of Nylstroom. Special Publication, Geological Society of South Africa, 1, 312–325.

Cohen, J., 1988. Statistical Power Analysis for the Behavioral Sciences (2nd Edition). Hillsdale, NJ: Erlbaum.

Cooksey, R.W., 2020. Illustrating Statistical Procedures: Finding Meaning in Quantitative Data (3rd Edition). Springer, 145pp.

Cox, D.P., 1986. Description of polymetallic veins. In: D.P. Cox and D.A. Singer (Editors), Mineral deposit models: U.S. Geological Survey Bulletin 1693, 125–129.

Council of Geoscience, 1978. 1:250000 geologic maps 2528 Pretoria and 2428 Nylstroom sheets, Pretoria.

Crocker, I.T., 1979. Metallogenic aspects of the Bushvled granite: Fluorite, tin and associated rare metal-carbonate mineralization. Spec. Publi. Geol. Soc. S. Afr., 5, 275–296.

Dancey, C.P. and Reidy, J., 2007. Statistics without Maths for Psychology. Pearson Education.

De Bruiyn, H., 1980. The geology of the acid phase of the Bushveld Complex, north of Pretoria -a geochemical statistical approach. Ph.D. thesis (unpublished), University of Free State, 171pp.

Du Plessis, C.P. and Walraven, F., 1990. The tectonic setting of the Bushveld Complex in Southern Africa part 1: structural deformation and distribution. Tectonophysics, 179, 305–319.

Elsenbroek, J.H., 1995. Instrumentation analytical technique for the analysis of regional geochemical samples used at the South African Council for Geoscience. Analyst, 120, 1535–1541.

Elsenbroek, J.H., 1996. An analytical report of the calibration on the Philips PW 1606 simultaneous wavelength dispersive X-ray fluorescence spectrometer. Internal report, Council for Geoscience, 1996–0236, 61pp.

Elston, W.E., 1992. Does the Bushveld–Vredefort system (South Africa) record the largest known terrestrial impact catastrophe? Abstract, International Conference on Large Meteorite Impacts, Planetary Evolution, Lunar and Planet Institute Contribution Series, 790, 23–24.

Falcon, L.M., 1985. Tin in South Africa. Journal of South African Mining Metallurgy, 85, 333–345.

Ehlers, D.L. and du Toit, M.C., 2002. Explanation of the Nylstroom metallogenic map sheet 2428. Explanation, Metallogenic Map Sheet 2428, 1:250 000, Council for Geoscience, 53pp.

Eriksson, P.G., Schreiber, U.M. and Reczko, B.F.F., 1994. Petrography and geochemistry of sandstones interbedded with the Rooiberg Felsite Group (Transvaal Sequence, South Africa): Implications for provenance and tectonic setting. J. Sediment. Res., A64, 836–846.

Eriksson, P.G, Reczko, B.F.F. and Callaghan, C.C., 1997. The economic mineral potential of the mid-Proterozoic Waterberg Group, northwestern Kaapvaal craton, South Africa. Mineralium Deposita, 32, 401–409.

FAO, 1988. Aspects of FAO's policies, programmes, budget and activities aimed at contributing to sustainable development. Document to the 94th Session of the FAO Council, Rome, 15–25 November 1988. Rome, FAO. CL 94/6.

FAO, 2001. Lectures notes on the major soils of the world. World Soil Resources Report 94. Rome: Food and Agriculture Organization of the United Nations, 126–320.

Garrett, R.G., 1973. Regional geochemical study of Cretaceous acidic rocks in the Northern Canadian Cordillera as a tool for broad mineral exploration. In: M.J. Jones (Editor), Geochemical Exploration 1972. Institution of Mining and Metallurgy, London, 203–219.

Good, N. and. de Wit, M.J., 1997. The Thabazimbi–Murchison Lineament of the Kaapvaal Craton, South Africa: 2700 Ma of episodic deformation. Journal of the Geological Society, London, 154, 93–97.

Govett, G.J.S., 1983. Rock geochemistry in mineral exploration. Handbook of Exploration Geochemistry vol. 3. Elsevier, Amsterdam, 57–58.

Govett, G.J.S. and Pantazis, T.M., 1971. Distribution of Cu, Zn, Ni, and Co in the Troodos pillow lava series, Cyprus. Inst. Min. Metall., Trans., Sect. B, 80, 27–46.

Govett, G.J.S. and Goodfellow, W.D., 1975. The use of rock geochemistry in detecting blind sulphide deposits —a discussion. Inst. Min. Metall., Trans., Sect., 84, 134–140.

Gunther, T., Haase, K.M., Klemd, R. and Teschner, C., 2018. Mantle sources and magma evolution of the Rooiberg lavas, Bushveld Large Igneous Province, South Africa. Contributions to Mineralogy and Petrology, 173:51.

Harmer, R.E. and Von Gruenewaldt, G., 1991. A review of magmatism associated with the Transvaal Basin — implications for its tectonic settings. South African Journal of Geology, 94, 104–122.

Harmer, R.E. and Farrow, D., 1995. An isotopic study of the volcanics of the Rooiberg Group: age implications and a potential exploration tool. Mineralium Deposita, 30, 188–195.

Harmer, R.E. and Armstrong, R.A., 2000. New precise dates on the acid phase of the Bushveld their implications. Abstract, Workshop on the Bushveld Complex, 18–21 November 2000, Burgersfort. University of the Witwatersrand, Johannesburg.

Hatton, C.J., 1995. Mantle plume origin for the Bushveld and Ventersdorp magmatic provinces. J. Afr. Earth Sci., 21, 571–577.

Hatton, C.J. and Schweitzer, J.K., 1995. Evidence for synchronous extrusive intrusive Bushveld magmatism. Journal of African Earth Science, 21, 579–594.

Hatton, C.J., 1988. Formation of the Bushveld Complex at a plate margin. Abstract, Congress of the Geological Society of South Africa, 22, 251–254.

Herselman, J.E., Steyn, C.E. and Fey, M.V., 2005. Baseline concentration of Cd, Co, Cr, Cu, Pb, Ni and Zn in surface soils of South Africa. South African Journal of Science, 101, 509–512.

Hunter, D.R., 1973. The localization of tin mineralization with reference to Southern Africa. Minerals Science Engineering, 5, 53–77.

Hunter, D.R., 1974. Some enigmas of the Bushveld Complex. Information Circular, Economic Geology Research Unit, University of the Witwatersrand, 82, 25pp.

Hunter, D.R., 1976. Some enigmas of the Bushveld Complex. Economic Geology, 71, 229–248.

Huston, D.L. and Large, R.R., 1987. Genetic exploration significance of the zinc ratio (100Zn/(Zn + Pb)) in massive sulphide systems. Economic Geology, 82, 1521–1529.

IUSS Working Group WRB, 2015. World reference base for soil resources 2014, update 2015. International soil classification system for naming soils and creating legends for soil maps. World Soil Resources Reports No. 106. FAO, Rome, 89pp.

Jahn, R., Blume, H. P., Asio, V. B., Spaargaren, O. and Schad, P., 2006. Guidelines for soil description (4th Edition). FAO, 11pp.

Kabata-Pendias, A., 2011. Trace Elements in Soils and Plants (4th Edition). CRC Press, 38–42.

Knox-Robinson, C.M. and Wyborn, L.A.I., 1997. Towards a holistic exploration strategy: using Geographic Information Systems as a tool to enhance exploration. Aust. J. Earth Sci., 44, 453–463.

Labuschagne, L.S., Holdsworth, R. and Stone, T.P., 1993. Regional stream sediment geochemical survey of South Africa. Journal of Geochemical Exploration, 47, 283–296.

Lenhardt, N. and Eriksson, P.G., 2012. Volcanism of the Palaeoproterozoic Bushveld Large Igneous Province: The Rooiberg Group, Kaapvaal Craton, South Africa. Precambrian Research, 214–215, 82–94.

Lenhardt, N., Masango, S.N., Jolayemi, O.O., Lenhardt, S.Z., Peeters, G. and Eriksson, P.G., 2017. The Palaeoproterozoic (~2.06 Ga) Rooiberg Group, South Africa: Dominated by extremely high-

grade lava-like and rheomorphic ignimbrites? New observations and lithofacies analysis. Journal of African Earth Sciences, 131, 213–232.

Mathez, E.A., VanTongeren, J.A. and Schweitzer, J., 2013. On the relationships between the Bushveld Complex and its felsic roof rocks, part 1: petrogenesis of Rooiberg and related felsites. Contributions to Mineralogy and Petrology, 166, 435–449.

Munro, B.H., 2005. Statistical Methods for Health Care Research. Lippincott Williams & Wilkins: Philadelphia, PA, USA, 1pp.

Nachtergaele, F., 2010. The classification of leptosols in the world reference base for soil resources. 19th World Congress of Soil Science, Soil Solutions for a Changing World (2010), 1–6.

Oberthür, T., Melcher, F., Fusswinkel, T., van den Kerkhof, A.M. and Sosa, G, M., 2018. The hydrothermalWaterberg platinum deposit, Mookgophong (Naboomspruit), South Africa. Part 1: Geochemistry and ore Mineralogy. Mineralogical Magazine, 82, 725–749.

Olivier, J., van Niekerk, H.J. and van der Walt, I.J., 2008. Physical and chemical characteristics of thermal springs in the Waterberg area in Limpopo Province, South Africa. Water SA., 34, 163–174.

Pohl, W.L., 2011. Economic geology: principles and practice. Metals, minerals, coal and hydrocarbons—introduction to formation and sustainable exploitation of mineral deposits. Wiley-Blackwell, 186–834.

Porwal, A. and Chudasama, B., 2016. Mineral prospectivity modelling. Workshop, Council for Geoscience, Pretoria, South Africa, 15–26 February.

Ratner, B., 2009. The correlation coefficient: Its values range between + 1 / − 1, or do they?. Journal of Targeting, Measurement and Analysis for Marketing, 17, 139–142.

Reedman, J. H., 1979. Techniques in mineral exploration. Applied Science. Publishers Ltd., London, 130 –138.

Rezaei, S., Shooshpasha, I. and Rezaei, H., 2018. Empirical Correlation between Geotechnical and Geophysical Parameters in a Landslide Zone. Earth Sci. Res. J., 22, 195–204.

Rhodes, R.C., 1975. New evidence for the impact origin of the Bushveld Complex, South Africa. Geology, 3, 549–554.

Rhodes, R.C. and Du Plessis, M.D., 1976. Notes on some stratigraphic relations in the Rooiberg felsite. Trans. Geol. Soc. S. Afr., 79, 183–185.

Rhodes, R.C., 1977. Petrochemical characteristics of Bushveld granite and Rooiberg felsite. Trans. Geol. Soc. S. Afri., 77, 93–98.

Robb, L. J., Robb, V.M. and Walraven, F., 1994. The Albert Silver Mine revisited: towards a model for polymetallic mineralization in granites of the Bushveld Complex, South Africa. Johannesburg, University of the Witwatersrand, Economic Geology Research Unit.

Robb, L. J., Freeman, L. A. and Armstrong, R. A., 2000. Nature and longevity of hydrothermal fluid flow and mineralisation in granites of the Bushveld Complex, South Africa. Transactions of the Royal Society of Edinburgh, Earth Science, 91, 269–281.

Schweitzer, J. K., 1987. The transition from the Dullstroom Basalt Formation to the Rooiberg Felsite Group, Transvaal Supergroup: a volcanological, geochemical and petrological investigation. Ph. D. thesis, University Pretoria, Pretoria, South Africa.

Schweitzer, J.K., Hatton, C.J. and De Waal, S.A., 1994. Economic potential of the Rooiberg Group — volcanic rocks in the floor roof of the Bushveld Complex. Geology Department, Pretoria University, Mineralium Deposita, 30, 168–177.

Schweitzer, J.K., Hatton, C.J. and De Waal, S.A., 1995a. Regional lithogeochemical stratigraphy of the Rooiberg Group, upper Transvaal Supergroup — a proposed new subdivision. South African Journal of Geology, 98, 245–255.

Schweitzer, J.K., Hatton, C.J. and de Waal, S.A., 1995b. Economic potential of the Rooiberg Group-volcanic rocks in the floor and roof of the Bushveld Complex. Mineralium Deposita, 30, 167–177.

Schweitzer, J.K., Hatton, C.J. and De Waal, S.A., 1997. Link between the granitic and volcanic rocks of the Bushveld Complex, South Africa. Journal of African Earth Science, 24, 95–104.

Sharpe, M.R., Bahat, D. and Von Gruenewaldt, G., 1981. The concentric elliptical structure of feeder sites to the Bushveld Complex and possible economic implications. Trans. Geol. Soc. S. Afr., 84, 239–244.

South African Committee for Stratigraphy (SACS), 1980. Stratigraphy of South Africa. Part 1. Lithostratigraphy of the Republic of South Africa, South West Africa/Namibia, and the Republics of Bophuthatswana, Transkei and Venda (L.E. Kent, compiler). Handbook Geological Survey of South Africa (Council for Geoscience), 8, 690pp.

Stolz, A.J., Large, R.R., Robinson, P. and Wedekind, R., 1994. Criteria for distinguishing between gold-bearing and barren ironstones at Tennant Creek, Northern Territory, Australia. Journal of Geochemical Exploration, 51, 247–264.

Tauson, L. V. and Kozlov, U. D., 1973. Distribution functions and ratios of trace element concentrations as estimators of ore-bearing potential of granites. In: M. J. Jones (Editor). Geochemical Exploration 1972. Institution of Mining and Metallurgy, London, 37–44.

Temperley, B.N., 1975. The Welgevonden fault of the central Transvaal and its thermal water. Geological Survey of South Africa, Groundwater Series, 2, 1–2.

Twist, D. and French, B.M., 1983. Voluminous acid volcanism in the Busheveld Complex: A review of the Rooiberg felsite. Bull. Volcanol., 46, 224–242.

Twist, D., 1985. Geochemical evolution of the Rooiberg silicic lavas in the Loskop Dam area, southeastern Bushveld. Economic Geology, 80, 1153–1165.

Van den Kerkhof, A.M., Sosa, G.M., Oberthür, T., Melcher, F., Fusswinkel, T., Kronz, A., Simon, K. and Dunkl, I., 2018. The hydrothermalWaterberg platinum deposit, Mookgophong (Naboomspruit), South Africa. Part II: Quartz chemistry, fluid inclusions and geochronology. Mineralogical Magazine, 82, 751–778.

Vantongeren, J.A., Mathez, E.A. and Kelemen, P.B., 2010. A felsic end to Bushveld differentiation. Journal of Petrology, 51, 1891–1912.

Walraven, F., Retief, E.A., Burger, A.J., Swanepoel, D.J. de V., 1987. Implications of new U-Pb zircon age dating on the Nebo Granite of the Bushveld Complex. S. Afr. J. Geol., 90, 344–351.

Walraven, F. and Hattingh E., 1993. Geochronology of the Nebo Granite, Bushveld Complex. South African Journal of Geology, 96, 31–41.

Walraven, F., 1997. Geochronology of the Rooiberg Group, Transvaal Supergroup, South Africa. Information Circular, vol. 316. Economic Geology Research Unit, University of the Witwatersrand, Johannesburg, South Africa.

Zeh, A., Ovtcharova, M., Wilson, A. H. and Schaltegger, U., 2015. The Bushveld Complex was emplaced and cooled in less than one million years – results of zirconology, and geotectonic implications. Earth and Planetary Science Letters, 418, 103–114.

Zimmermann, H.J. and Zysno, P., 1980. Latent connectivities in human decision making. Fuzzy Set Systems, 4, 37–51.

Zimmermann, H.J., 1985. Fuzzy Set Theory — its applications. Kluwer-Nijhoff Publishing, Boston-Dordrecht-Lancaster, 363pp.

APPENDICES

Appendix 1: Statistics Summary and classification of Logged Data

Table A1.1. The statistical summary of the soil logged data for ore-forming and pathfinder elements.

	Logged Data							
	Minimum	**Maximum**	**Range**	**Mean**	**Std. Deviation**	**Mean + Std. Dev. (68 %)**	**Mean + 1.64485xStd. Dev. (90 %)**	**Mean + 2x Std. Dev. (95 %)**
Log_MnO	-2.138167002	.249540765	2.387707767	-.90666401821	.177607563444	-.729056454762	-0.614526217	-0.551448891
Log_Cu	.731991449	2.422753941	1.690762492	1.79750772339	.160716626966	1.958224350361	2.061862467	2.118940977
Log_Pb	1.202692611	3.018126052	1.815433441	2.20629351217	.194937099343	2.401230611513	2.5269358	2.596167711
Log_Zn	1.443536781	3.659338023	2.215801242	2.42813169135	.137267082770	2.565398774119	2.653915452	2.702665857

Analytical Values				
	Mean	**Mean + Std. Dev. (68 %)**	**Mean + 1.64485xStd. Dev. (90 %)**	**Mean + 2x Std. Dev. (95 %)**
MnO (%)	0.12	0.19	0.24	0.28
Cu (ppm)	63	91	115	132
Pb (ppm)	161	252	336	395
Zn (ppm)	268	368	451	504

Appendix 2: Detection Limits of Major and Trace elements and the Precision of the in-house Powder Briquette Monitors

Table A2.1 The analysed elements and their lower levels of determination.

	Lower levels of detection (LLD)
SiO_2 (%)	0.01
TiO_2 (%)	0.01
Al_2O_3 (%)	0.01
Fe_2O_3 (%)	0.01
MnO (%)	0.001
MgO (%)	0.01
CaO (%)	0.01
Na_2O (%)	0.01
K_2O (%)	0.01
P_2O_5 (%)	0.001
As (ppm)	4
Ba (ppm)	5
Ce (ppm)	10
Co (ppm)	4
Cr (ppm)	4
Cu (ppm)	2
Ga (ppm)	2
Hf (ppm)	5
Nb (ppm)	3
Ni (ppm)	2
Pb (ppm)	3
Rb (ppm)	3
Sc (ppm)	3
Sr (ppm)	2
Th (ppm)	3
U (ppm)	3
V (ppm)	4
W (ppm)	3
Y (ppm)	3
Zn (ppm)	3
Zr (ppm)	3

Table A2.2 The precision of the in-house powder briquette monitors.

Element (n = 110)	Mean	Standard Deviation	Minimum	Maximum	Range	Precision (%)
TiO_2 (%)	6.43	0.03	6.34	6.49	0.15	1
MnO (%)	1.39	0.07	1.25	1.45	0.2	10
Fe_2O_3T (%)	14.2	0.2	13.9	14.6	0.66	3
Sc (ppm)	202	4	195	213	18	4
V (ppm)	2 000	13	1 953	2 023	70	1
Cr (ppm)	1 822	7	1 802	1 837	35	1
Co (ppm)	1 002	16	970	1 024	54	3
Ni (ppm)	1 039	2	1 030	1 043	13	0.4
Cu (ppm)	562	2	558	567	9	0.7
Zn (ppm)	516	6	508	526	18	2
As (ppm)	165	3	156	172	16	4
Rb (ppm)	569	2	563	572	9	1
Sr (ppm)	337	0.78	335	339	4	0.5
Y (ppm)	146	0.65	144	147	3	1
Zr (ppm)	831	1.5	828	835	7	0.4
Nb (ppm)	161	0.5	161	162	1	0.6
Sn (ppm)	9	1.3	5	12	7	29
Sb (ppm)	13	4.7	3	23	20	72
Ba (ppm)	1 069	14	1 029	1 104	75	3
W (ppm)	18	3	12	24	12	33
Pb (ppm)	1 435	10	1 408	1 456	48	1
Th (ppm)	71	1	69	74	5	3
U (ppm)	14	1	11	17	6	14

Appendix 3: Multivariate Analysis: Correlation Coefficient

Table A3.1 The correlations between major oxides and trace elements.

Correlations																																				
	SiO2	TiO2	Al2O3	Fe2O3	MnO	MgO	CaO	Na2O	K2O	P2O5	As	Ba	Ce	Co	Cr	Cu	Ga	Hf	Mo	Nb	Nd	Ni	Pb	Rb	S	Sb	Sc	Sn	Sr	Ta	Th	U	V	W	Y	Zn	Zr
SiO2	1																																			
TiO2	.369**	1																																		
Al2O3	.450**	.611**	1													0 - 0,5	Poor																			
Fe2O3	,061	.369**	.525**	1												0,5 - 0,6	Fair																			
MnO	.212**	.320**	.328**	.456**	1											0,6 - 0,7	Good																			
MgO	.090*	-,071	,029	.134**	.157**	1										0,7 - 0,8	Very Good																			
CaO	.260**	.247**	.208**	.122**	.403**	.129**	1									0,8 - 1	Excellent																			
Na2O	.075*	-.114**	-,031	,021	.089*	.704**	,041	1																												
K2O	.382**	,055	.241**	-.161**	-,051	-,044	.162**	,068	1																											
P2O5	.206**	.554**	.509**	.397**	.439**	,045	.539**	,043	.113**	1																										
As	.197**	-,027	-,058	-.314**	-.170**	-,063	,016	,038	.331**	-,033	1																									
Ba	.337**	.258**	.337**	.163**	.227**	,070	.455**	,049	.678**	.279**	-,005	1																								
Ce	.079*	.164**	.411**	.144**	.085*	-,061	-,010	-,032	.352**	.226**	.176**	.317**	1																							
Co	-.096**	.421**	.333**	.582**	.496**	.109**	,052	,042	-.231**	.376**	-.151**	-,016	.187**	1																						
Cr	.335**	.688**	.483**	.320**	.276**	-,066	.178**	-.078*	-,044	.518**	,070	-,003	.080*	.315**	1																					
Cu	.210**	.394**	.470**	.450**	.514**	.125**	.166**	.081*	-,071	.358**	-.140**	,070	.073*	.419**	.365**	1																				
Ga	.086*	.143**	.384**	.483**	.138**	.098**	,018	,023	.160**	.082*	-,044	.271**	.369**	.221**	,009	.115**	1																			
Hf	.662**	.469**	.430**	.214**	.269**	,049	.099**	-,001	.101**	.162**	.104**	.195**	,042	.100**	.433**	.274**	.134**	1																		
Mo	-,014	-,044	.203**	.344**	.127**	.133**	-,036	,044	-.185**	.099**	-,054	-.084*	.132**	.137**	.079*	.130**	.210**	-.086*	1																	
Nb	.247**	.396**	.357**	.240**	-,050	-,058	-.157**	-,002	.366**	.182**	.149**	.278**	.357**	.124**	.203**	.088*	.343**	.298**	-,018	1															
Nd	.104**	.156**	.395**	.096**	-,013	-.095**	.110**	-.078*	.322**	.111**	.107**	.430**	.696**	-,021	-,022	.074*	.311**	.098**	,055	.287**	1														
Ni	.122**	.778**	.619**	.611**	.450**	,032	.114**	-,052	-.179**	.522**	-.175**	,046	.144**	.703**	.658**	.539**	.253**	.290**	.132**	.258**	,034	1													
Pb	.165**	.143**	.340**	.232**	.392**	.123**	.076*	.148**	.096**	.317**	.257**	-,021	.281**	.263**	.256**	.623**	.084*	.135**	.258**	.077*	.116**	.258**	1												
Rb	.334**	.312**	.458**	,014	.089*	-,021	.105**	.080*	.801**	.272**	.243**	.544**	.459**	,013	.140**	.208**	.217**	.208**	-.179**	.418**	.382**	.154**	.282**	1											
S	.310**	.336**	.460**	.171**	.306**	,019	.757**	-,017	.301**	.702**	.133**	.378**	.177**	,060	.350**	.196**	,040	.156**	,032	-,006	.189**	.195**	.214**	.282**	1										
Sb	-,039	-,012	-,022	,035	-.078*	.074*	-.073*	.090*	-,058	-,034	.238**	-.076*	,062	,050	,013	-,053	.087*	-,019	.106**	,038	,032	,025	.122**	-,057	-,069	1									
Sc	-,066	.267**	.300**	.400**	.136**	.235**	.073*	.141**	-,040	.196**	-.135**	.169**	.130**	.285**	.152**	.149**	.284**	,011	.119**	.128**	.154**	.379**	,067	,062	.087*	.123**	1								
Sn	.094*	.222**	.281**	.368**	.295**	-.146**	,035	-.072*	,026	.287**	-.164**	,035	.078*	.221**	.260**	.461**	.157**	.242**	,064	.317**	,046	.291**	.213**	.190**	.118**	-.138**	,018	1							
Sr	.355**	.257**	.228**	-.110**	.129**	,020	.518**	,061	.675**	.323**	.322**	.738**	.291**	-.130**	,062	,063	.100**	.200**	-.124**	.222**	.396**	-,071	.152**	.534**	.507**	,025	,007	-,013	1						
Ta	-,038	-.099**	,058	.335**	,068	.093*	-.188**	.118**	,035	-.130**	,066	.130**	.149**	.174**	-.122**	,064	.304**	.173**	.113**	.230**	.161**	,063	.144**	,041	-.214**	,044	.155**	.126**	,001	1					
Th	.336**	.405**	.568**	.403**	.091*	,012	-,069	,037	.418**	.297**	,055	.350**	.495**	.255**	.226**	.282**	.420**	.316**	.082*	.738**	.377**	.387**	.260**	.564**	.116**	-,016	.209**	.336**	.226**	.248**	1				
U	.369**	.382**	.607**	.477**	.302**	,016	,031	-,010	.321**	.248**	-,056	.367**	.366**	.263**	.216**	.408**	.380**	.448**	.089*	.375**	.317**	.373**	.317**	.572**	.127**	-.098**	.158**	.367**	.201**	.283**	.587**	1			
V	.118**	.781**	.412**	.499**	.331**	.087*	.098**	-,003	-.216**	.448**	-.106**	,004	,032	.624**	.626**	.445**	.095**	.238**	.077*	.241**	-,063	.850**	.179**	.073*	.086*	.089*	.340**	.184**	-.083*	-,013	.282**	.260**	1		
W	.195**	.150**	.218**	.120**	.093*	,069	-.176**	.212**	.358**	.125**	.334**	.127**	.356**	.160**	.095**	.323**	.214**	.290**	-,033	.511**	.229**	.183**	.453**	.574**	-,025	,037	,046	.322**	.189**	.384**	.581**	.469**	.092*	1		
Y	.413**	.399**	.645**	.328**	.136**	,029	.179**	,025	.416**	.269**	.157**	.518**	.582**	.140**	.160**	.210**	.443**	.398**	,055	.522**	.699**	.265**	.173**	.564**	.277**	,058	.242**	.174**	.437**	.217**	.659**	.567**	.160**	.421**	1	
Zn	.333**	.330**	.459**	.179**	.576**	,061	.335**	,042	.243**	.346**	-,019	.328**	.082*	.137**	.249**	.571**	.098**	.282**	,014	-,051	.138**	.319**	.521**	.362**	.372**	-.139**	,071	.220**	.327**	,018	.157**	.372**	.159**	.221**	.249**	1	
Zr	.796**	.571**	.616**	.396**	.360**	,038	.326**	,011	.373**	.445**	.184**	.413**	.225**	.141**	.523**	.344**	.244**	.684**	,050	.436**	.229**	.404**	.267**	.457**	.461**	,015	.134**	.275**	.387**	,060	.549**	.508**	.335**	.341**	.593**	.372**	1

**. Correlation is significant at the 0.01 level (2-tailed).

*. Correlation is significant at the 0.05 level (2-tailed).

Appendix 4: Anomaly Predictor Maps of Zn, Pb, Cu and Mn

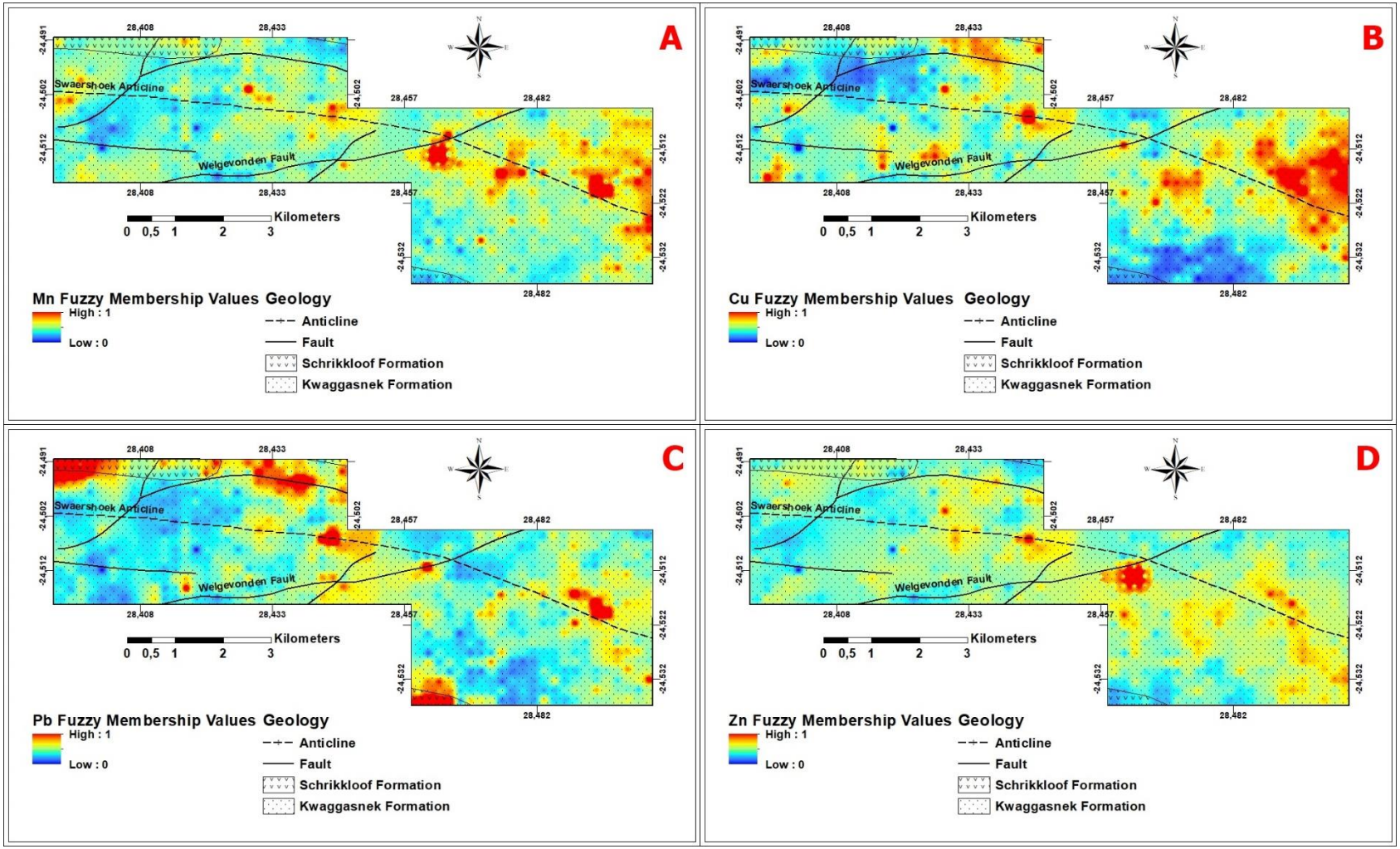

Figure A4.1 Anomaly fuzzy membership value maps. (A) Fuzzy membership values map of Mn, (B) Fuzzy membership values map of Cu, (C) Fuzzy membership values map of Pb and (C) Fuzzy membership values map of Zn.

Appendix 5: Predictor Map of Pathways

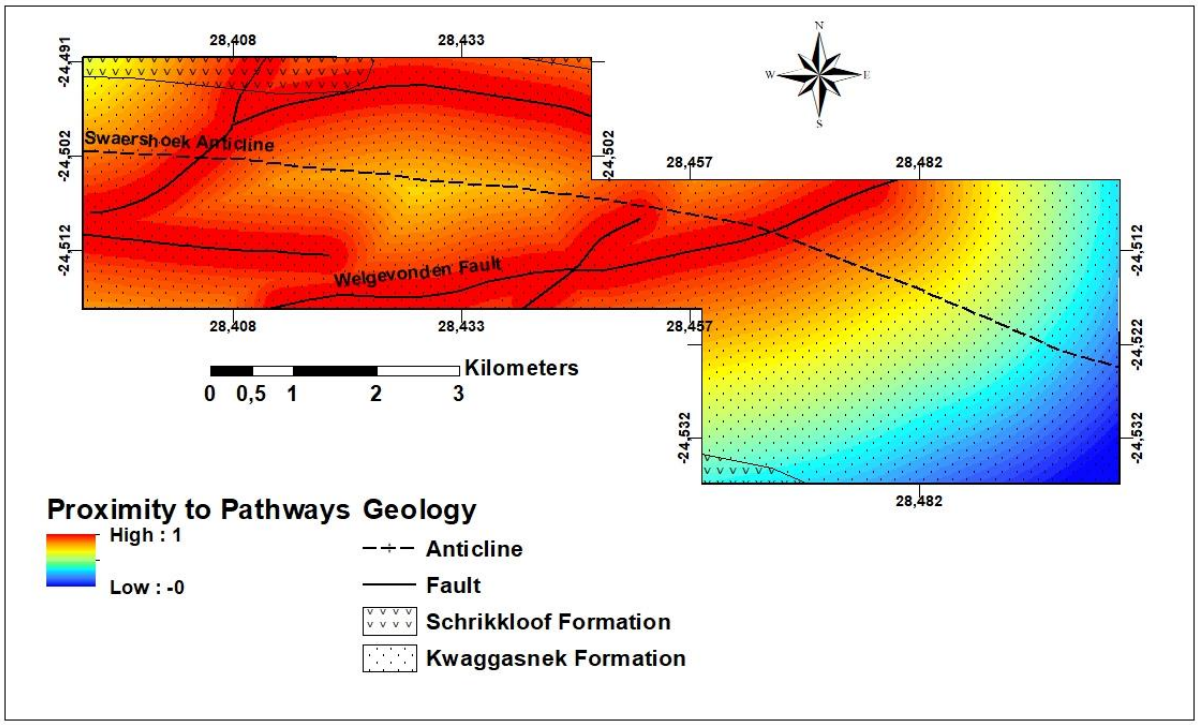

Figure A5.1 The fuzzy membership values map of the proximity to pathways produced from structures.

Appendix 6: Predictor Map of Traps

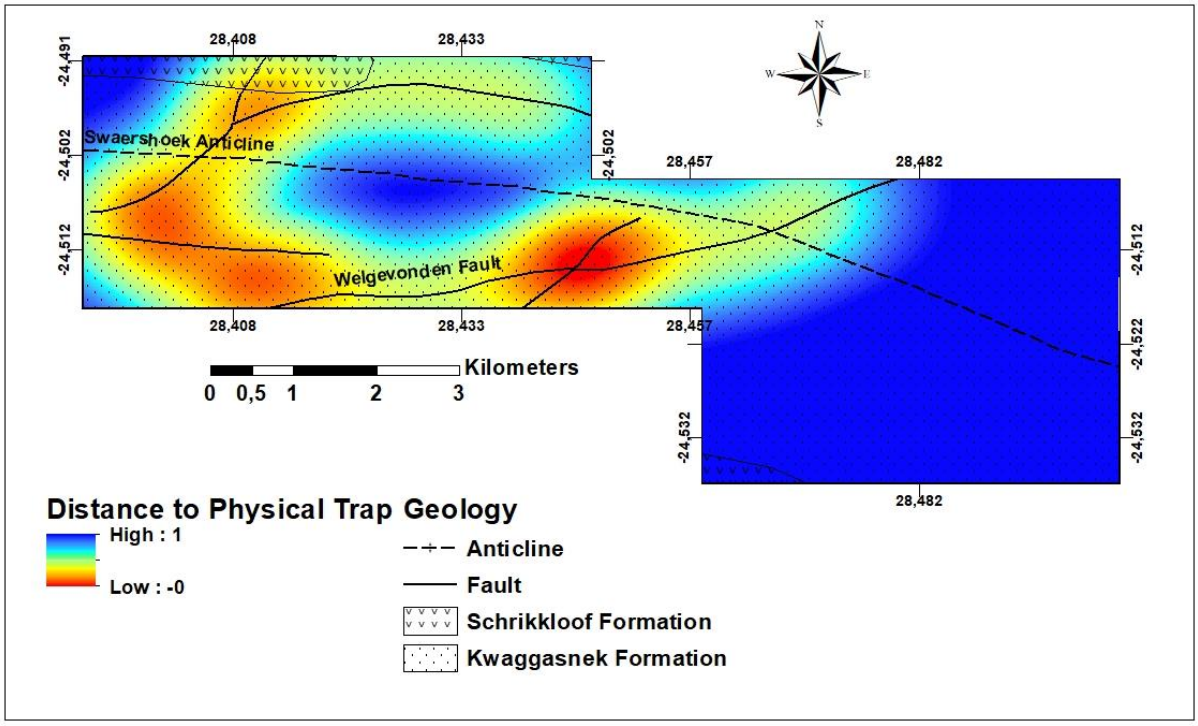

Figure A6.1 The fuzzy membership values map of the distance to physical traps produced from structural densities.

Appendix 7: Fuzzy Mineral Potential Maps of Zn-Pb-Cu-Mn

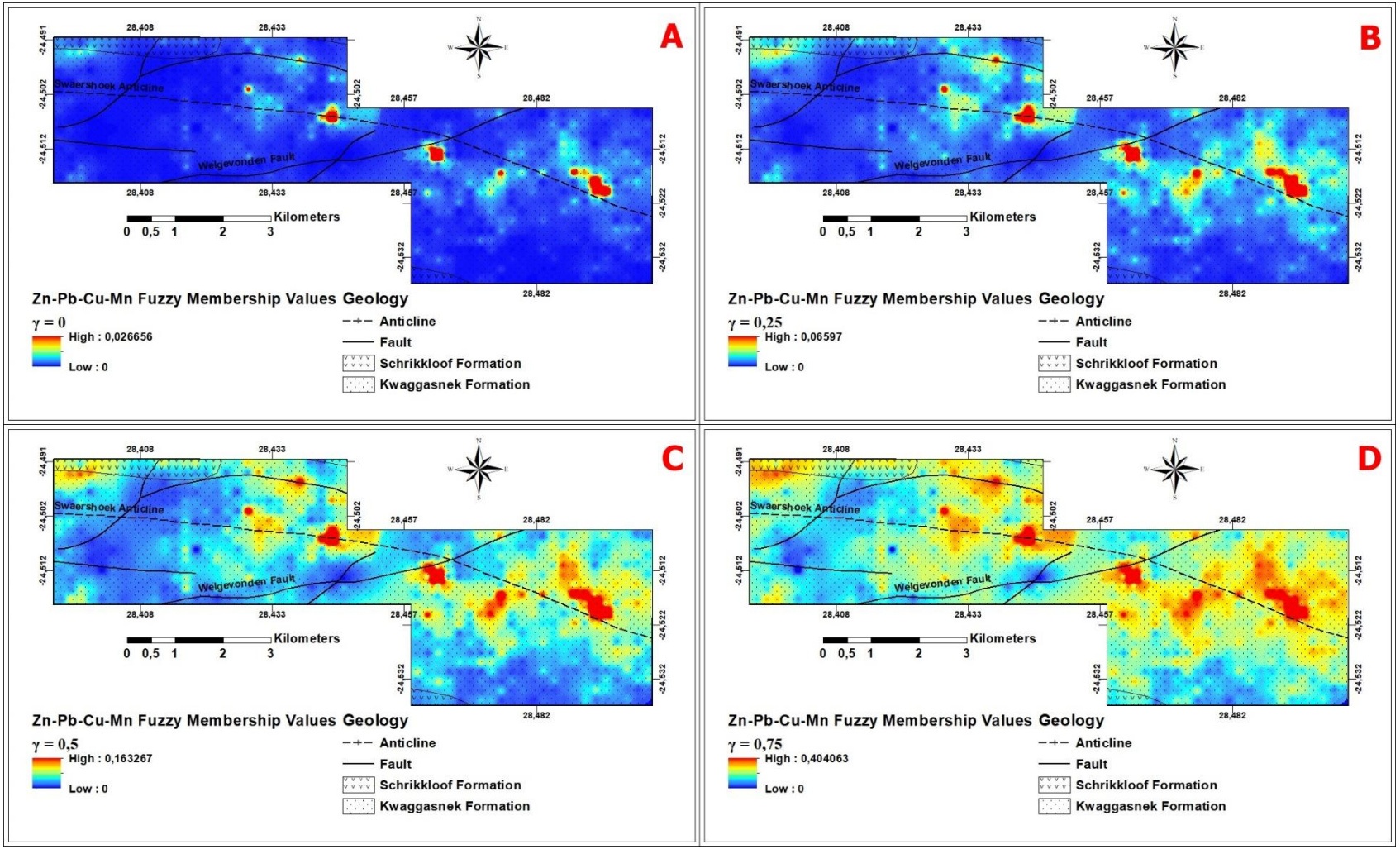

Figure A7.1 Membership value map of overlaid proximity to physical traps, proximity to pathways and Zn, Pb, Cu, Mn anomalies for (A) γ = 0, (B) γ = 0.25, (C) γ = 0.5 and (D) γ = 0.75.

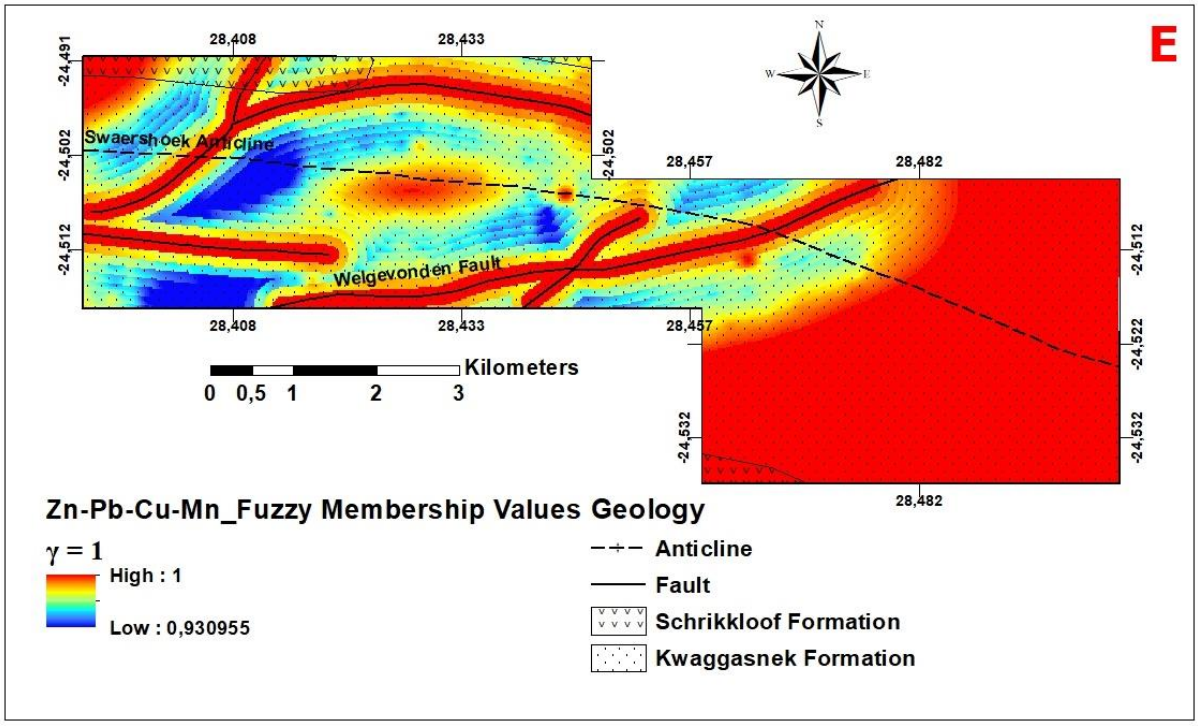

Figure A7.2 Membership value map of overlaid proximity to physical traps, proximity to pathways and Zn, Pb, Cu, Mn anomalies for γ = 1.

Appendix 8: Regional Geochemical Data of Rock Samples

Table A8.1 Trace geochemical data of regional rock samples (Mathez *et al*., 2013).

SAMPLE NAME	ROCK NAME	ROCK TYPE	Sc (ppm)	Cr (ppm)	Co (ppm)	Ni (ppm)	Cu (ppm)	Zn (ppm)	Ga (ppm)	Rb (ppm)	Sr (ppm)	Y (ppm)	Zr (ppm)	Nb (ppm)	Ba (ppm)	Hf (ppm)	Pb (ppm)	Th (ppm)
s_15 [17453]	RHYOLITE [17453]	VOL	6	4	88	0	0	93	16	227	40	74	466	22	1075	14	14	26
s_16 [17453]	RHYOLITE [17453]	VOL	7	6	77	4	42	199	16	268	53	62	449	21	1546	0	13	26
s_17 [17453]	RHYOLITE [17453]	VOL	7	9	69	0	14	157	18	206	100	58	418	20	1002	0	12	25
s_18 [17453]	RHYOLITE [17453]	VOL	7	8	88	0	12	291	18	280	57	67	468	23	1200	0	15	27
s_19 [17453]	RHYOLITE [17453]	VOL	7	7	72	0	14	147	17	216	86	63	426	20	1140	0	9	27
s_20 [17453]	RHYOLITE [17453]	VOL	5	4	124	0	0	177	12	224	48	70	520	26	1011	11	13	26
s_21 [17453]	RHYOLITE [17453]	VOL	6	6	78	0	13	115	18	252	137	76	548	26	1040	0	10	25
s_22 [17453]	RHYOLITE [17453]	VOL	7	7	92	21	5	268	20	206	144	70	531	27	773	12	17	26
s_23 [17453]	RHYOLITE [17453]	VOL	6	5	66	9	13	193	20	200	43	77	560	26	872	13	10	25
s_24 [17453]	RHYOLITE [17453]	VOL	6	6	69	0	9	131	17	187	99	65	467	21	953	13	16	29
s_26 [17453]	RHYOLITE [17453]	VOL	9	8	60	3	15	106	17	205	89	58	429	20	685	13	10	26
s_27 [17453]	RHYOLITE [17453]	VOL	6	7	61	0	12	155	18	190	83	64	441	22	1038	0	12	28
s_28 [17453]	RHYOLITE [17453]	VOL	8	5	52	0	10	202	18	170	63	67	455	20	321	14	9	26
s_31 [17453]	RHYOLITE [17453]	VOL	5	4	126	0	4	63	13	224	248	75	515	24	901	13	9	24
s_32 [17453]	RHYOLITE [17453]	VOL	9	1	133	21	27	71	15	228	265	82	530	26	344	13	9	24
s_33 [17453]	RHYOLITE [17453]	VOL	6	1	135	7	6	26	16	222	226	77	545	26	784	13	8	28
s_34 [17453]	RHYOLITE [17453]	VOL	6	6	71	0	11	164	19	256	60	66	438	21	1352	13	16	26
s_35 [17453]	RHYOLITE [17453]	VOL	6	5	69	1	13	124	17	177	90	70	436	23	839	0	10	27
s_36 [17453]	RHYOLITE [17453]	VOL	6	5	50	0	10	110	17	178	56	63	431	21	1096	12	9	24
s_37 [17453]	RHYOLITE [17453]	VOL	5	4	71	0	13	156	17	182	62	63	442	23	1243	16	7	24
s_38 [17453]	RHYOLITE [17453]	VOL	6	5	59	0	1	147	18	238	102	86	573	29	1473	0	10	26
s_39 [17453]	RHYOLITE [17453]	VOL	10	6	55	21	19	132	16	176	98	72	464	22	1161	0	8	22